EUROPEAN ORGANIZATION FOR NUCLEAR RESEARCH

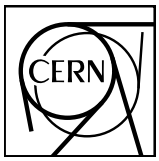

ALICE-PUBLIC-2023-001
12 May 2023

Physics of the ALICE Forward Calorimeter upgrade

ALICE Collaboration *

Abstract

The ALICE Collaboration proposes to instrument the existing ALICE detector with a forward calorimeter system (FoCal), planned to take data during LHC Run 4 (2029–2032). The FoCal detector is a highly-granular Si+W electromagnetic calorimeter combined with a conventional sampling hadronic calorimeter, covering the pseudorapidity interval of $3.4 < \eta < 5.8$. The FoCal design is optimized to measure isolated photons at most forward rapidity for $p_{\mathrm{T}} \gtrsim 4$ GeV/c.

In this note we discuss the scientific potential of FoCal, which will enable broad exploration of gluon dynamics and non-linear QCD evolution at the smallest values of Bjorken x accessible at any current or near-future facility world-wide. FoCal will measure theoretically well-motivated observables in pp and p–Pb collisions which are sensitive to the gluon distribution at small x at low to moderate Q^2, based on isolated photon, neutral meson, and jet production and correlations in hadronic collisions, and the measurement of vector meson photoproduction in ultra-peripheral collisions. These FoCal measurements will provide incisive tests of the universality of linear and non-linear QCD evolution in different collision systems over an unprecedented kinematic range, in particular when combined with the comprehensive experimental program at the EIC and other forward measurements at RHIC and the LHC. FoCal will also carry out measurements at very forward rapidity in Pb–Pb collisions, enabling novel probes of the Quark-Gluon Plasma based on jet quenching phenomena and long-range correlations of neutral pions, jets, and photons.

*See Appendix A for the list of collaboration members

Contents

1 Introduction

The ALICE Collaboration proposes to install a new, high-precision FOrward CALorimeter system (FoCal) [1]. FoCal consists of a pioneering highly-granular, longitudinally-segmented silicon-tungsten (Si+W) electromagnetic calorimeter (FoCal-E) and a conventional highly-granular metal-scintillator hadronic calorimeter (FoCal-H). FoCal will cover pseudorapidity $3.4 < \eta < 5.5$ over the full azimuth, and up to $\eta = 5.8$ with partial azimuthal coverage, for measurements of prompt and isolated photons (γ), identified π^0 and other neutral mesons, J/ψ and its excited states, W and Z bosons, inclusive jets, and their correlations (di-hadron, di-jet, γ+hadron, γ+jet, etc.). FoCal will be installed during LHC Long Shutdown 3 (LS3) and will take data during LHC Run 4, which is currently scheduled for the period 2029–2032. FoCal will record data for pp, p–Pb, and Pb–Pb collisions, triggered on both hadronic interactions and on Ultra-Peripheral Collisions (UPCs). These data will probe the partonic structure of hadronic matter with unprecedented reach in momentum fraction Bjorken-x, down to $x \sim 10^{-6}$ for small and moderate momentum transfer Q^2. [1] This note presents the physics capabilities of FoCal, with focus on key photon and jet observables, and discusses their theoretical interpretability. It also discusses the larger experimental program to measure saturation phenomena at RHIC, the LHC, and the Electron Ion Collider (EIC) [2], and how to utilize this broad suite of data for comprehensive understanding of the small-x structure of matter.

[1] Bjorken-x refers to the momentum fraction carried by partons in the proton or in the nucleus.

The primary scientific goal of FoCal is the study of **gluon saturation**. New phenomena are expected to emerge at very small-x, which is probed by collisions at high energy [3]. At large x QCD evolution is linear: as x decreases, partons split in processes such as $q \to qg$ and $g \to q\overline{q}$, and gluon density $g(x)$ increases like a power law $xg(x) \propto x^{-\delta/2}$, where the power δ is determined by fitting to data. However, at sufficiently small x, the density increases to the extent that partons overlap and recombine. This recombination leads to a reduction in gluon density relative to linear projections, otherwise known as gluon shadowing [4]. This growth cannot continue unabated as x is reduced; due to the gluon self-interaction the gluon density eventually saturates, leading to a new state of gluon-saturated matter. This matter is characterized by a dynamically-generated saturation momentum $Q_{\rm sat}$; the density of gluons with momentum less than $Q_{\rm sat}$ is subject to saturation effects, while the density of gluons with momentum larger than $Q_{\rm sat}$ is governed by linear QCD evolution. Since the gluon density grows as x decreases, saturation effects are expected to be strongest at small x. Saturation effects at a given value of x are likewise larger in heavy nuclei: ${Q_{\rm sat}}^2 \sim A^{1/3}$, where $\sim A$ is the nuclear mass [3, 5].

Observation of non-linear QCD evolution and gluon saturation would be a landmark in physics, and this search has been the focus of intensive theoretical and experimental effort for three decades. Various inclusive and coincidence observables are predicted theoretically to be sensitive to saturation phenomena in hadronic proton-nucleus collisions and in UPCs with proton and nuclear beams at the LHC and at RHIC. However, QCD phenomena evolve only logarithmically in x and Q^2, and experimental observation and study of non-linear QCD evolution requires "logarithmically" broad coverage in $\left(x, Q^2\right)$, including large x and large Q^2 where saturation effects are expected to be small, in order to calibrate the probes.

For a calculational approach such as the Color-Glass Condensate (CGC) [5] to provide a universal description of the small-x structure of matter, it must self-consistently describe measurements of saturation-sensitive observables at small-x and low Q^2 in multiple collision systems. The most compelling program to explore non-linear QCD evolution at small-x is therefore **multi-messenger,** combining measurements from forward pA collisions at RHIC and LHC with those from Deep Inelastic Scattering (DIS) and diffractive interactions in eA collisions at EIC, in order to cover a broad range in $\left(x, Q^2\right)$ with multiple observables which probe saturation in a way that is rigorously interpretable theoretically. This program will provide a wide-ranging set of universality tests of linear vs. non-linear QCD: is saturation required by such data, and does it provide a unified and coherent description of the full suite of observables; i.e. is it therefore a universal description of hadronic matter at small-x?

Forward pA measurements enabled by FoCal provide key elements of this program, because of its unique coverage at very small x. We stress the importance of the theoretical interpretability of such measurements, which requires that factorization is respected for the corresponding observable. In this note we present several FoCal observables for which that is currently the case: isolated direct photons and their correlations, inclusive hadron and inclusive jet production, and dijet observables sensitive to the Transverse Momentum Dependent (TMD) gluon distribution [6].

At the LHC, forward measurements which probe saturation are also being carried out by the LHCb Collaboration. The LHCb detector [7, 8] is a single-arm spectrometer with tracking, particle identification, and calorimetry, with forward acceptance $2 < \eta < 5$. LHCb will carry out several important measurements in the small-x region in Run 3 and 4, notably that of the Drell-Yan (DY) cross section for dimuon masses above 5 GeV/c which probe the sea-quark distribution, as well as high-precision measurements of open charm and bottom meson production [9].

The study of QCD matter at extreme gluon density is also one of the primary goals of the Electron-Ion Collider (EIC). As discussed in the following, the FoCal and the EIC saturation physics programs are complementary, together providing incisive probes of saturation physics over wide kinematic range.

We also discuss the comparison of this broad range of measurements from different experiments and collision systems with linear and non-linear QCD calculations. The natural framework for such a com-

parison is Bayesian Inference, which is in growing usage in the Nuclear Physics community [10–12]. However, its application to the study of saturation requires development. The calculation of NLO corrections for inclusive and coincidence observables in pA collisions at the LHC is likewise an active area in the theory community [13, 14]. Development in both areas will be required to fully exploit FoCal measurements for this scientific program.

FoCal measurements would also have significant impact on Quark-Gluon Plasma (QGP) studies. Calculations of heavy-ion collisions may include gluon saturation effects to model the initial state, based on the notion of a weak-coupling phase prior to QGP formation. The duration of such a phase has direct impact on the extraction of various QGP properties from data, for instance quantitative constraints on specific shear viscosity. These in turn have consequences on our understanding of the nature and evolution of high temperature strongly interacting matter that the universe consisted of just after the Big Bang.

In addition to the study of saturation at small-x, the FoCal scientific program includes the following key components:

Long range correlations and thermalization effects: Azimuthal correlations that are long range in η, the so-called "ridge", have been observed in pp and p–Pb collisions [15]. Correlation measurements between neutral mesons or photons in FoCal with particles measured in the central ALICE detector or forward muon system (MFT), constitute an unexplored large range in pseudorapidity separation (up to $|\Delta\eta| \sim 9$). In particular, such studies promise to disentangle initial state contributions, and isolate the role of the initial state spatial anisotropies. This will enable unique constraints on saturation based models that attempt to describe such spatial anisotropies. The long range correlations will also provide key information on the novel final state mechanisms contributing to the momentum anisotropy. These have been postulated to arise from local thermalization effects, which lend themselves to a hydrodynamic description. A number of unique measurements are proposed to test these effects.

Jet quenching at forward rapidity: One of the hallmark observations in heavy-ion collisions is the modification of hadron and jet production due to the interaction of energetic partons in the QGP [16]. FoCal will provide measurements of high-p_{T} neutral meson, photon and jet production at larger rapidity than in present measurements, allowing us to map the QGP density as a function of rapidity and explore the effect of longitudinal flow on jet quenching effects. Since the fraction of quark-initiated jets is larger than at midrapidity, these measurements also explore the difference between energy loss for quark and gluon jets.

2 Partonic kinematics in current data and planned experiments

2.1 Kinematics overview

Figure 1 shows an overview of the x and Q coverage for measurements of various current and planned experiments which probe hadronic structure. The left figure shows EM probes (i.e. direct photon and Drell-Yan measurements) from hadronic collisions at LHC, with the coverage of direct photon measurements by FoCal and Drell-Yan measurements by LHCb highlighted in red and blue, respectively. The right figure shows the coverage of hadronic and UPC measurements at RHIC and LHC. LHCb coverage for measurements of e.g. light hadrons and open charm and bottom are marked in blue, while those for which FoCal has acceptance for e.g. neutral mesons and jets at small x are marked in red. Not shown is the coverage of LS3 upgrades of ATLAS and CMS, which include new tracking systems covering $|\eta| < 4$. CMS will also have partial PID coverage and the forward HGCAL in $|\eta| < 3$.

Hadronic collision systems, such as pp and pA interactions, do not provide direct access to $\left(x, Q^2\right)$ of the interaction. For hadronic collision systems in this figure, the momentum fraction x probed via partons emitted with transverse momentum p_{T} at rapidity y in collisions with a centre-of-mass energy $\sqrt{s}$ is approximated at Leading Order (LO, i.e. $2 \to 2$ processes) as

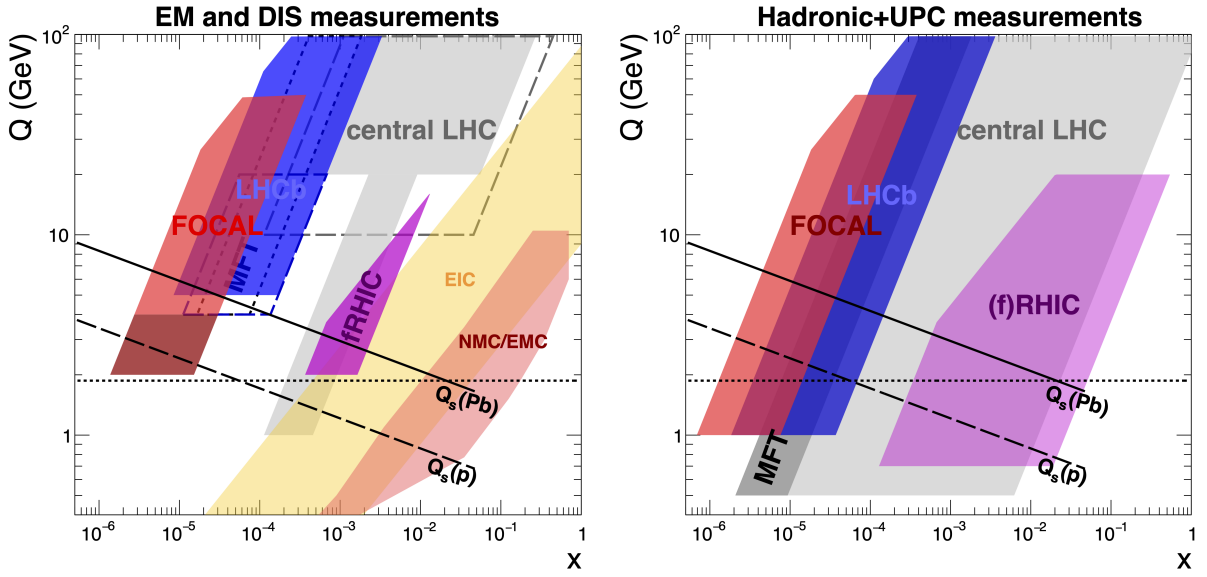

Fig. 1: Partonic kinematics in terms of momentum-fraction x and momentum-transfer Q calculated for various measurement channels within the experimental acceptance of current data and planned experiments which probe hadronic structure. Left panel: EM probes (i.e. direct photon and Drell-Yan measurements) from hadronic collisions, and DIS measurements including the future EIC project; right panel: hadronic and UPC measurements at RHIC and LHC. The estimated saturation scales for proton and Pb are also indicated as discussed in the text. The horizontal dashed line indicates the kinematic cuts above which data are usually included in the determination of PDFs. At HERA, and hence possibly at EIC, pQCD fits worked down to even $Q \approx 0.8$ GeV. Possible measurements with the CMS HGCAL are denoted with dashed gray line, indicating that it is not clear if EM measurements related to saturation such as the measurement of direct photons can be done with HGCAL which is optimized for high-energy jets or photons from Higgs decays. The same notation has been used to indicate the possible direct photon performance for LHCb and Drell-Yan capabilities for the MFT.

$$x_{1,2} \approx \frac{2p_{\mathrm{T}}\exp(\pm y)}{\sqrt{s}}, \tag{1}$$

where x typically denotes the negative-rapidity case x_2. In this approximation, measurements at large y and low p_{T} for a given $\sqrt{s}$ are most sensitive to the smallest values of x . Eq. 1 neglects non-perturbative fragmentation effects, which are relevant in particular for hadronic observables. For pA collisions at the LHC, $\sqrt{s_{\mathrm{NN}}} = 8.8$ TeV [2], while for RHIC we use $\sqrt{s_{\mathrm{NN}}} = 0.2$ TeV.

The left figure also shows the coverage for regions probed by nuclear DIS measurements [17–20], including the EIC [2], as well as direct photon and Drell-Yan measurements by the RHIC cold nuclear upgrade program [21], for which STAR has constructed forward detectors covering $2.5 < \eta < 4$ [22]. [3]

Figure 1 shows that FoCal and LHCb measurements reach much smaller x than other existing and planned measurements, with FoCal able to reach to the smallest x measurable prior to the far-future LHeC [23] and FCC [24]. Both LHCb and FoCal photon measurements are planned which extend to even lower p_{T} and lower Q. The corresponding regions for these challenging measurements are shown in the left panel of Fig. 1 as dark (FoCal) and open (LHCb) trapezoids. For FoCal, the main challenges at very low p_{T} are the large background of decay photons and the increasing contribution from fragmentation

[2] For pp collisions at 14 TeV, FoCal could probe to even smaller $x \sim 5 \times 10^{-7}$.

[3] The performance of the ALICE muon arm to measure DY has not been explored. Hence, the corresponding acceptance ($2.5 < \eta < 4$) (labelled as MFT) is only shown with a dashed line.

photons. For LHCb, a technique is being developed to reconstruct direct photons which convert to an electron-positron pair in the detector material in the tracker [25,26]; however, this approach suffers from small reconstruction efficiency and consequently relatively large uncertainty. More information about the comparison between FoCal and LHCb photon performances is provided in Ref. [1].

At a given value of x, the saturation scale is given by

$$Q_{\rm sat}^2 \approx \frac{x g_{\rm A}(x,Q^2)}{\pi R_{\rm A}^2} \propto A^{1/3} x^{-\lambda}\,, \tag{2}$$

where $g_{\rm A} = A\,g$, g is the gluon PDF of a proton, $R_{\rm A}$ the radius of the nucleus, A the nuclear mass number and the exponent $\lambda \approx 0.3$ [27,28]. Qualitatively, $Q_{\rm sat}$ increases with the gluon density, i.e. at smaller x and for heavier nuclei (by up to factor 6 in case of Pb). For perturbative calculations to work well in the saturated regime, the saturation scale should be an order of magnitude larger than the QCD scale $\Lambda_{\rm QCD} \approx 0.2$ GeV/c.

Fig. 1 shows the value of $Q_{\rm sat}$ determined from Eq. 2, with normalization obtained by setting its value to 1.7 GeV/c for $A = 1$ at $x = 10^{-4}$ [29]. At high parton density or small x, non-linear QCD evolution is expected to play a role near the saturation scale. A smooth, not abrupt, transition is expected from the linear to the non-linear region as a function of x, and the absolute magnitude of $Q_{\rm s}$ is theoretically not well established.

FoCal and EIC will probe the structure of protons and nuclei at small x in a complementary manner. It is the combination of EIC and FoCal measurements, together with other forward measurements at RHIC and the LHC, which provide the widest lever arm in $\left(x, Q^2\right)$ space and broadest range of observables to explore the non-linear description of QCD evolution and saturation phenomena, and test its universality.

2.2 Inclusive and coincidence production at the LHC: comparison of channels

While Fig. 1 shows phase-space acceptance, which is the starting point for comparing the capabilities of different experiments and facilities, it does not indicate the quality of measurements in terms of statistical or systematic precision, or their theoretical interpretability. In this section we present more detailed comparison of the partonic kinematics coverage for several inclusive production channels at the LHC (photons, D-meson, π^0), and photon-jet coincidences (see Sec. 5.1 for discussion of photon production in terms of direct, fragmentation, and prompt processes, and the experimental technique of isolation). The calculations utilize the PYTHIA event generator [30] (partonic processes at Leading-Order plus Leading Log to all orders; hadronization via the Lund string model; multiple-parton interactions; underlying event), and JETPHOX [31] for calculating the inclusive photon cross section at NLO.

Figure 2 compares the x_2 distribution from this calculation for prompt photons in two rapidity intervals within the FoCal acceptance, together with that for D^0-mesons within the LHCb acceptance in published data [32]. The left panel demonstrates that prompt photon production probes a lower range in Bjorken-x with narrower distributions than D-meson production, where the fragmentation process introduces additional momentum spread. The right panel shows the median and the 90% interval of the gluon-x (x_2) distribution as a function of the transverse momentum of the produced particle. At lower $p_{\rm T}$, smaller x is probed, as expected. For D-mesons at very low $p_{\rm T}$ there is an increase in median x, due to the finite mass of the D-meson and possibly to multiple parton interactions. While calculation of the effect of multiple-parton interactions is model-dependent, the study does make it clear that the theory description is expected to break down at low $p_{\rm T}$.

A more accurate exploration of the Bjorken-x sensitivity of direct photon and D meson production at forward rapidity at the LHC, using NLO pQCD calculations with JETPHOX, has been reported in [31, 33]. The main result is reproduced in Fig. 3, which shows that the gluon-x (x_2) distribution for direct

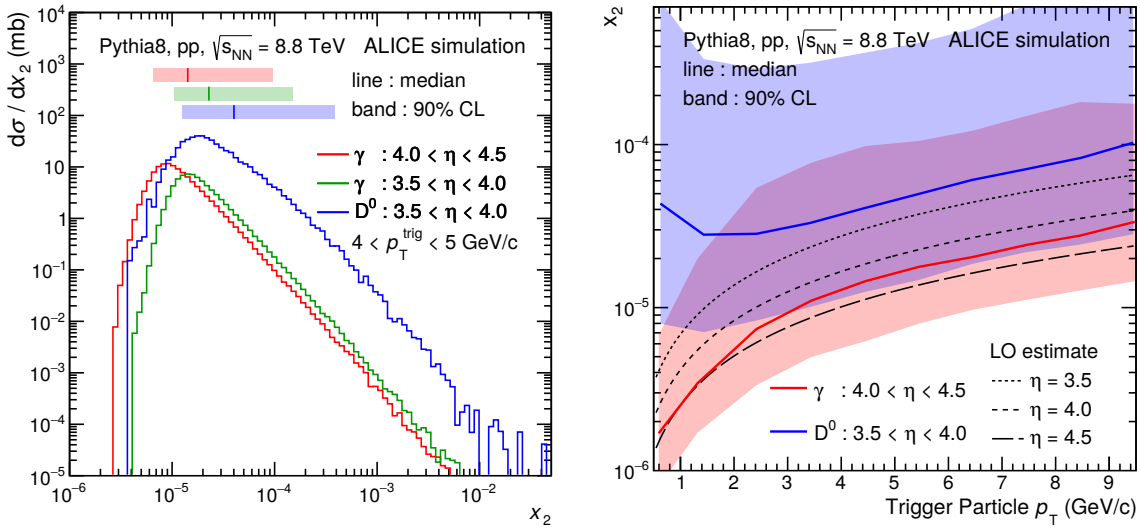

Fig. 2: (Left) Distribution of the momentum fraction of the gluons (x_2) contributing to production of D mesons and prompt photons in the PYTHIA event generator (v8.235) for $4 < p_T < 5$ GeV/c. The bars above the distribution indicate the median and the interval that contains 90% of the distribution. (Right) Median and 90% spread of the gluon-x (x_2) distribution as a function of p_T. Figures from [1].

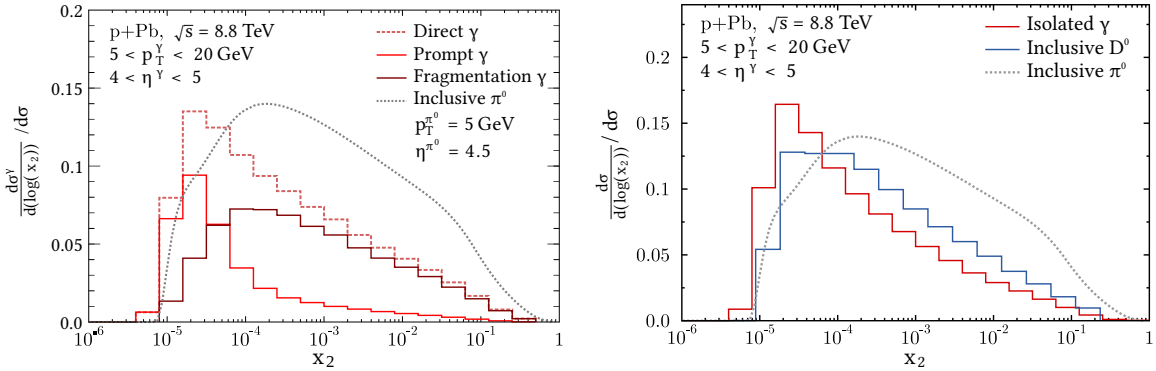

Fig. 3: (Left) Distribution of gluon-x (x_2) probed by direct photon production at forward rapidity in p–Pb collisions at 8.8 TeV as calculated in JETPHOX using EPS09 structure functions [31]. The different components of direct photon production are shown separately. For comparison, the x_2 distribution for pion production with similar kinematics is also shown. (Right) Comparison of gluon-x (x_2) distribution for isolated γ, pion and D-meson production from NLO pQCD calculations [31, 33].

photons is indeed peaked at small values, as expected. Comparison of the contribution of prompt and fragmentation photons reveals that both components have sensitivity to small x; however, fragmentation photons show a strong tail towards larger x.

The distribution corresponding to neutral pion production shows a similar (or only slightly weaker) sensitivity to the small x-region than fragmentation photons. The sensitivity of the photon measurement to small x improves significantly when fragmentation processes are suppressed by isolation cuts, as discussed in Sec. 5.1. Compared to isolated photons, D mesons probe slightly larger x, with also a broader distribution, due to fragmentation effects. For the case of constant suppression of gluons in nuclei compared to protons, D-meson and isolated-photon production measurements are equally sensitive to the gluon distribution, while for the case of suppression appearing only at small x, the isolated photon measurement would be significantly more sensitive due to its lower reach in x. Under all scenarios, the strongest physics program is one in which both D-mesons and isolated photons probe small-x, with significantly different experimental and theoretical systematic uncertainties.

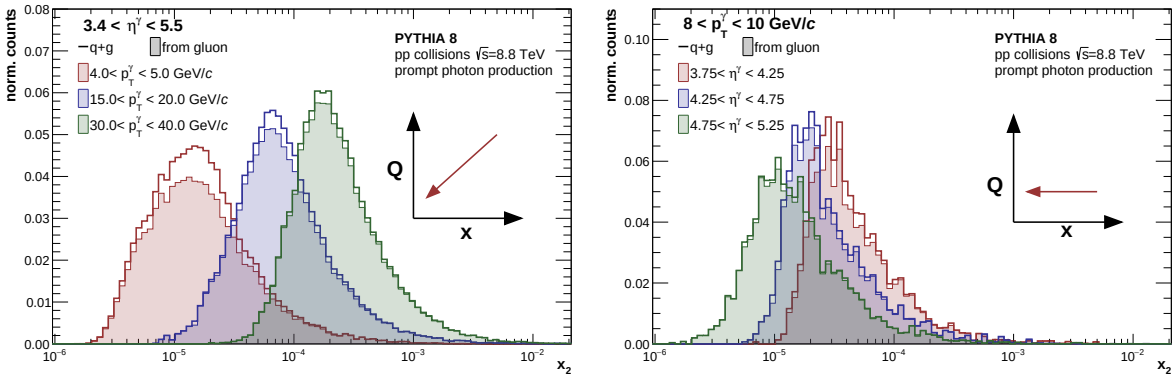

Fig. 4: Prompt photons in FoCal: effect of kinematic cuts on x_2 distribution, calculated by PYTHIA using the simulation of qg$\rightarrow \gamma$q processes in pp collisions at 8.8 TeV. Left panel: x_2 distributions for selected intervals in $p_{\mathrm{T}\gamma}$ for the full acceptance in η_γ. Right panel: x_2 distributions for selected intervals in η_γ for $8 < p_{\mathrm{T}\gamma} < 10$ GeV/c. Unfilled histograms are for all processes, while the filled histograms are for processes where x_2 corresponds to a gluon.

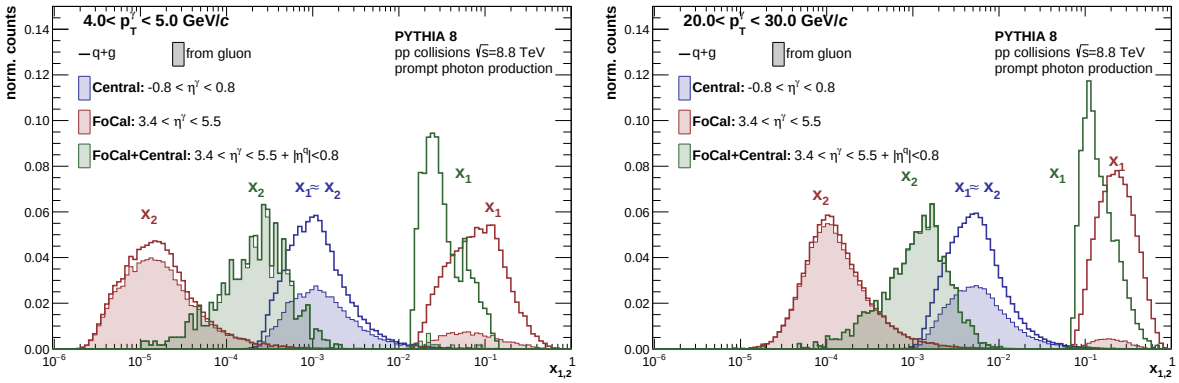

Fig. 5: Bjorken x_1 and x_2 of quarks and gluons probed by prompt photons measured only with FoCal (red), with FoCal combined with the existing central tracking and calorimeter systems of ALICE (green) or only the latter (blue) for $4 < p_{\mathrm{T}}{}^{\gamma} < 5$ GeV/c (left panel) and $20 < p_{\mathrm{T}}{}^{\gamma} < 30$ GeV/c (right panel). The curves are obtained using the simulation of signal qg$\rightarrow \gamma$q processes in pp collisions at 8.8 TeV with PYTHIA. Unfilled histograms are for all processes, while the filled histograms are for processes where x_2 corresponds to a gluon.

Figure 4 shows dependence of the x_2 distribution on the photon kinematics within the FoCal acceptance. It is evident that, purely within the FoCal acceptance, significant variation in the x_2 distribution can be achieved by selecting the photon kinematics. Comparison of the open and filled histograms confirms that small values of x_2 probe almost entirely gluons.

In addition, the combined information provided by FoCal and the central tracking and calorimeter systems of ALICE can be used to significantly enhance the kinematic coverage as shown in Fig. 5. The figure shows both the x_1 (high rapidity) and x_2 (low rapidity) distributions for $4 < p_{\mathrm{T}\gamma} < 5$ GeV/c (left panel) and $20 < p_{\mathrm{T}\gamma} < 30$ GeV/c (right panel). Combining measurements in FoCal with those from the ALICE central detector probes the full phase space of x_2. The coincidence measurement of a photon measured within FoCal with the measurement of a (quark) jet at midrapidity probes intermediate x_2, between the forward–forward and midrapdity–midrapidity measurements provided either by FoCal or the central ALICE detectors alone.

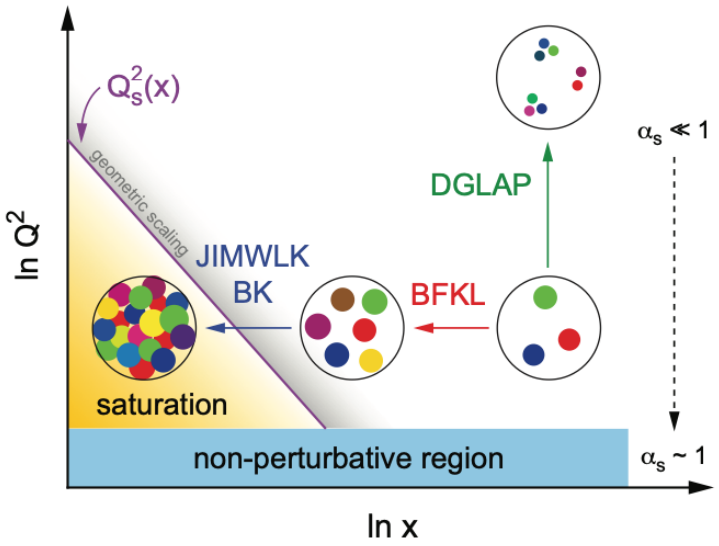

Fig. 6: Map of QCD evolution as a function of (Q,x). The evolution towards large Q^2 can be described by DGLAP, and that towards small (but not too small) x by BFKL. At very small x, where the gluon density is very high, non-linear effects become significant and other evolution equations (BK or JIMWLK) are required.

3 Partonic structure at small-x and saturation: theory

A map of QCD evolution is shown in Fig. 6. The DGLAP evolution equations [34–36] are valid at moderate to large Q^2 and moderate to large x, where the parton densities are not large. For intermediate values of Q^2 but small values of x, the BFKL equations [37], which use k_T factorization, describe the evolution.

One of the key features of evolution in this regime is that the gluon density increases as x is reduced. [4] This is because the DGLAP and BFKL evolution equations are linear, only incorporating parton splitting processes, so that parton densities only increase towards small x and large Q^2. However, at small enough x, the presence of abundant soft gluons arising from gluon splitting leads to high parton densities, so that parton recombination, in particular gluon fusion due to gluon self-interaction, becomes significant. QCD evolution in this regime is therefore non-linear, and is described by the JIMWLK [38] or BK equation [39, 40]. This non-linearity limits the growth of gluon density, with gluon generation and annihilation processes in equilibrium at the dynamically-generated gluon saturation scale $Q_{\rm sat}$.

In order to eludicate the general features of gluon saturation we use the Color-Glass Condensate (CGC) framework, which is the most common theoretical approach for describing the dynamics of gluon-saturated matter. In the following we summarize key elements of CGC theory, and point out the deep connection between observables in DIS and pA via the dipole scattering amplitude. This discussion follows Ref. [5], and we refer the reader there for further details and citations to specific concepts and results.

The CGC is an effective field theory where the separation of scales follows from the observation that, because of time dilation at high energy, the random distribution of color sources ρ at large-x evolves much more slowly than the natural time scale of the strong interaction, and can therefore be regarded effectively as frozen during the interaction. This distribution serves as the source of the dynamical gauge fields A^μ at small-x. The dynamics of the CGC are governed by the JIMWLK evolution equation which describes how $W[\rho]$, the statistical distribution of large-x source density ρ, evolves towards small-x. Saturation in the CGC is characterized by an emergent scale $Q_{\rm sat}$, at which the gluon occupation number

[4] The sea-quark contribution also rises strongly, due to gluon splitting. However, since gluons are the dominant degrees of freedom at small x, one usually discusses these small-x phenomena in terms of gluon distributions only.

at small-x becomes $\mathcal{O}(1/\alpha_S)$.

The CGC framework enables the calculation of n-point gluon correlation functions and their evolution with x order-by-order in perturbation theory, given a non-perturbative distribution of sources at an initial scale x_0. In the CGC approach the $W[\rho]$ distribution is **universal**; the same distribution appears in calculations of inclusive quantities in eA and pA collisions, and in UPC photoproduction.

In lepton-induced DIS the virtual photon fluctuates into a $q\bar{q}$ pair, which then interacts with the proton or nuclear target. The inclusive DIS interaction cross section is then

$$\sigma_{\gamma^* T} = \int_0^1 \mathrm{d}z \int \mathrm{d}^2\mathbf{r}_\perp |\psi^{\gamma^* \to q\bar{q}}(z, \mathbf{r}_\perp)|^2 \sigma_{\mathrm{dipole}}(x, \mathbf{r}_\perp), \tag{3}$$

where $\psi(z, \mathbf{r}_\perp)$ is the $q\bar{q}$ component of the virtual photon and $\sigma_{\mathrm{dipole}}(x, \mathbf{r}_\perp)$ is the cross section for $q\bar{q}$ scattering off the target. Applying the optical theorem, the dipole scattering cross section can be written in terms of the dipole forward scattering amplitude $\mathbf{T}(\mathbf{x}_\perp, \mathbf{y}_\perp)$. At LO,

$$\sigma^{\mathrm{LO}}_{\mathrm{dipole}}(x, \mathbf{r}_\perp) = 2 \int \mathrm{d}^2\mathbf{b}\, T_{\mathrm{LO}}(\mathbf{b} + \frac{\mathbf{r}_\perp}{2}, \mathbf{b} - \frac{\mathbf{r}_\perp}{2}). \tag{4}$$

Here, T_{LO} is written in terms of infinite fundamental Wilson lines on the light-cone $U(\mathbf{x}_\perp)$ encoding the interaction between the quark and the target color field as

$$T_{\mathrm{LO}} = 1 - \frac{1}{N_c} \langle \mathrm{tr}(U(\mathbf{x}_\perp) U^\dagger(\mathbf{y}_\perp)) \rangle, \tag{5}$$

where N_c is the number of colors. The average over the distribution of initial configurations is indicated by

$$\langle \ldots \rangle = \int [D\rho]\, W_{\Lambda_0^-}[\rho](\ldots), \tag{6}$$

where Λ_0^- indicates the longitudinal momentum scale which separates static color sources from dynamic color fields.

Turning now to pA collisions, in the dilute-dense hybrid factorization approach these are treated as the collisions of a dilute proton with a dense nucleus. Inclusive production is then described as the scattering of a parton from the proton off the target nucleus color field. The amplitude M_{LO} for this scattering is proportional to the Fourier transform of a Wilson line, and its square has the form

$$|M|^2_{\mathrm{LO}} \propto \int \mathrm{d}^2\mathbf{b}\, \mathrm{d}^2\mathbf{r}_\perp e^{i\mathbf{p}_\perp \cdot \mathbf{r}_\perp} T_{\mathrm{LO}}(\mathbf{b} + \frac{\mathbf{r}_\perp}{2}, \mathbf{b} - \frac{\mathbf{r}_\perp}{2}), \tag{7}$$

where T_{LO} is the same dipole scattering amplitude used to calculate the DIS interaction cross section. While the above expressions are specific to LO, this correspondence likewise holds at higher perturbative order. This correspondence is also general, and does not rely upon the specific implementation of the CGC. It establishes the deep theoretical connection between inclusive observables in lepton induced DIS and in pA collisions, and provides the basis for the tests of universality we propose by comparing selected FoCal and other pA measurements with those carried out at the EIC. This deep connection between pA collisions and the EIC has also recently been emphasized in the EIC Yellow Report, Sect. 7.5.4 [41].

More complex final states, containing correlations of pairs of photons, hadrons, and jets, can likewise be calculated based on the product of four Wilson lines which correspond to a quadrupole operator. In order to ensure that the process can be factorized into the universal distribution of sources $W[\rho]$, all such observables must be sufficiently "inclusive", in the sense of not imposing a restriction on the number of accompanying gluons in the interaction.

4 Search for non-linear QCD evolution: general considerations

The hallmark of gluon saturation is the non-linear evolution of gluon density at small x and low Q^2. A comprehensive experimental program to search for gluon saturation phenomena requires broad coverage in both x and Q^2, with measurements both at low $\left(x, Q^2\right)$ and at high x or Q^2, where saturation effects are expected to be negligible and the dynamics are expected to be well-described by linear QCD evolution.

Section 2 shows the FoCal acceptance in $\left(x, Q^2\right)$ for several measurement channels and compares it to that of published data and to current and other future experiments. While FoCal covers unique phase space at small $\left(x, Q^2\right)$, its scientific program to explore non-linear QCD evolution must also satisfy the following criteria:

- Observables that are sensitive to non-linear QCD evolution must be rigorously interpretable theoretically, so that precise, quantitative comparison of data and theory can be made. For hadronic collisions, this means that the theoretical description of such observables factorizes,i.e. their measurement is sensitive to the same QCD operator that can be probed in corresponding measurements in an eA DIS experiment in a different kinematic regime.
- Such observables must be measurable with good precision over a wide kinematic range, specifically high statistical precision and systematic accuracy over a broad range in $\left(x, Q^2\right)$ [5]. This includes the range in which saturation effects are predicted to be significant, and the range in which they are predicted to be negligible, to be able to turn off the effects.
- Observables should minimize sensitivity to poorly-controlled non-perturbative effects in theory calculations, especially modeling of hadronization.

The proposed FoCal measurements, combined with other pA measurements at LHC and RHIC, and with eA DIS measurements at EIC, comprise a wide-ranging set of universality tests of non-linear QCD evolution: does saturation provide a unified and coherent description of the full suite of observables, and is it therefore the universal description of the high gluon density regime?

Different observables are sensitive to different operators [42,43]. Inclusive observables and some coincidence channels can be calculated using the dipole operator, while other coincidence observables require inclusion of the quadrupole operator. This distinction has practical consequences for the FoCal scientific program, since quadrupole operator calculations at NLO are calculationally more complex than calculations dependent primarily on the dipole operator.

The establishment of factorization, which requires pQCD calculations beyond LO, is challenging; at present this has been done for a handful of FoCal observables, which we discuss in Sec. 5. Extending such calculations to observables dependent on the quadrupole operator, to enable full exploitation of FoCal capabilities, presents an additional theory challenge.

Sections 5 and 6 discuss specific FoCal observables sensitive to gluon saturation, based on current theoretical calculations and general considerations. In brief, observables that are expected to be clearly interpretable in terms of gluon saturation effects, with sensitivity to the dipole cross section, include the following:

- inclusive isolated photon production (has not yet been calculated at NLO but necessary theoretical tools are in place);
- isolated photon+jet (same as inclusive isolated photons);
- inclusive jets;

[5] Systematic uncertainty smaller than 10% is a suitable benchmark

– dijet photoproduction in UPCs;

– cross section ratios of J/ψ and $\psi(2S)$ production on ion vs. on proton targets in UPCs.

Observables which require additional developments include the following:

– γ-π^0 correlation: calculation of the partonic-level process only requires the dipole cross section, but the π^0 Fragmentation Function presents an additional uncertainty which is harder to control theoretically. This channel could be reclassified as "cleanly interpretable" if there is sufficient theoretical confidence in the π^0 FF at NLO.

– dijets and dihadrons: quadrupole evolution at NLO needs to be constructed and solved. This is doable in principle but is numerically complex - a dedicated theory effort is needed;

– the cross section ratio for exclusive production of J/ψ and $\psi(2S)$ in UPCs. The main uncertainty is the scale dependence at NLO.

New observables sensitive to saturation physics are currently still only at the conceptual level but show promise, for instance the measurement of energy-energy correlators [44, 45].

4.1 Quantitative comparison of data and theory

Quantitative testing of the universality of linear or non-linear QCD will require rigorous, unbiased comparison of complex measurements from different experiments and collider facilities.

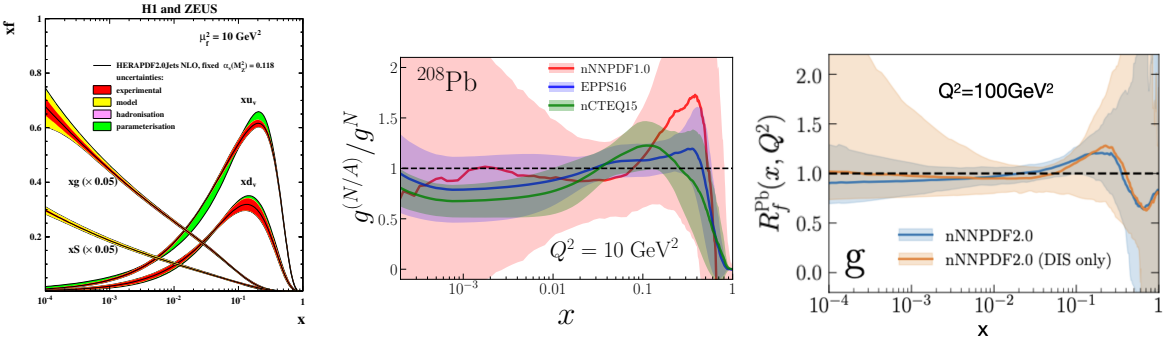

Fig. 7: Left: PDFs from HERAPDF2.0, which have been determined from charm data, jet data and low energy data as well as the HERA-I and II high energy inclusive data. Middle: Comparison of the nuclear modification between the nNNPDF1.0, EPPS16 and nCTEQ15 fits versus x at $Q^2 = 10$ GeV^2 for the gluon PDF in Pb. Data above $Q^2 = 3.5$ GeV^2 were included for nNNPDF, while for EPPS16 and nCTEQ15 data down to 1.7 GeV^2 (including light hadrons), as well as high Q^2 W, Z and dijet data were used. Right: Comparison of the nuclear modification of the gluon density between the nNNPDF2.0, based only on DIS data, and nNNPDF2.0 nuclear PDFs, which include electroweak boson production data from the LHC in the fit. In all cases, the nuclear PDFs have been normalized by the respective proton PDFs, and 90% confidence-level uncertainty bands are drawn. Figures are from [46–48]

A common approach for this purpose is global fitting to determine proton and nuclear Parton Distribution Functions (PDFs) based on collinear perturbative QCD, as shown in Fig. 7. The main experimental input for such global fits comes from DIS measurements in which a virtual photon, W or Z boson is exchanged. These measurements probe the quark density directly, with the gluon density derived indirectly from the Q^2-evolution of the measured cross sections. As shown in the left panel of Fig. 7, PDFs for protons are well-constrained by DIS measurements over a broad kinematic range, although the gluon distribution uncertainties become larger than 20% at small x and Q^2 (around 10^{-3} and 10 GeV^2, respectively) [49]. Data from hadronic collisions are also used in global PDF fits, in particular dilepton production from the Drell-Yan (DY) process and electroweak boson production (γ, Z, W). These final states are of special interest since they comprise elementary particles that are generated directly, without fragmentation and hadronisation processes which require phenomenological modeling for comparison to theory. When the

kinematic coverage of the available measurements is limited, parametrisations are used together with the DGLAP evolution equations [34–36] to interpolate the areas covered by measurements and to extrapolate into unconstrained regions of the (x, Q^2) phase space, and hence such data are not adding new constraints. Additional data at small x and low to moderate Q^2 may generate tension in such global fits, requiring the inclusion of non-linear evolution in x as described by the JIMWLK/BK equation [50] (see Sec. 3).

To illustrate the current state of knowledge of the gluon density in nuclei, the middle and right panels of Fig. 7 show the nuclear modification of the gluon distribution (quantified as the ratio of nuclear over proton PDF) and its uncertainty for different nuclear PDFs [41, 47, 51, 52]. The different parameterizations exhibit a large spread for small values of x, reflecting the lack of constraint due to the limited set of relevant measurements, in particular with nuclear targets. Since current DIS, photon production, and DY measurements with nuclear targets do not constrain nuclear PDFs at small x (below 10^{-2}), determination of the nPDFs in that region at present relies on extrapolation from large to small x and Q using linear evolution equations, and the resulting uncertainties may consequently be underestimated. Furthermore, analysis of nuclear PDFs requires a parametrisation of small-x behaviour which imposes a specific shape; for example, EPPS16 [52] uses a parametrisation for the nuclear modification which is constant at small x. Using such a parametrisation reduces the nominal uncertainties at small x, but does not reflect the fact that no experimental information is available.

At small x, the main measurements that are available are W, Z and dijet production, which however have large $Q \approx 90$ GeV, and thus do not provide strong constraints at small Q. The EPPS16 [52] and nCTEQ15 [51] fits include both these measurements and light-hadron production data measured at midrapidity at RHIC. The nNNPDF analysis [47], which relies purely on inclusive DIS measurements of neutral-current structure functions on nuclear targets and NNLO calculations, uses a broad set of parametrisations which explore a larger range of possible x-dependencies at $x > 10^{-2}$, resulting in significantly larger uncertainties at smaller x.

We note that nPDF global fits are a highly-integrated representation of a vast body of data based on collinear QCD, requiring the assumption of functional form for the PDFs, and typically assume Gaussian uncertainties using the Hessian approximation of experimental errors for global χ^2 minimization [53]. In addition, nPDF global fits require the specification of initial conditions that are sensitive to non-perturbative physics and must be extracted by fitting to data; this procedure can mask the difference between linear and non-linear evolution [54]. As such, global PDF fits may provide only limited tests of universality of linear vs. non-linear evolution, with limited discriminating power to resolve tensions between data sets and between data and theory.

An alternative approach to consider is that of Bayesian Inference, whose utilization in nuclear physics is growing rapidly [10–12, 55]. Bayesian Inference enables the incorporation of heterogeneous datasets, including the full experimental uncertainty covariance and theoretical uncertainties, and providing statistical tools to quantify the tension between posterior distributions of high-dimensional data. However, Bayesian Inference analyses can be computationally expensive, requiring Machine Learning approaches for efficient emulation and calculation of likelihoods. The application of Bayesian Inference to comprehensive universality tests of linear and non-linear QCD evolution still requires significant development.

5 Search for non-linear QCD evolution in hadronic collisions: specific channels

In the following we present a detailed discussion of selected FoCal observables, in terms both of theoretical interpretability and of statistical precision and kinematic reach.

Projection of statistical precision requires an assumption about the integrated luminosity that will be recorded during LHC Run 4 (2029–2032). Current estimates (spring 2023) for LHC Run 4 are as follows:

– pp at $\sqrt{s}$=8.8 TeV: 5 days[6], $\mathscr{L}$=3 pb^{-1};

– p–Pb at $\sqrt{s}$=8.8 TeV: 3 weeks, $\mathscr{L}$=300 nb^{-1};

– Pb–Pb at $\sqrt{s_{\rm NN}}$=5.02 TeV: 3 months; $\mathscr{L}$=7 nb^{-1};

– pp at $\sqrt{s}$=14 TeV: $\approx$ 18 months, $\mathscr{L}$=150 pb^{-1};

However, assumptions about integrated luminosity made far in advance are by their nature uncertain, since the LHC and FoCal instrumental capabilities, and the Run 4 run plan, will continue to develop. In addition, the projection of statistical precision itself need not be precise; the purpose of such projections is to provide only qualitative (or perhaps, semi-quantitative) guidance about the potential physics reach of the measurements. For the projections in this note we therefore utilize convenient "round number" estimates for the integrated luminosity at $\sqrt{s}$=8.8 TeV, which are easily scaled to current best estimates:

– pp at $\sqrt{s}$=8.8 TeV: $\mathscr{L}$=1 pb^{-1};

– p–Pb at $\sqrt{s}$=8.8 TeV: $\mathscr{L}$=100 nb^{-1};

5.1 Direct photon and π^0 production: theory

Direct photons refer to all photons not originating from decays [56]. Prompt photons are direct photons which are produced directly at the parton interaction vertex, and not from parton fragmentation. Prompt photon measurements provide access to the parton kinematics since they couple directly to the incoming quarks, and unlike hadrons are not affected by final state effects. The dominant prompt photon production process at the LHC is quark-gluon scattering (Compton process, Fig. 8a), with smaller contribution from quark-anti-quark annihilation (Fig. 8b). For processes at next-to-leading order (NLO) and higher order, direct photons are also generated by bremsstrahlung (Fig. 8c) and by parton fragmentation (Fig. 8d). Both processes involve the parton-to-photon fragmentation distribution , which is poorly known at present.

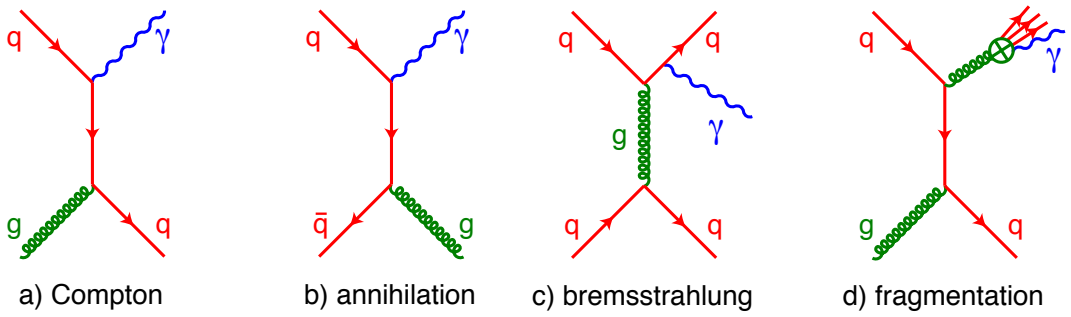

Fig. 8: Feynman diagrams for direct photon production. Prompt photons are directly produced at leading order by the a) quark-gluon Compton process, and b) quark-antiquark annihilation process. Fragmentation photons are produced at next-to-leading order from c) bremsstrahlung from a quark, and d) emission during the gluon fragmentation process.

At LHC energies, a large fraction of prompt photons are produced in the fragmentation process, complicating the relation between the kinematic variables of the measured photon and those of the incoming partons, and hence their PDFs [57]. However, bremsstrahlung and fragmentation photons are accompanied by hadronic fragmentation products, and the contribution of these processes can be largely suppressed by application of photon isolation selections, as illustrated in Fig. 9. The application of the isolation cut ensures that the dominant process is the quark-gluon Compton scattering process, where the measured photon is directly sensitive to the gluon PDF. For precise comparison with calculations these selection criteria are also applied in the calculations.

[6] A few more days for the pp reference run may be justifiable at a later stage.

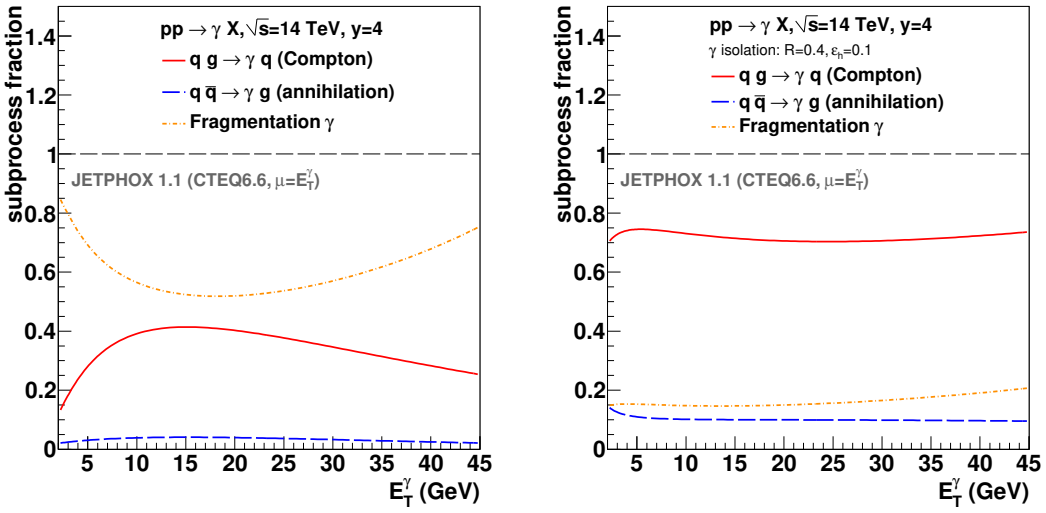

Fig. 9: Relative contributions without (left) and with (right) isolation of the qg-Compton, $q\bar{q}$ annihilation, and fragmentation subprocesses in NLO direct photon production in pp collisions at $\sqrt{s} = 14$ TeV at the LHC at forward rapidity obtained with JETPHOX. Figures are taken from [58].

Theoretical calculations using the dilute-dense hybrid factorization approach described in Sec. 3 have been carried out for forward inclusive hadron production [59–61] and photon production [62–68], together with their correlations. At the operator level, while inclusive production is sensitive primarily to the dipole operator for both light hadrons [59] and photons [62], photon-hadron correlations depend only on the dipole operator, whereas di-hadron correlations depend on the quadrupole operator [42, 43, 62, 68].

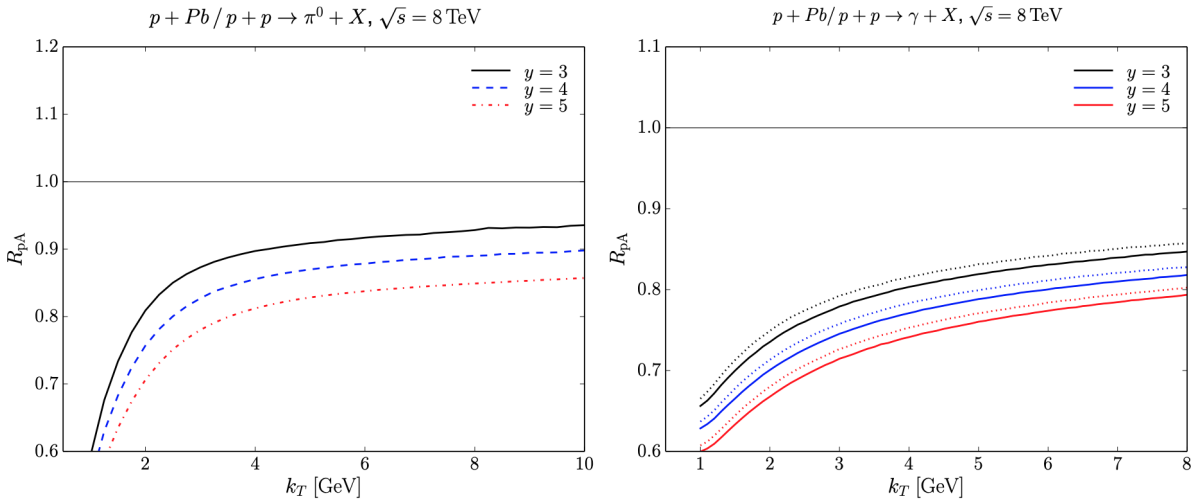

Fig. 10: Theoretical calculations for R_{pPb} of inclusive production at various values of forward rapidity using the dipole formalism, in pp and p–Pb collisions at $\sqrt{s_{\mathrm{NN}}}$=8 TeV [65]. The horizontal axis, which is labelled k_{T}, corresponds to the experimentally observable transverse momentum, p_{T}. Left panel: π^0. Right panel: isolated prompt photon. Solid lines correspond to isolation with R=0.4, dotted lines to isolation with R=0.1.

Forward inclusive hadron production in pA collisions has been calculated in the dipole framework at NLO [59], and at NLO with threshold resummation at Leading Log (LL) accuracy [60,61]. Factorization is proven in the dipole framework for forward inclusive photon production [64], which has also been calculated at NLO [66].

Nuclear effects on inclusive production are quantified by the nuclear modification factor R_{pPb}, which is

the ratio of cross sections calculated or measured in p–Pb collisions and pp collisions normalized by A (i.e. $A = 208$ for Pb).

While the theoretical framework for calculating inclusive photon and π^0 distributions in the dipole framework at NLO is in place, at present there are no predictions available at NLO for experimentally observable distributions. Figure 10 shows such a calculation at LO, using the dipole formalism to predict $R_{\rm pPb}$ for inclusive π^0 and isolated prompt photon production at forward rapidity in pp and p–Pb collisions at $\sqrt{s_{\rm NN}}$=8 TeV [65].

Isolation is commonly applied in prompt photon measurements to suppress the contribution of fragmentation processes, enhancing sensitivity to the Compton process which probes the gluon density directly. In the CGC framework, isolated photon distributions were likewise found to be more sensitive to gluon saturation effects [62]. However, Fig. 10 shows little sensitivity to the radius R of the isolation cone, though this feature should be revisited with an NLO calculation. The figure shows marked suppression due to saturation for both π^0 and photons at low $p_{\rm T}$ (labelled $k_{\rm T}$ in the figure), but with strikingly different $p_{\rm T}$-dependence. This difference arises [65] because π^0s are fragments of jets, with broad variation in the jet momentum fraction z carried by the π^0. The π^0 population observed at a given transverse momentum $p_{\rm T}$ therefore includes contributions from jets with large $k_{\rm T} > Q_{\rm sat}$ in the target, resulting in little nuclear modification. In contrast, the LO process to generate a photon is the Compton process, in which the photon $p_{\rm T}$ is largely balanced by an unobserved jet, and it is the momentum imbalance $k_{\rm T}$ which should be compared to $Q_{\rm sat}$. The authors caution, however, that this simple picture may be modified substantially when NLO effects are taken into account.

The calculations in Fig. 10 provide a valuable step towards quantitative prediction of FoCal measurements. They illustrate what can be learned by measuring and comparing inclusive production of both π^0 and prompt photons over a broad range in $p_{\rm T}$, including very low $p_{\rm T}$, to test and constrain the theoretical formalism.

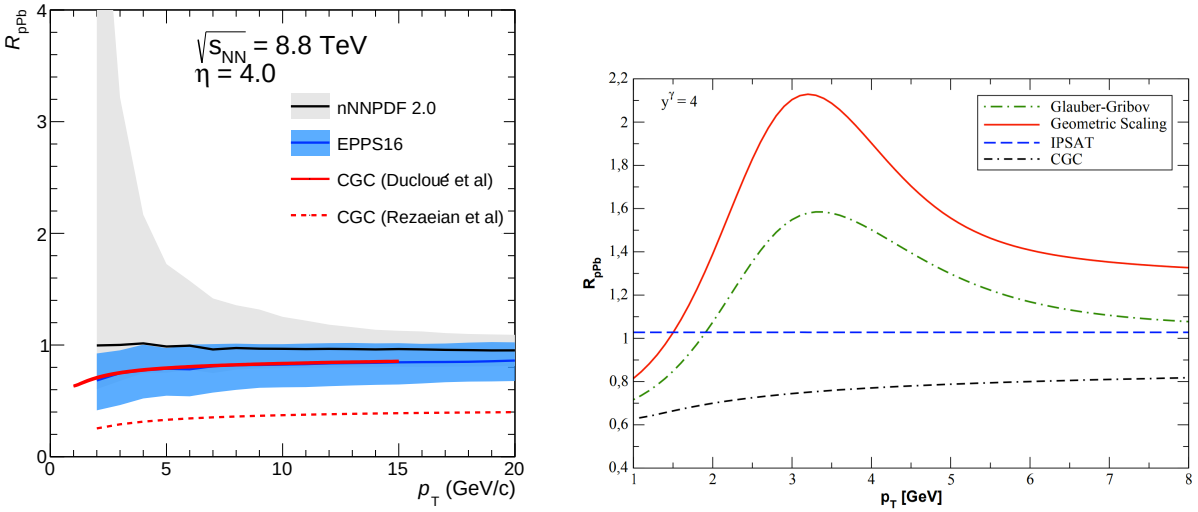

Fig. 11: Left: Nuclear modification factor and uncertainties for isolated photons at $\eta = 4$ for $\sqrt{s_{\rm NN}} = 8.8$ TeV calculated using EPPS16 [52] and nNNPDF2.0 [48] nuclear PDFs, compared to two CGC calculations [65, 69]. Only the PDF uncertainties are shown. Right: Nuclear modification factor $R_{\rm pA}$ for prompt photon production at $\sqrt{s_{\rm NN}} = 8$ TeV shown for various models using the color dipole approach [70] compared to the CGC [65] calculation.

Additional predictions for $R_{\rm pPb}$ of isolated photons at $\eta = 4$ and its uncertainties are shown in Fig. 11. The left panel shows calculations using the EPPS16 and nNNPDF2.0 nuclear PDFs in the collinear pQCD

framework. The central values differ by about 10–15% between the calculations but the uncertainties, which originate from uncertainties in the nuclear PDFs, are much larger than that difference. Note in particular nNNPDF2.0, which by design is not constrained by hadron data.

Two calculations of photon production in the CGC framework are shown for comparison. The more recent LO calculation [65], discussed above, predicts only moderate suppression below unity, while the earlier calculation by a different group [69, 71] shows strong suppression, $R_{\mathrm{pPb}} \approx 0.4$. The right panel demonstrates significant variation in the results of calculations incorporating non-linear QCD evolution in the color dipole approach [70] and the LO CGC calculation [65] at low momentum.

5.2 Direct photon and π^0 production: experiment

The key measurement proposed for FoCal is that of the isolated photon inclusive p_{T} spectra at forward rapidity in pp and p–Pb collisions at 8.8 TeV in Run 4 at the LHC.

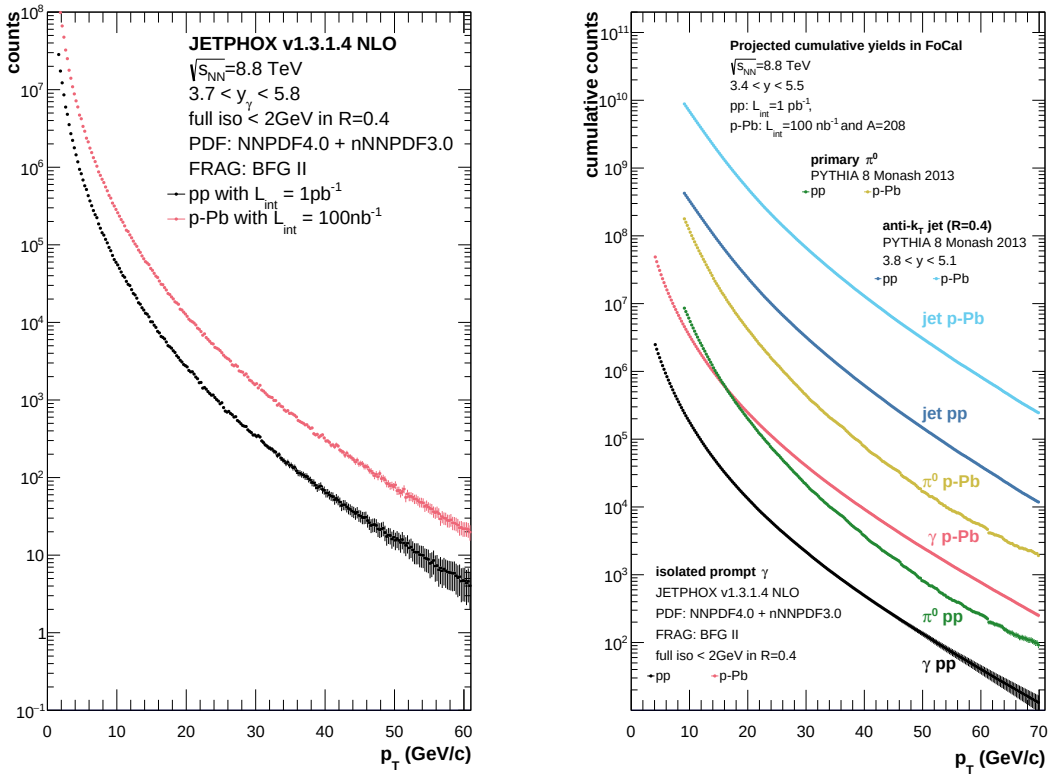

Fig. 12: Projected counts in the FoCal acceptance of inclusive isolated prompt photon, π^0 and jet production measured in pp and p–Pb collisions at $\sqrt{s_{\mathrm{NN}}} = 8.8$ TeV for integrated luminosities of 1 pb^{-1} and 100 nb^{-1} in pp and p–Pb collisions, respectively. The prompt production cross section is obtained at NLO using JETPHOX [72] and recent (n)PDFs, while the π^0 and jet yields are calculated using PYTHIA 8 Monash tune. Left: differential yield vs p_{T} for prompt photons. Right: cumulative counts above a p_{T} threshold for prompt photons, π^0, and jets.

Figure 12 shows projections of the statistics achievable in FoCal measurements of inclusive isolated photon, π^0 and jet production in pp and p–Pb collisions at $\sqrt{s_{\mathrm{NN}}} = 8.8$ TeV during LHC Run 4. For the photon measurements, statistical precision better that 10% will be achieved up to ~ 50 GeV in pp collisions and beyond 70 GeV in p–Pb collisions. The kinematic range of FoCal photon measurements therefore includes both the region in which saturation effects may be evident, at low p_{T}, and the region where saturation effects are expected to be negigible, at $p_{\mathrm{T}} \sim$ few 10s of GeV. The kinematic reach of FoCal measurements of inclusive π^0 and jets span even wider ranges. The figure also shows that observables relying on comparison between pp and p–Pb collisions at the same collision energy will be limited in their statistical precision by the pp reference data.

Fig. 13 shows a published measurement of the nuclear modification factor for isolated photons at high

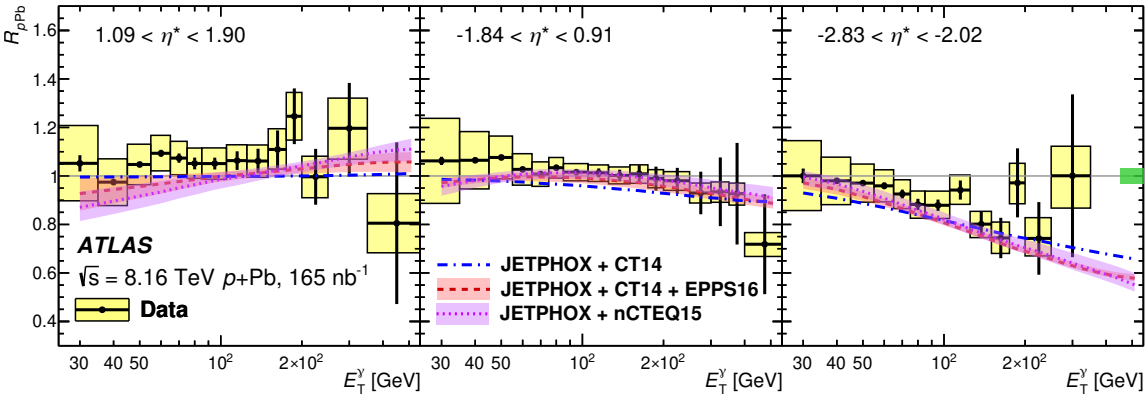

Fig. 13: Isolated photon R_{pPb} versus p_{T} for different intervals of centre-of-mass pseudorapidity measured by ATLAS [73], compared to calculations from JetPhox with various (n)PDFs. Positive values of η^* correspond to forward and negative to backward rapidity.

p_{T} [73], which does not exhibit significant suppression at forward rapidity. FoCal will extend these measurements an order of magnitude lower in p_{T} and to much larger rapidity. ALICE will likewise carry out low-p_{T} direct photon measurements at midrapidity, as done in [74]. These central and forward measurements in the same experiment will probe a broad range in $\left(x, Q^2\right)$ by photons (Fig. 5). We expect that these data will play a central role in the search for non-linear evolution effects.

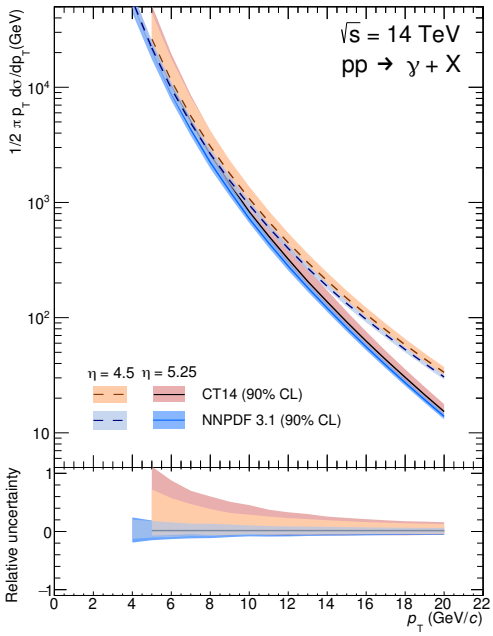

Fig. 14: Isolated photon spectra in pp collision at 14 TeV for $\eta = 4.5$ and $\eta = 5.25$ with the CT14 [49] (red lines and bands) and NNPDF3.1 [75] proton PDF (blue lines and bands). The bands shows the effect of the uncertainties on the PDFs on the calculated cross section, ignoring fragmentation scale uncertainties. The lower panels shows the relative uncertainties on a linear scale.

Figure 14 shows the p_{T}-differential cross section of inclusive prompt photons in the FoCal acceptance for pp collisions at $\sqrt{s}$=14 TeV, calculated at NLO using INCNLO [76] with two different choices of PDF. The uncertainty bands have magnitude 20–50%. If smaller systematic uncertainty can be achieved in this FoCal measurement, it will provide significant new constraints on the proton PDF. Furthermore, at low p_{T} this measurement probes $x \sim 5 \times 10^{-7}$; saturation effects may be observable even in the proton at such small x, for instance in the ratio of direct photon and pion spectra at $y = 5$ [77, 78].

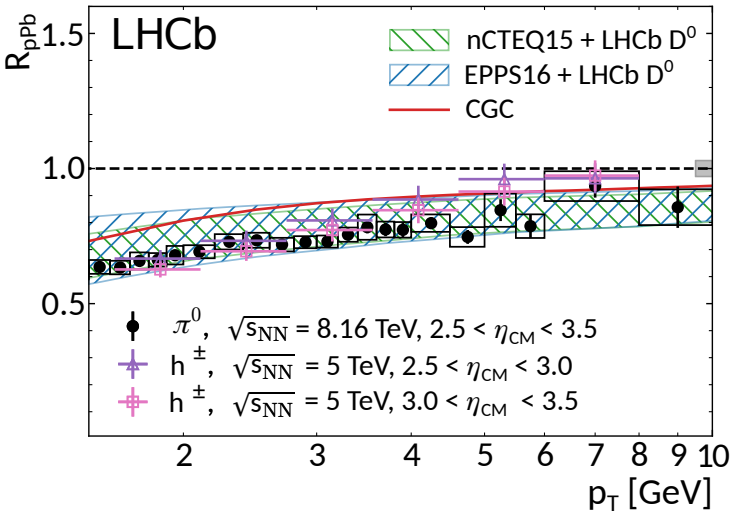

Fig. 15: Measurement of the π^0 nuclear modification factor at forward rapidity ($2.5 < \eta < 3.5$) by LHCb [79]. Error bars show the statistical uncertainty, while the open boxes show the systematic uncertainties. The solid gray boxes show the overall normalization uncertainties from the luminosity estimate and efficiency correction factors. The results are compared to pQCD calculations using nuclear PDFs [31, 80] and a CGC calculation [81].

Figure 15 shows a recent measurement by the LHCb Collaboration of $R_{\rm pPb}$ of π^0 in p–Pb collisions at 8.16 TeV, in the acceptance $2.5 < \eta_{\rm CM} < 3.5$ [79]. Also shown are calculations based on linear QCD evolution with nuclear shadowing, and on non-linear evolution in the CGC framework at LO. While the CGC calculation is somewhat disfavored in the comparison, the calculation is at LO, and the acceptance may not be sufficiently forward to probe the deep saturation region. FoCal data will extend this measurement to significantly larger rapidity.

In pp and p–Pb collisions, FoCal measurements of $\mathrm{Z} \to e^+e^-$ and $\mathrm{W} \to e$ [83] may be possible, providing additional constraints to nuclear PDFs at high Q^2.

5.3 Photon and hadron-triggered correlations

Photon and hadron-triggered correlations in the forward region of pA collisions also probe small-x gluon dynamics, but with different sensitivity than inclusive yields. In the dilute-dense picture, a large-x parton from the proton scatters off the coherent small-x gluon field in the nucleus, which results in both yield suppression and angular decorrelation. While measurement of correlated yield suppression probes gluon density, similar to measurements of inclusive production, measurement of angular decorrelation is in addition sensitive to the coherence of the gluonic wavefunction.

The choice of a hadron trigger and a hadron, rather than the jet, as the recoil object has advantages for probing low $k_{\rm T} \sim Q_{\rm sat}$, though the calculation of hadrons in the final state requires the use of Fragmentation Functions, which have additional theoretical uncertainties relative to calculations of photon or jet correlations. It is clear, however, that a comprehensive experimental program must exploit all such correlations. We discuss γ+hadron and hadron+hadron correlations here; γ+jet and dijet correlations are discussed in Sec. 5.4.

Figure 16 shows a recent STAR measurement of $\pi^0 + \pi^0$ correlations in the forward region in pp, p–Al, and p–Au collisions at $\sqrt{s_{\rm NN}}$=200 GeV [82]. The two panels show different selections in trigger and associated particle $p_{\rm T}$. A marked yield suppression is observed for nuclear targets, with larger suppression for larger target mass A, qualitatively consistent with expectations from the CGC picture. However, no A-dependent broadening is observed, consistent with a previous measurement by PHENIX at RHIC [84], but in contrast to general expectations from the CGC picture.

Figure 17 shows a theoretical calculation of forward di-hadron azimuthal correlations at RHIC, compared

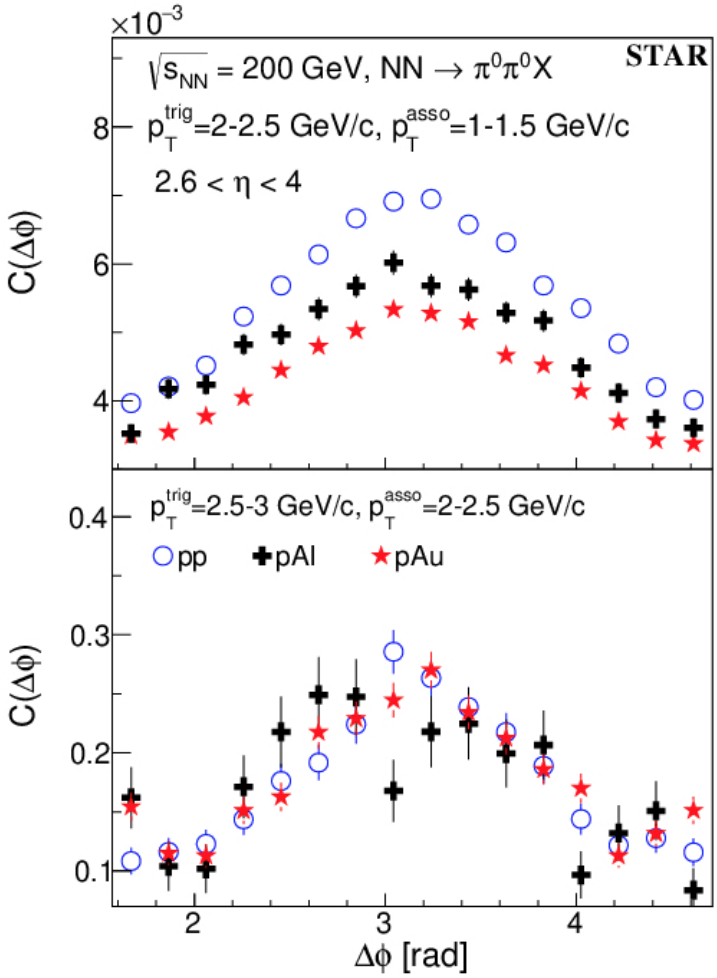

Fig. 16: Azimuthal angular separation of π^0-π^0 pairs at forward rapidity ($2.6 < \eta < 4.0$) in pp, p–Al and p–Au collisions at $\sqrt{s_{\rm NN}}$=200 GeV, for two different intervals in trigger and associated $p_{\rm T}$, measured by the STAR Collaboration at RHIC [82].

to preliminary STAR data similar to those in Fig. 16 [85]. The calculation incorporates the dilute-dense CGC framework augmented by Sudakov radiation, and interpolates between the non-linear CGC and linear high-energy factorization pictures. The CGC description of di-hadron correlations requires calculation of the quadrupole operator [42, 43], which in this calculation is approximated. The effect of Sudakov radiation is found to be essential to describe such correlations in pp collisions; such effects grow in magnitude with $p_{\rm T}$, in contrast to effects expected due to saturation. Sudakov radiation must therefore be taken into account in any comparison of such calculations with data. Quantitative comparison of these calculations with the data in Fig. 16 are not yet published.

Figure 18 shows a prediction of the azimuthal angular distributions of $\pi^0 + \pi^0$ pairs in pp and p–Pb collisions at $\sqrt{s_{\rm NN}}$=8.8 TeV within the FoCal acceptance, using the same calculations as in Fig. 17 [85]. Both trigger and associated particles are selected within $4 < p_{\rm T} < 5$, which is not at the limit of FoCal measurement capabilities. A slight broadening of the angular distribution in p–Pb is predicted, which sets a challenging benchmark for measurements in this channel. Note however that these calculations are carried out at LO, while extension to NLO is needed for assessment of the theoretical uncertainty.

A parallel calculation for γ+π^0 correlations is also of interest, since the required theoretical framework is significantly different [42, 43]. As an example, Fig. 19 shows a prediction for this channel using a different theoretical approach within the CGC framework. Modification of the recoil yield due to

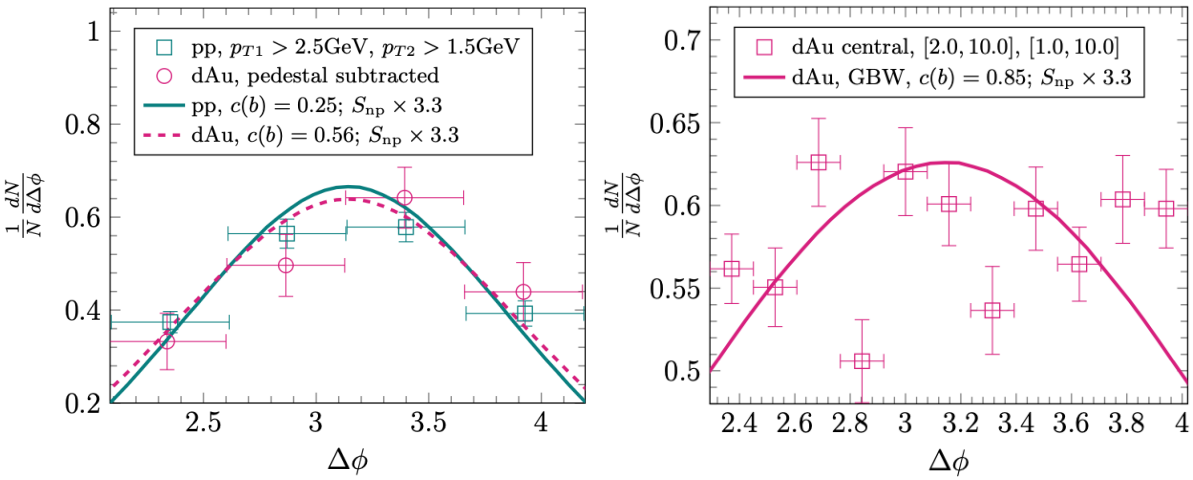

Fig. 17: Theoretical calculations of $\pi^0 + \pi^0$ correlations compared to a preliminary STAR data similar to those in Fig. 16, but for d–Au interactions selected for high event activity ("central" d–Au collisions) [85]. Calculations are based on the dilute-dense CGC framework with the addition of Sudakov radiation at small-x, and interpolate between CGC formalism and high-energy factorization.

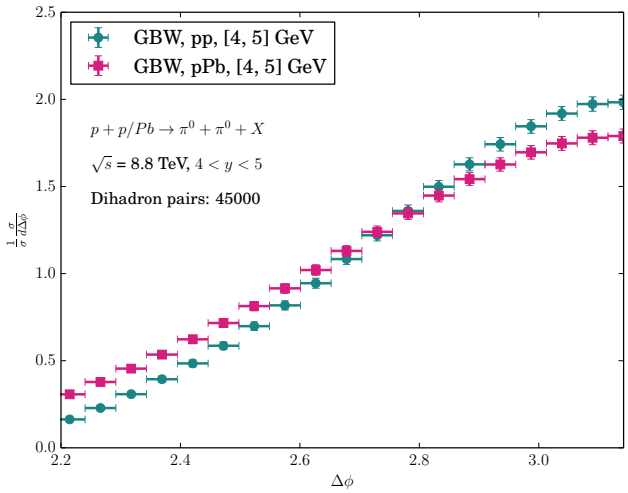

Fig. 18: Prediction of azimuthal angular distributions of $\pi^0 + \pi^0$ pairs in pp and p–Pb collisions at $\sqrt{s_{\rm NN}}$=8.8 TeV, within the FoCal acceptance, based on the same calculation as in Fig. 17 [85].

saturation effects is also observed in this case.

5.4 Jets, γ+jet, and dijets

Forward inclusive jet production has been calculated within the dilute-dense CGC framework at NLO, utilizing the dipole scattering amplitude [86–88]. An IR-safe NLO calculation which incorporates a realistic jet reconstruction algorithm (anti$-k_{\rm T}$) shows the validity of rapidity factorization in this channel [87]. While the effect of multiple scattering of the projectile parton in the CGC is to induce additional $k_{\rm T} \sim Q_{\rm sat}$, such effects are significant only for very low-$p_{\rm T}$ jets. This presents an experimental challenge to observe saturation effects in inclusive jet production measurements.

Forward di-jet observables may therefore have better sensitivity than inclusive jet measurements to saturation effects at small-x. That is because there are three momentum scales in the forward di-jet process [89]: $Q_{\rm sat}$, which characterizes gluon-saturated matter at small-x; $p_T^{\rm jet}$ of the individual jets in the pair; and the momentum imbalance $k_{\rm T}$ of the dijet pair, which also corresponds to the transverse momen-

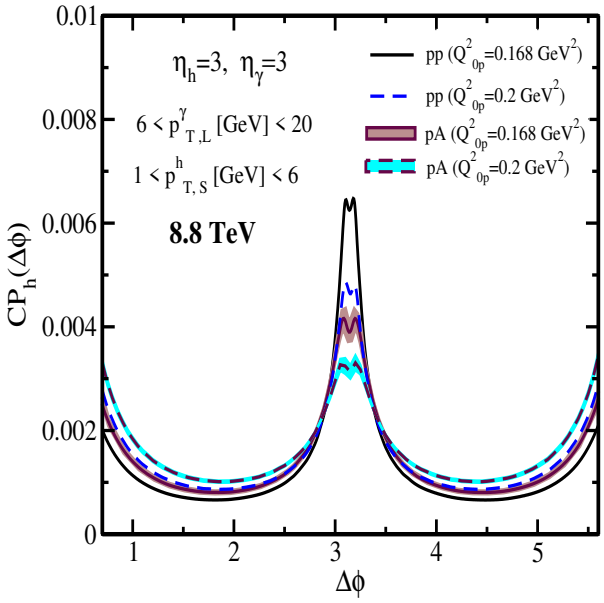

Fig. 19: Prediction of γ–π^0 correlations as a function of azimuthal angle difference at forward rapidity, in minimum-bias pA and pp collisions at $\sqrt{s_{\rm NN}}$=8.8 TeV, using a CGC approach with the running coupling BK equation and various initial saturation scales [63].

tum of the small-x gluons involved in the hard scattering. For jet measurements in practice, the value of $p_T^{\rm jet}$ is typically much larger than $Q_{\rm sat}$, while the magnitude of $k_{\rm T}$ ranges from similar to $Q_{\rm sat}$ to much larger, and thereby spans a range to interpolate between the low $\left(x, Q^2\right)$ limit of a transverse momentum-dependent (TMD) factorization framework to the high-Q^2 limit where high-energy factorization applies. For $Q_{\rm sat} \ll k_{\rm T} \sim p_T^{\rm jet}$, non-linear effects are negligible and the description of forward dijets involves hard matrix elements and a single TMD gluon distribution, while for $Q_{\rm sat} \sim k_{\rm T} \ll p_T^{\rm jet}$, non-linear effects persist and several different TMD distributions are required. The dijet channel is therefore promising approach to studying parton saturation, whose effects may be observable by varying $k_{\rm T}$ between $p_T^{\rm jet}$ and $Q_{\rm sat}$.

Figure 20 shows a recent calculation of the $\Delta\Phi$ dependence of di-jet $R_{\rm pPb}$ in the FoCal acceptance at $\sqrt{s_{\rm NN}} \sim 8$ TeV using the KaTie MC code [90–92]. KaTie is based on the Improved TMD (ITMD) factorization approach, whose domain of validity is $Q_{\rm sat} \ll p_T^{\rm jet}$. The ITMD formalism in Katie is augmented by resummation of Sudakov logarithms, and by non-perturbative corrections due to hadronization and showers using the PYTHIA event generator. While the calculation exhibits negligible dependence on $\Delta\Phi$ due to saturation effects, its uncertainties relative to the central values show that the precision of the current calculation is sufficient to provide strong discrimination of saturated and non-saturated gluon density, and thereby also set the precision needed in FoCal measurements.

Correlations with jets in the final state and with different triggers probe different QCD operators within the dilute/dense framework, providing significant variation to test its universality. In the ITMD approach, photon+jet coincidences are sensitive only to the dipole TMD distribution, which also governs the DIS interaction cross section, while dijet production in pA probes several different TMDs, and in DIS its description requires the quadrupole operator [89].

Figure 21 shows a KaTie calculation ofγ+jet coincidence events in the FoCal acceptance for pp and p–Pb collisions at 8.16 TeV. The left panel shows the $p_{\rm T}$-distributions of photon and jet; saturation effects are negligible, as expected since $Q_{\rm sat} \ll p_T^{\rm jet}$. The right panel shows the distribution of azimuthal separation $\Delta\varphi \sim k_{\rm T}/p_T^{\rm jet}$ for $p_T^{\gamma}, p_T^{\rm jet} > 10$ GeV/c, which exhibits greater sensitivity to saturation effects.

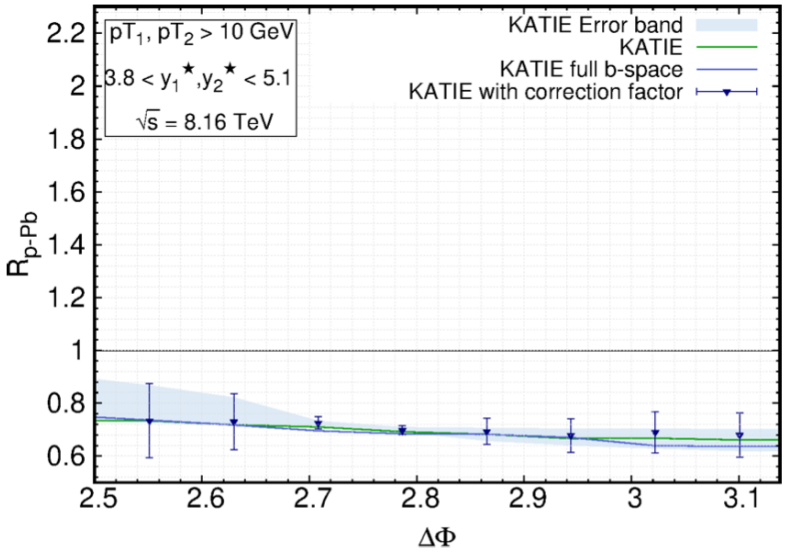

Fig. 20: Prediction of R_{pPb} for di-jets as a function of the opening angle $\Delta\Phi$ in the FoCal acceptance, for p–Pb and pp collisions at $\sqrt{s_{\mathrm{NN}}}$=8.16 TeV, calculated using the KaTie MC code [90]. The blue error band is the uncertainty due to the variation in the factorization scale. The data points show R_{pPb} obtained from Katie scaled by the non-perturbative correction factors from PYTHIA, with error bars showing the cumulative uncertainty of the factorization scale and non-perturbative corrections.

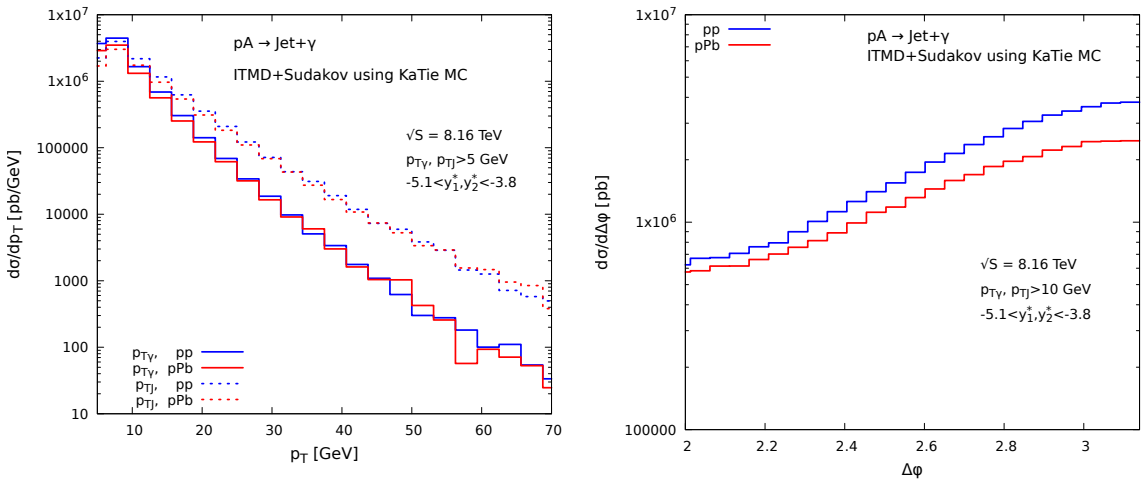

Fig. 21: KaTie MC calculation of recoil jet distributions for γ+jet coincidences in the FoCal acceptance for pp and p–Pb collisions at 8.16 TeV. Left panel: γ and recoil jet p_{T}-distributions. Right panel: azimuthal separation $\Delta\varphi$.

Figure 22 shows the $\Delta\varphi$ dependence of R_{pPb} for γ+jet and di-jet coincidences with several p_{T} thresholds from the same calculation as used for Fig. 21, further illustrating the magnitude of saturation effects. The two channels exhibit similar behavior, with 30% yield suppression in the back-to-back configuration (low k_{T}) for the 10 GeV threshold, and gradual weakening of the suppression towards greater acoplanarity (larger k_{T}). However, the γ+jet and dijet channels have markedly different theoretical descriptions; this is another opportunity for FoCal to carry out multiple measurements with different theoretical and experimental systematic dependencies, to probe the universality of the saturation picture at small-x.

Finally, we note that a CMS measurement of forward di-jet momentum imbalance and η-dependence of yield in p–Pb collisions [93] has been incorporated into a recent nPDF fit and found to have significant constraining power [53]. However, while the jet acceptance of these measurements ($4 < \eta < 5.2$) overlaps that of FoCal, the magnitude of jet p_{T} are $p_{\mathrm{T}}^{\mathrm{leading}} > 120$ GeV/c and $p_{\mathrm{T}}^{\mathrm{subleading}} > 30$ GeV/c, making

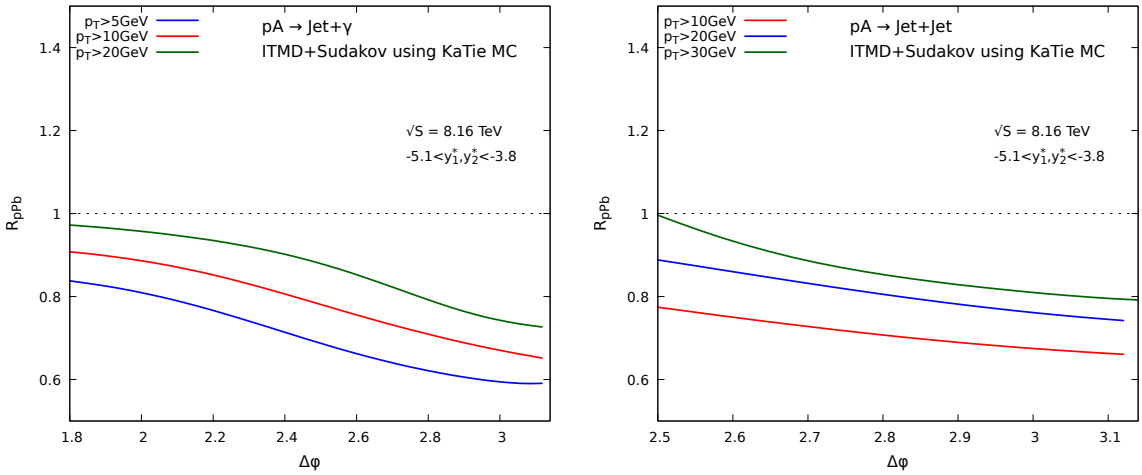

Fig. 22: R_{pPb} dependence on $\Delta\varphi$ for various p_{T}-thresholds, from the same calculation as Fig. 21. Left: γ+jet; right: di-jet channel. Note the different choices of the threshold and the different color coding in the two panels.

precise dijet imbalance measurements at the saturation scale Q_{sat} ∼few GeV/c challenging. FoCal will carry forward jet and di-jet measurements at much lower p_{T}, which will complement and extend these and forthcoming forward jet measurements from CMS.

5.5 Heavy flavor

For completeness we also discuss the theoretical status of forward heavy flavor production that is measurable by the LHCb collaboration [32], and which is likewise a key component of comprehensive program to test the universality of linear and non-linear QCD evolution. D-meson production is directly sensitive to the gluon density since the dominant production process for $c\bar{c}$ production is gluon fusion, $gg \to c\bar{c}$.

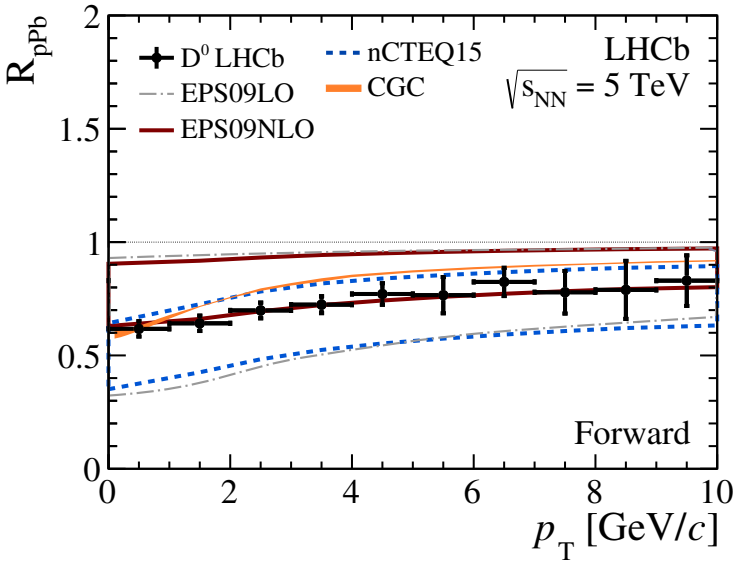

Fig. 23: R_{pPb} for prompt D^0 in acceptance $2.5 < |y^*| < 4.0$ for $p_{\mathrm{T}} < 6$ GeV/c and $2.5 < |y^*| < 3.5$ for $6 < p_{\mathrm{T}} < 10$ GeV/c, for p–Pb collisions at $\sqrt{s_{\mathrm{NN}}} = 5.02$ TeV, measured by LHCb [32]. Theoretical calculations are also shown, using linear QCD evolution with nuclear PDFs [51, 94], and a CGC-based [95] framework. In the case of nCTEQ15 the two (blue-dashed) lines indicate the spread of the theoretical uncertainty of the calculation.

LHCb has reported a precise measurement of prompt D-meson production at forward rapidity $2.5 < y < 4.0$ [32], which also probes small-x. Figure 23 shows this measurement of the relative inclusive yield, R_{pPb}, as a function of p_{T}. Forward production of prompt D-mesons is observed to be suppressed in p–Pb

compared to pp collisions, with $R_{\rm pPb} \sim 0.6$ at low $p_{\rm T}$, increasing slowly with $p_{\rm T}$. This directly confirms that the shadowing at small x is strong.

The measured suppression is in line with expectations based on the various nuclear PDF sets, which are also shown in the figure. The suppression of charm production in the calculations with nuclear PDFs is a direct result of the reduced gluon density at $x \lesssim 10^{-2}$ (see Fig. 7). The calculated values of $R_{\rm pPb}$ range from about 0.3 to 0.9, reflecting the current uncertainties in the nuclear modification of the small-x gluon density. This is because the NMC data which initially identified shadowing [17–19]only constrain the nuclear PDFs on the large x side of the shadowing region, near $x = 10^{-2}$.

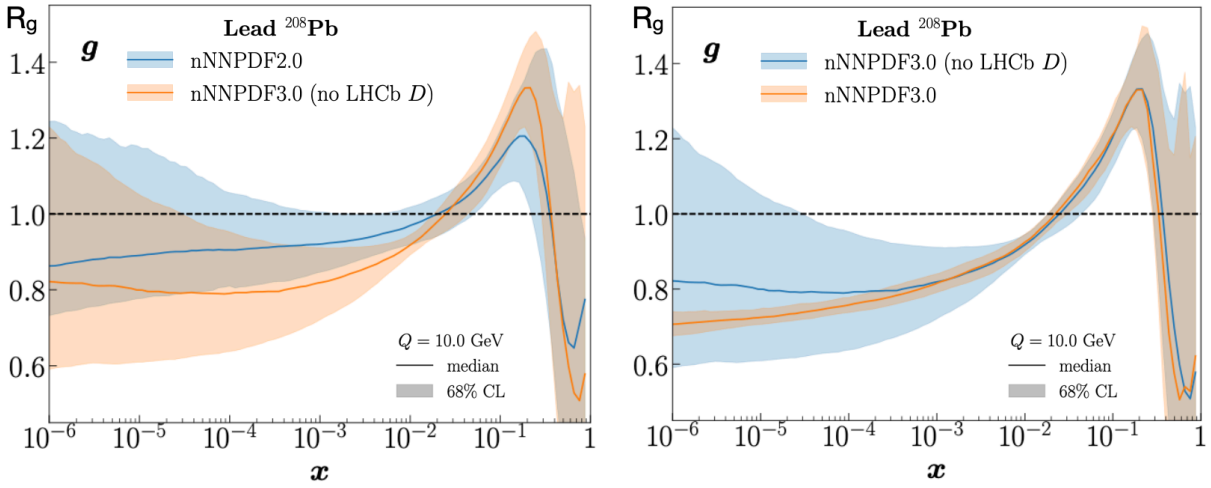

Fig. 24: Comparison of $R_{\rm g}$ for nNNPDF2.0 vs. nNNPDF3.0 without charm (left) and for nNNPDF3.0 with charm and without charm [96]. Uncertainties are at 65% confidence level.

Including the D-meson data in the determination of the nuclear PDFs only slightly influences the central value, but reduces the uncertainties by up to a factor 2 [80] [7]. However, a quantitative determination of the magnitude of gluon shadowing based on hadron production measurements is complicated by the fact that hadronic final state effects (rescattering) may also influence the distribution. The recently observed flow-like long-range correlations [98–102], discussed in Sec. 7, need to be taken into account in the interpretation of the measurements.

Despite these concerns, recent nuclear PDFs [53,96] have included the precise LHCb charm data [32] in their global fits. As an example, the gluon density modification $R_{\rm g}$ is shown in Fig. 24 for the nNNPDF3.0 nuclear PDF, with and without the LHCb charm data. Significant suppression of $R_{\rm g}$ at small x is obtained with small systematic uncertainties, even at x values well below 10^{-5}. Comparison of precise forward photon and charm measurements will allow one to test factorization and universality of the nuclear PDFs.

6 Small-x studies using ultra-peripheral heavy-ion collisions

Ultra-peripheral collisions (UPCs) are the energy frontier for photon-mediated interactions, probing collisions at γp center of mass energies above 1 TeV [103–105], which far exceeds the energy accessible at the HERA ep collider. For γ–A collisions, the maximum γ–N center of mass energies are 700 GeV and 1.5 TeV in Pb–Pb and p–Pb collisions respectively. With its far forward geometry, Focal is the best-suited LHC detector subsystem to exploit this energy; it will probe the gluon densities of protons and heavy ions down to Bjorken$-x$ values below 10^{-6} [106].

In UPC, the photons come from the Lorentz-boosted electromagnetic fields of the colliding ions. These fields can be treated as a flux of quasi-real photons. In vector meson photoproduction, these photons

[7] Note that the updated PDFs introduce a tension with the ALICE midrapidity D^0 meson nuclear modification factor [97].

fluctuate to quark-antiquark dipoles (virtual vector mesons) which then interact elastically with the target nucleus, emerging as real vector mesons. For production of a vector meson with mass M_V at rapidity y, the photon energy and Pomeron x value are [107]

$$k = \gamma M_V \exp(\pm y) \tag{8}$$

and

$$x = \frac{M_V}{\gamma m_p} \exp(\mp y) \tag{9}$$

The $\pm$ and $\mp$ signs are present because, for coherent photoproduction, there is an ambiguity about which nucleus emitted the photon and which is the target. This ambiguity can be resolved in *pA* collisions, where the photon is usually emitted by the heavy nucleus. In Pb–Pb collisions, one method to resolve the ambiguity is by considering events with different nuclear breakup conditions, as will be discussed below. With this, in lead-lead collisions at $\sqrt{s_{\rm NN}} = 5.6$ TeV, J/ψ photoproduction at $y = 5.8$, near the edge of the Focal acceptance, probes the target at $x = 5 \times 10^{-7}$; for pp collisions, the Lorentz boosts are higher, so reaching targets down to $x = 2 \times 10^{-7}$. For vector meson photoproduction, the hard scale comes from the heavy-quark masses, so $Q^2 = (M_V/2)^2$, or $Q^2 \approx 2.25$ GeV^2. Different Q^2 values can be probed with different mesons, including the ψ' and the low mass vector meson states. In pQCD, vector meson photoproduction is actually described by a generalized parton distribution; this difference may be bridged by the use of a Shuvayev transformation [108]. And, recent NLO calculations have pointed to the presence of a significant quark contribution at that order, along with a significant scale dependence [109]. The scale dependence can be treated by comparing cross sections on proton and lead targets, while the quark contribution can become part of fits to extract parton distributions, as is already done with direct photons.

The signature for coherent vector meson photoproduction decaying to e^+e^- will be very distinctive in FoCal —two electromagnetic showers back-to-back in azimuthal angle, with nothing else present in the event (except for some neutrons in the zero degree calorimeters). The rates for these processes are large, even at large $|y|$ [105–107].

6.1 Physics measurements in ultra-peripheral p–Pb collisions

The ALICE collaboration has studied the energy dependence of the J/ψ photoproduction cross section in p–Pb collisions, and found that it continues to follow the power law seen by HERA: $\sigma(\gamma \mathrm{p} \to \mathrm{J}/\psi \mathrm{p}) \propto W_{\gamma p}^{\delta}$, with $\delta = 0.70 \pm 0.05$ [110]. In LO pQCD, this gives a gluon density that evolves as $xg(x) \propto x^{-\delta/2}$. Saturation would reduce the high-energy cross section below this power law. ALICE measurements [110, 111], extending down to $x \sim 10^{-5}$, showed no deviation from this behaviour, although the statistical error was large. An alternative explanation for the reduction of the cross section could be large higher order corrections, but no such calculations exist. Also early work has indicated that such corrections will lead to an increase of the cross section [112]. The FoCal detector will access an unexplored kinematic regime at even smaller x where a different trend in the growth of the cross section might occur. While the LHCb collaboration has studied exclusive J/ψ in pp collisions at $\sqrt{s} = 7$ TeV [113,114] and $\sqrt{s} = 13$ TeV [115], their analyses of $\sigma(\gamma \mathrm{p})$ are strongly model dependent because of the ambiguity in the photon direction present in symmetric colliding systems (see Refs. [106, 116] for details).

There are three published models that use non-linear QCD to make predictions at high energies, namely, the Hot Spot model (CCT) [119], the NLO BFKL [120] and the CGC-based (MS) calculations [121].

To illustrate the prospects of observing saturation effects with FoCal, the projection of the energy dependence of the J/ψ photoproduction cross section in the FoCal acceptance was obtained using the NLO BFKL model [120]. It is shown in Fig. 25, while Fig. 26 shows the ratio of the NLO BFKL projection to the same power-law used to fit the ALICE data. The figures demonstrate that if saturation occurs, as predicted by these models, the future FoCal UPC measurements would provide the first observation of the deviation from the power-law trend at high energies. These figures are based on a simplified model of

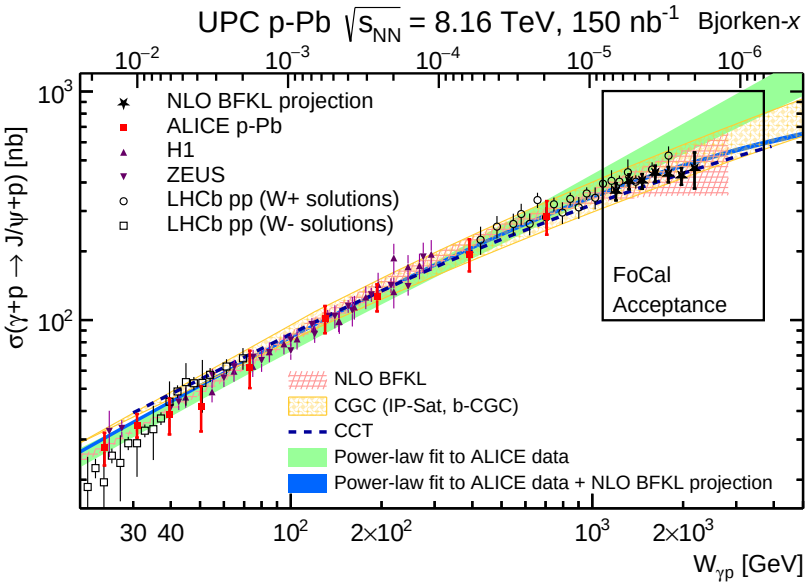

Fig. 25: Figure from [106]. Current ALICE data [117](full red squares) from p–Pb UPCs at $\sqrt{s_{\rm NN}} = 5.02$ TeV is shown, along with data from HERA [112, 118] and LHCb [113–115]. The FoCal acceptance in $W_{\gamma p}$ for exclusive J/ψ photoproduction on protons is shown by the black box. The black stars show the expected FoCal results, based on the NLO BFKL model. In all cases, the error bars are the quadratic sum of the statistical and systematic uncertainties. The green band shows the fit of the existing data to a power-law, while the blue band shows a possible future fit to the data using a modified power-law function which saturates at large $W_{\gamma p}$ [106]. Also shown are three theory calculations.

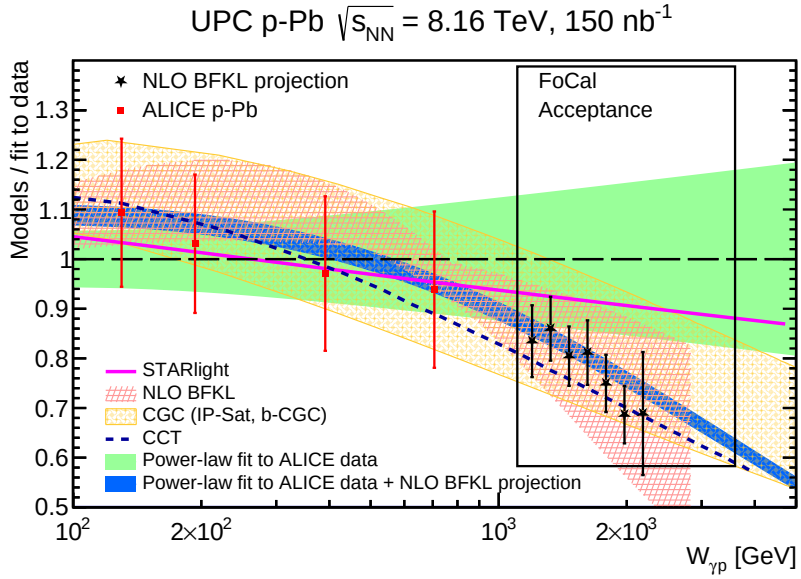

Fig. 26: Ratio of the ALICE data, NLO BFKL projection and theoretical models shown in Fig. 25 to the power-law fit through the ALICE data points. The green band shows the uncertainty of the power-law fit to the existing ALICE data while the blue band shows the reduction of the fit uncertainty at high energy when the ALICE data is combined with the NLO BFKL projected points and fitted to the formula presented in [106]. The FoCal energy reach corresponding to its acceptance is illustrated with a box. Figure from [106].

the FoCal performance, conservatively assuming a 60% efficiency at $\eta < 5$, and not extending to higher pseudorapidities. In the projected pseudorapidity range this is lower, on the average, than obtained from

detailed simulations. Since the photon flux decreases exponentially in rapidity, the projected data points for FoCal do not cover the energy reach which is illustrated with a box on these figures.

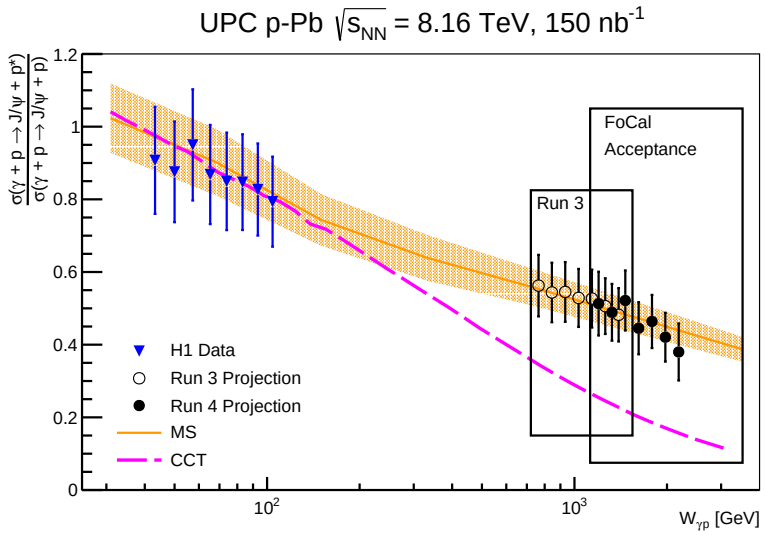

Fig. 27: Energy dependence of the ratio of dissociative to exclusive J/ψ photoproduction cross sections as a function of $W_{\gamma p}$. The full triangles correspond to the H1 measurement [112]. The projected data are shown with open and full circles for the measurements with the ALICE muon detectors during Run 3 and the ALICE FoCal detector during Run 4, respectively. The corresponding kinematic regions are indicated by the two boxes. The projected points were obtained using STARlight [122] for the exclusive process, and the BM model prediction for the dissociative process. Theoretical calculations based on the CCT and MS saturation models are also shown. The projected points are also smeared randomly according to the Gaussian distribution with the width corresponding to the expected statistics of each measurement. The points show the statistical and systematic uncertainties added in quadrature. Figure from [106].

The ratio of the cross sections between $\psi(2S)$ and J/ψ is also predicted to be sensitive to gluon saturation [123]. These two vector mesons have different wave functions, different energy evolution of their color dipole sizes. Figure 28 shows the H1 and ZEUS data [124, 125], and the projected STARlight events within the FoCal acceptance. The HERA points are compared to two different types of model calculations: the calculations based on the color dipole model (GBW) and on the BGK model, respectively [123]. For these two types of calculations, the linear and the non-linear (saturation) predictions are shown. There is a clear separation between the linear and the non-linear calculation, making this ratio a very promising measurement to observe gluon saturation at the LHC. The comparison between these two different sets of calculations, the GBW and BGK, provide some estimate of the theoretical uncertainty. The figure also shows the kinematic region that can be explored utilizing the ALICE muon spectrometer during Run 3.

In addition, the dissociative process ($\gamma p \to J/\psi p^*$) has received recent interest [119, 126, 127]. The Good-Walker paradigm relates incoherent photoproduction to event-by-event fluctuations in the nuclear configuration, including gluonic hot spots, and, for heavier ions, fluctuations in the positions of the nucleons [128]. Although there are theoretical issues with separating coherent and incoherent production in the Good-Walker paradigm [129], the separation appears to work in practice. Studies of HERA data using this approach [126] found evidence for a proton with large fluctuations. With FoCal, as shown in Fig. 27, these measurements could be extended to considerably lower x than was possible at HERA; ion targets can also be studied. Of particular interest is the search for the possible onset of the black-disk regime, where the incoherent cross section reaches a maximum, and then declines with further increases in photon energy [130]. The observation of a significant reduction of the cross section as energy increases would be a signature of gluon saturation at high energies.

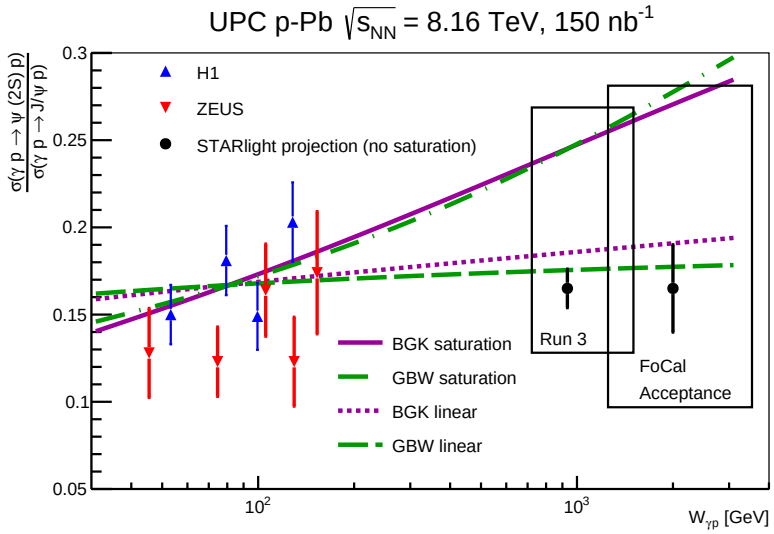

Fig. 28: Energy dependence of the ratio between $\psi(2S)$ and J/ψphotoproduction cross sections. The points correspond to the HERA data (full triangles) measured by the H1 and ZEUS collaborations, respectively [124,125], and to the STARlight projections (full circles). For the STARlight projected points only the statistical uncertainty is shown based on the number of expected events multiplied by the reconstruction efficiency. Theoretical calculations based on BKG and GBW saturation models and their corresponding linearized versions [123], are also shown. The two boxes illustrate the kinematic regions that can be explored utilizing the ALICE muon detectors during Run 3 and the ALICE FoCal detector during Run 4, respectively.

6.2 Physics measurements in ultra-peripheral Pb–Pb collisions

Exclusive photonuclear production of vector mesons (VMs) has been studied by several experiments in ultra-peripheral Pb–Pb collisions at the LHC [131–136]. In particular, J/ψ photoproduction is measured using nuclear targets to study gluon shadowing. ALICE has studied J/ψ photoproduction at both midrapidity and in the forward region, revealing significant shadowing at medium and small x down to 10^{-5} and $Q \approx M_{J/\psi}/2$. The major experimental issue is resolving the two-fold ambiguity as to which nucleus emitted the photon, and which was the target. The directional ambiguity can be addressed by studying events with neutrons in different directions and possibly by also studying photoproduction in peripheral hadronic collisions [119, 137]. Figure 29 shows the $\sigma(\gamma\mathrm{Pb})$ cross section for coherent J/ψ photoproduction in ultra-peripheral Pb–Pb collisions as function of $W_{\gamma\mathrm{Pb}}$. The uncertainty of the measurement results from propagating the experimental uncertainties of the $d\sigma/dy$s in the various neutron configurations (see Ref. [106] for details). At present, no experimental data exist for this measurement although ALICE has an ongoing analysis and CMS has recently presented preliminary results. Note that LHCb does not have ZDCs installed at present or for Run 4, making ALICE with FoCal the only experiment capable of carrying out this analysis to probe down to x values of about 2×10^{-6}.

In addition to a measurement of structure functions at small Bjorken-x, the FoCal coherent photoproduction data could also be used to study the evolution of the nuclear shape with Q^2, at smaller x values than previously [138, 139]. By studying how the apparent nuclear shape changes with decreasing x in J/ψ photoproduction on lead targets, ALICE can search for the onset of gluon saturation using a new approach.

Finally, the study of dijet photoproduction in UPCs is also of great interest. The photoproduction of dijets was explored by the ATLAS collaboration [140] as a promising probe to access a wide range of x values above 10^{-4} at $Q > 7$ GeV/c, while CMS has studied angular correlations of diffractive dijets [141]. FoCal will have a competitive advantage over ATLAS and CMS because of the high-granularity detection and the forward rapidity coverage.

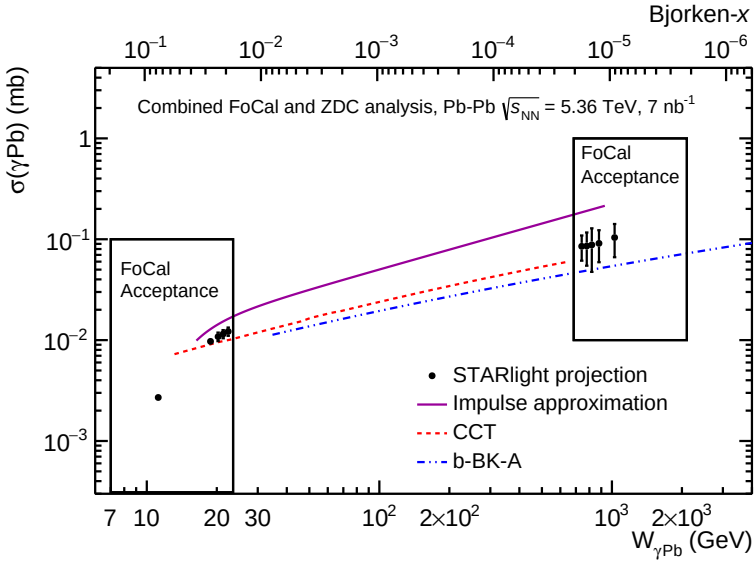

Fig. 29: STARlight [122] projection (full black circles) for the cross section of coherent J/ψ photoproduction in ultra-peripheral Pb–Pbcollisions shown as a function of the photon-lead center-of-mass energy $W_{\gamma\mathrm{Pb}}$. To separate the two photon directions, this analysis will use both FoCal and ZDC detectors. Predictions from the impulse approximation, CCT and b-BK models are also shown. The two boxes indicate the FoCal detector acceptance for the two explored kinematic regions.Figure from [106].

7 Long-range correlations in pp and p–Pb collisions

The situation regarding the sensitivity of hadronic observables to the initial state, in particular the gluon density, has been greatly enriched by unexpected features discovered in small systems at RHIC and the LHC [15, 142]. Among those is the "double ridge", a two-hadron correlation in the relative azimuthal angle $\Delta\varphi$ extending over a large range in $\Delta\eta$, as shown in the left panels of Fig. 30 and Fig. 31. The

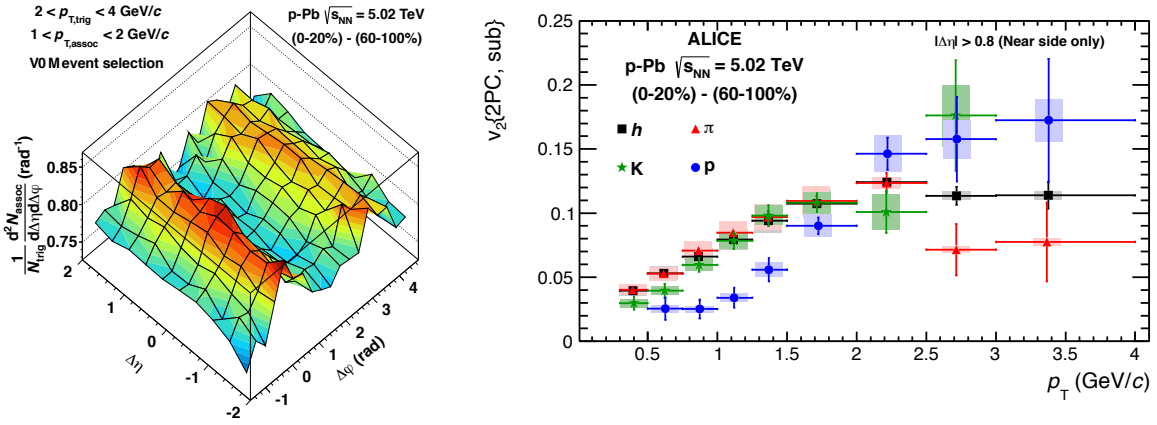

Fig. 30: (Left) Per-trigger particle associated yield in $\Delta\varphi$ and $\Delta\eta$ for pairs of charged particles with $2 < p_{\mathrm{T,trig}} < 4$ GeV/c and $1 < p_{\mathrm{T,assoc}} < 2$ GeV/c in p–Pb collisions at $\sqrt{s_{\mathrm{NN}}} = 5.02$ TeV for the 0–20% event class after subtraction of the yield obtained in the corresponding 60–100% event class [143]. (Right) The v_2 values extracted from two-particle correlations in p–Pb collisions at $\sqrt{s_{\mathrm{NN}}} = 5.02$ TeV for hadrons (black squares), pions (red triangles), kaons (green stars) and protons (blue circles) as a function of p_{T} in the 0–20% event class after subtraction of the 60–100% event class [98].

structure of the correlation in $\Delta\varphi$ can be well described by a Fourier decomposition with a dominant second order coefficient v_2, also known as *elliptic flow* [145]. By now, v_2 has been measured for numerous hadrons, including open and hidden charm [98–102, 146]; examples are shown in the right panels of Fig. 30 and Fig. 31.

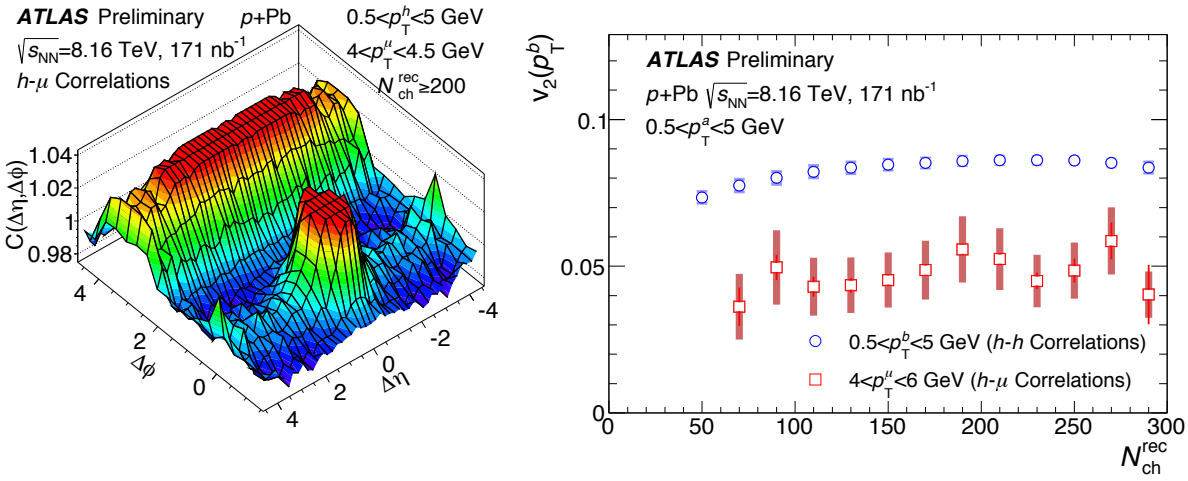

Fig. 31: (Left) Two-particle hadron–μ correlation functions as a function of $\Delta\eta$ and $\Delta\varphi$ for high-multiplicity p–Pb collisions at 8.16 TeV measured by ATLAS [144]. (Right) Corresponding v_2 values extracted from the correlation functions for associated hadrons and muons.

The mechanisms causing these correlations are not fully understood, and two sources have been identified: an anisotropy in the initial state momentum distribution [147, 148]; and an anisotropy in the spatial distribution that is imprinted on the momentum distributions by final state scattering [149, 150]. In analogy to heavy-ion collisions, final-state scattering can arise from from a hydrodynamic response. This occurs if the system is in local thermal equilibrium, with pressure gradients driving the system to global equilibrium. The hydrodynamic response generates collective motion from the conversion of initial spatial anisotropy to momentum anisotropy. This mechanism would generate the observed dependence of the light flavor v_2 values as a function of hadron mass, which is characteristic of a hydrodynamic response. On the other hand, measurements of J/ψ v_2 in small systems can be explained by initial state momentum anisotropies only, expected from saturation models [151]. Attempts to model J/ψ v_2 using only final state effects have proven unsuccessful so far [152]. Therefore, both initial and final state momentum anisotropies may have competing contributions, which calls for future measurements to disentangle these effects in small systems.

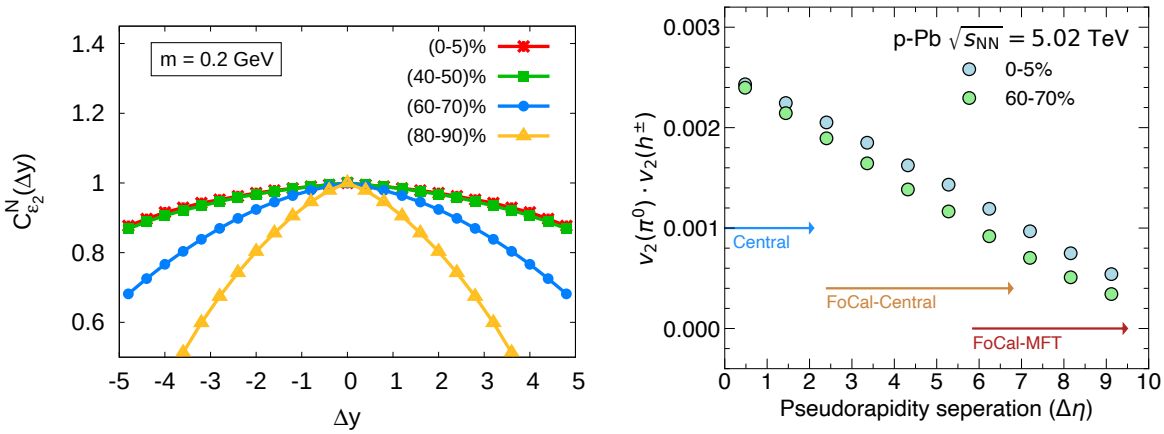

Fig. 32: (Left) Decorrelations in the initial state eccentricity as a function of rapidity difference in p–Pb collisions at LHC energies in different multiplicity classes [153]. (Right) An estimation of v_2^2 measurements using neutral pions from FoCal (or TPC/EMCal at $|\Delta\eta| \lesssim 2$) with respect to charged hadrons from other detectors in ALICE for p–Pb collisions. See text for more details.

FoCal can play a leading role in disentangling initial and final state momentum anisotropies by measuring

long-range correlations in unexplored kinematic regimes. This can be achieved by measuring azimuthal correlations between particles at forward rapidity with FoCal, and at mid/backward rapidity using the ALICE Central TPC/MFT detectors. The measurement could be done in the same manner as those shown in the left panel of Fig. 31.

As mentioned, for small systems, a key question is to what extent initial state momentum anisotropies contribute to the momentum anisotropies observed in the final state. Measuring anisotropic flow vs. the rapidity difference of the outgoing particles is critical for addressing this question. Recent studies have shown that, for differences of $|\Delta\eta| < 1$, initial state momentum anisotropies play a significant role, but at larger $|\Delta\eta|1$ the observed momentum anisotropy should be dominated by final state effects [153, 154]. The momentum anisotropies at $|\Delta\eta| > 1$ are therefore speculated to only result from a hydrodynamic response to initial state spatial anisotropies. The 3+1D IP-Glasma model, which incorporates gluon saturation effects, predicts a decorrelation between second order initial state anisotropies over large rapidity differences in p–Pb collisions at LHC energies [153]. The decorrelations resulting from such a calculation are shown in the left panel of Fig. 32 as a function of different multiplicity classes (e.g. 0-5% represent collisions with the highest number of produced particles, 80-90% the lowest). The normalized (N) correlation function at different rapidities y_1 and y_2 vs the rapidity difference is defined as:

$$C^N_{\varepsilon_2}(\Delta y) = \frac{\langle \varepsilon_2(y_1)\varepsilon_2(y_2)\rangle}{\sqrt{\langle \varepsilon_2(y_1)^2\rangle\langle \varepsilon_2(y_2)^2\rangle}} \tag{10}$$

where $\varepsilon_2(y)$ is the eccentricity at rapidity y. It is 1 when the eccentricities are the same at different rapidities y_1 and y_2 i.e. fully correlated, and 0 if they are fully de-correlated. The decorrelation is most pronounced at the largest rapidity separations for p–Pb collisions with the lowest multiplicity (80–90%).

In the right panel of Fig. 32, we present an estimation of v_2^2 using FoCal and other ALICE detectors in p–Pb collisions, to illustrate the effect of the decorrelations on this observable. The FoCal can be used to measure π^0 hadrons at forward rapidities, and the EMCal at midrapidity. The TPC ($|\eta| < 1$) or MFT ($-3.6 < \eta < -2.5$) can be used to measure charged hadrons (in the case of the MFT, muons from charged hadron decays). We use the decorrelation predictions from the left panel and measurements of v_2 vs. η in d–Au collisions from PHENIX at the top RHIC energy [155] for this estimation. A Fourier decomposition of the ridge provides a measurement of v_2^2, hence the product $v_2(\pi^0) \times v_2(h^{\pm})$ for the y-axis. This can be obtained using two particle correlations of $v_2(\pi^0)$ and $v_2(h^{\pm})$ vs. $\Delta\eta$ and $\Delta\phi$, as shown in the left panels of Fig. 30 and Fig. 31. It is clear that the FoCal provides a unique opportunity to investigate decorrelation effects, as the differences between low and high multiplicity events occur at the largest rapidity separations. Such differences ultimately test initial state models, that are now in the process of pursuing a 3D description of the dynamical evolution of nuclear collisions (3+1D). The majority of current hydrodynamic models only evolve the system vs. time in the transverse direction (2+1D). Whether saturation based models are a key component is a critical question — for example, the (non-saturation) AMPT model also predicts similar effects for decorrelations of initial state spatial anisotropies [156]. In addition, correlations of forward isolated photons with midrapidity hadrons are of interest. These test mechanisms at work in the initial stages of the collisions, as isolated photons should suffer very little influence from final state interactions. The mass scaling related to the hydrodynamic response at forward rapidities can also be tested with measurements of heavier mesons (η, ω), also utilizing very long range correlations to minimize the contributions from initial state momentum anisotropies.

Finally, gluon saturation at small x has also been postulated to be the source of quantum entanglement effects [157]. These could lead to instant thermalization based on the potential equivalence of entanglement and thermodynamic entropy. This is due to the fact that entropy is already generated in the initial state for partons, which provides a means for fast entropy maximization needed for thermalization of hadrons in the final state. In order to study this type of parton-hadron duality, using FoCal ALICE can

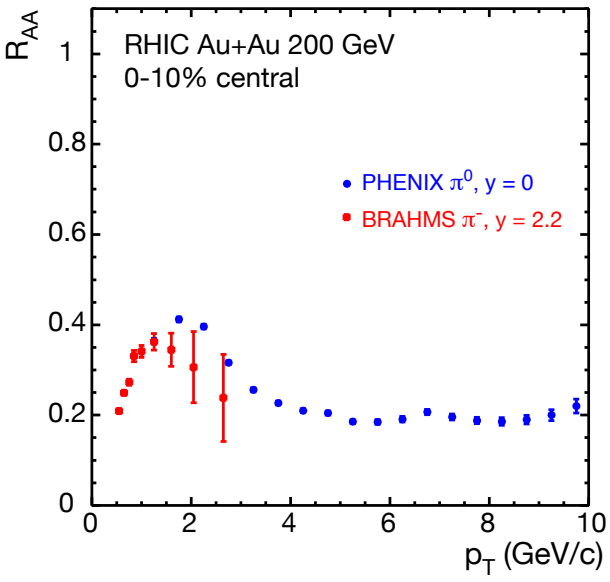

Fig. 33: Nuclear modification factor R_{AA} as a function of p_{T} for identified pion production in central Au–Au collisions at RHIC. Shown are measurements of π^0 at midrapidity by PHENIX [159] (blue symbols) and of π^- at $\eta = 2.2$ by BRAHMS [160] (red symbols). Only statistical errors are shown.

complement the EIC measurements in ep and eA systems via measurements in pp, pA and AA collisions. The survival of the coherent state as a function of system size can be measured through particle multiplicities and quantum tomographic correlation functions of particles from small-x processes [158]. FoCal will be useful also for such studies in an x region of $10^{-6} < x < 10^{-5}$ that is not yet accessible experimentally. The final state entropy is determined from hadron multiplicity distributions, which can be measured in the neutral channel using FoCal.

8 Exploration of jet quenching in Pb–Pb collisions at large rapidity

One of the hallmark results from high-energy heavy-ion collisions is the observed suppression of high-p_{T} particle production compared to the expected scaling with the number of binary nucleon–nucleon collisions. This suppression arises from parton energy loss due to interactions of the high-energy partons with the QGP, usually called jet quenching, before they fragment into high-p_{T} hadrons [16].

As of yet, the knowledge on the rapidity dependence of the single hadron or jet suppression is very limited. At RHIC, the only forward measurements of hadron spectra in central Au–Au collisions have been performed by the BRAHMS experiment. Figure 33 shows results of the nuclear modification factor (R_{AA}) of the forward negative pion production compared to the results for neutral pions at midrapidity as measured by PHENIX. A suppression is apparent in both modification factors. However, while the midrapidity measurements are of relatively high precision, the forward measurements suffer from large uncertainties, and are of very limited reach in transverse momentum. This is due partially to the steeper momentum spectra at high rapidities and partially due to the fact that there is no large acceptance detector for high rapidity at RHIC. Given the large statistical uncertainties, no strong statement about the rapidity dependence of R_{AA} at RHIC can be made. At the LHC, the nuclear modification factor has been measured out to $\eta \approx 2$, see right panel of Fig. 34; this covers however only a small fraction of the available dynamic range in rapidity. These measurements are unfortunately not conclusive – no clear systematic trend can be identified in the data, also because of the limited range in pseudorapidity.

Jet quenching at high rapidities is of interest because the conditions of the hot and dense matter do change with rapidity, although this dependence is not expected to be strong as one can see from pseudorapidity densities of charged particles, which do not vary very strongly. In addition to variations in the medium

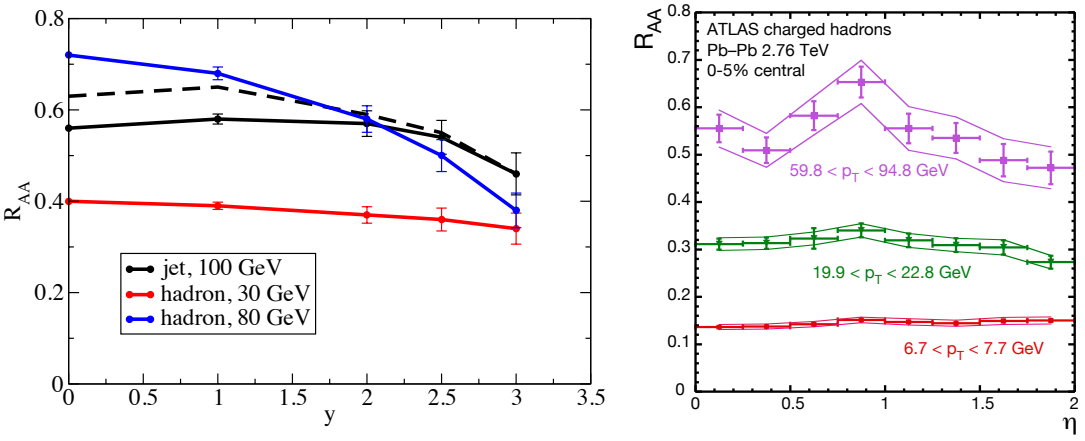

Fig. 34: Nuclear modification factor $R_{\rm AA}$ of jets and hadrons in central Pb–Pb collisions at $\sqrt{s_{\rm NN}} = 2.76$ TeV. (Left) $R_{\rm AA}$ of jets and hadrons as a function of rapidity as calculated with YaJEM [161]. (Right) $R_{\rm AA}$ for charged hadrons in different $p_{\rm T}$ intervals as a function of pseudorapidity measured in ATLAS [162].

properties, there are other rapidity dependent effects relevant for parton energy loss measurements, e.g. the relative mixture of quark vs. gluon contributions, which is modified due to the contributions of larger Bjorken-x for one of the primary partons, and the slope of the initial parton spectrum, which is strongly modified when one gets closer to the kinematic limit at high rapidity. The latter can be particularly important for the measurement of the single hadron nuclear modification factor, as shown in the left panel of Fig. 34. In fact, while high-$p_{\rm T}$ hadrons at midrapidity originate from a broad distribution of parton $p_{\rm T}$, this source of uncertainty is reduced at high rapidity, where the kinematic range of parton $p_{\rm T}$ is limited. In addition, this effect would lead to a stronger suppression at large rapidity compared to midrapidity. Jets and intermediate $p_{\rm T}$ hadrons show very little rapidity dependence of the suppression, while the dependence is very strong for high $p_{\rm T}$ hadrons, an effect that is likely due to the strong modification in the parton spectrum.

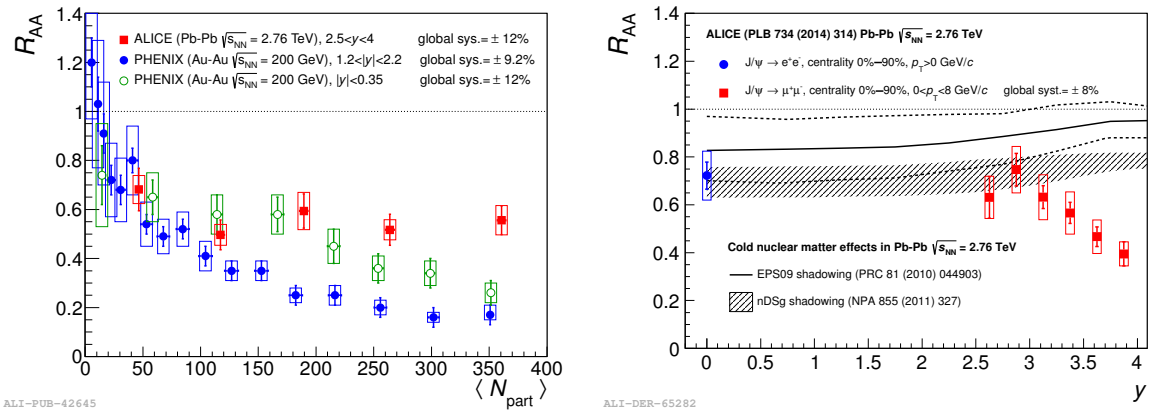

Fig. 35: (Left) Inclusive J/ψ $R_{\rm AA}$ as a function of the number of participating nucleons measured in Pb–Pb collisions at $\sqrt{s_{\rm NN}} = 2.76$ TeV compared to PHENIX results in Au–Au collisions at $\sqrt{s_{\rm NN}} = 200$ GeV at midrapidity and forward rapidity [163]. (Right) Inclusive J/ψ $R_{\rm AA}$ as a function of rapidity measured in Pb–Pb collisions at $\sqrt{s_{\rm NN}} = 2.76$ TeV with a comparison to theoretical predictions including nuclear shadowing [164].

The measurements of the nuclear modification factor of neutral pions in a more forward rapidity range with FoCal will allow to explore this region in more detail. To make these measurements most useful requires FoCal coverage that (partially) overlaps with the Muon Spectrometer, as we discuss now. The

study of parton energy loss and the medium density at forward rapidity is also important to interpret the existing measurements of quarkonium production at forward rapidity. To illustrate some of the open questions in charmonium production and suppression, the left panel of Fig. 35 compares the nuclear modification of J/ψ production at RHIC and LHC. The smaller suppression of J/ψ at the LHC compared to RHIC is now generally interpreted as an interplay of Debye-screening, which is dominant at RHIC and leads to a strong suppression, and an additional final state production mechanism (statistical hadronisation or kinetic recombination), which becomes important at LHC and compensates part of the suppression. Our understanding is unfortunately complicated by the different rapidity coverage of the measurements.

Further indications for the rapidity dependence can be found in a comparison of midrapidity and forward rapidity measurements of J/ψ suppression in Pb–Pb collisions by ALICE as displayed in the right panel of Fig. 35. While the suppression seems to be small and very similar for $|y| < 0.8$ and $y = 3$, R_{AA} decreases significantly for $y > 3$. This decrease is not explained by nuclear shadowing, as is seen from the comparison to the theoretical curves shown in the figure. Possibly there are other initial state effects that play a role here (like gluon saturation as discussed earlier), or the properties of the medium do change significantly as a function of rapidity. In addition to π^0 measurements, for which the FoCal performance in heavy-ion collisions has been evaluated in detail as discussed in the next sections, we also expect that FoCal can provide measurements of the heavier η and ω mesons.

Furthermore, measurements of isolated photons and jets will be possible using the electromagnetic and hadronic sections of the calorimeter enabling measurements of isolated photon and jet R_{AA} up to about $y \approx 5$.

9 Summary

The FoCal detector consists of a highly-granular Si+W electromagnetic calorimeter combined with a conventional sampling hadronic calorimeter, covering $3.4 < \eta < 5.5$.

The main goals of the FoCal science program are to:

- Explore gluon dynamics and non-linear QCD evolution at the smallest values of Bjorken x using theoretically well-motivated observables in pp and p–Pb which are sensitive to the gluon distribution at small x at low to moderate Q^2, such as isolated photon, neutral meson, and jet production and their correlations in hadronic collisions, and the measurement of vector meson photoproduction in ultra-peripheral collisions.
- Investigate the origin of flow-like effects by measurements of particle and jet correlations over a large range in rapidity in pp and p–Pb collisions;
- Quantify parton energy loss at forward rapidity by measuring the neutral meson and jet nuclear modification factors at high-p_{T} in Pb–Pb collisions.

Other measurements will be possible but are not further emphasized in this document, such as the measurements of (di-)jets in ultra-peripheral collisions, W, Z in pp and p–Pb collisions and direct photon production and photon interferometry (HBT) as well as centrality and reaction plane determination in Pb–Pb collisions. Lastly, measurements of $E_{\mathrm{EM}}/E_{\mathrm{had}}$ possibly accessible by FoCal at forward rapidity are important in interpreting data from cosmic-ray air showers.

Acknowledgments

We thank N. Armesto, K. Eskola, I. Helenius, J. Jalilian-Marian, P. Kotko, Y. Kovchegov, T. Lappi, H. Mäntysaari, H. Paukkunen, M. Sievert, and R. Venugopalan for valuable discussions. We thank Y. Kovchegov for substantial contributions to Sec. 3 and Sec. 4, and P.Kotko for providing Fig. 21 and Fig. 22.

The ALICE Collaboration would like to thank all its engineers and technicians for their invaluable contributions to the construction of the experiment and the CERN accelerator teams for the outstanding performance of the LHC complex. The ALICE Collaboration gratefully acknowledges the resources and support provided by all Grid centres and the Worldwide LHC Computing Grid (WLCG) collaboration. The ALICE Collaboration acknowledges the following funding agencies for their support in building and running the ALICE detector: A. I. Alikhanyan National Science Laboratory (Yerevan Physics Institute) Foundation (ANSL), State Committee of Science and World Federation of Scientists (WFS), Armenia; Austrian Academy of Sciences, Austrian Science Fund (FWF): [M 2467-N36] and Nationalstiftung für Forschung, Technologie und Entwicklung, Austria; Ministry of Communications and High Technologies, National Nuclear Research Center, Azerbaijan; Conselho Nacional de Desenvolvimento Científico e Tecnológico (CNPq), Financiadora de Estudos e Projetos (Finep), Fundação de Amparo à Pesquisa do Estado de São Paulo (FAPESP) and Universidade Federal do Rio Grande do Sul (UFRGS), Brazil; Bulgarian Ministry of Education and Science, within the National Roadmap for Research Infrastructures 2020¿2027 (object CERN), Bulgaria; Ministry of Education of China (MOEC) , Ministry of Science & Technology of China (MSTC) and National Natural Science Foundation of China (NSFC), China; Ministry of Science and Education and Croatian Science Foundation, Croatia; Centro de Aplicaciones Tecnológicas y Desarrollo Nuclear (CEADEN), Cubaenergía, Cuba; Ministry of Education, Youth and Sports of the Czech Republic, Czech Republic; The Danish Council for Independent Research — Natural Sciences, the VILLUM FONDEN and Danish National Research Foundation (DNRF), Denmark; Helsinki Institute of Physics (HIP), Finland; Commissariat à l'Energie Atomique (CEA) and Institut National de Physique Nucléaire et de Physique des Particules (IN2P3) and Centre National de la Recherche Scientifique (CNRS), France; Bundesministerium für Bildung und Forschung (BMBF) and GSI Helmholtzzentrum für Schwerionenforschung GmbH, Germany; General Secretariat for Research and Technology, Ministry of Education, Research and Religions, Greece; National Research, Development and Innovation Office, Hungary; Department of Atomic Energy Government of India (DAE), Department of Science and Technology, Government of India (DST), University Grants Commission, Government of India (UGC) and Council of Scientific and Industrial Research (CSIR), India; National Research and Innovation Agency - BRIN, Indonesia; Istituto Nazionale di Fisica Nucleare (INFN), Italy; Japanese Ministry of Education, Culture, Sports, Science and Technology (MEXT) and Japan Society for the Promotion of Science (JSPS) KAKENHI, Japan; Consejo Nacional de Ciencia (CONACYT) y Tecnología, through Fondo de Cooperación Internacional en Ciencia y Tecnología (FONCICYT) and Dirección General de Asuntos del Personal Academico (DGAPA), Mexico; Nederlandse Organisatie voor Wetenschappelijk Onderzoek (NWO), Netherlands; The Research Council of Norway, Norway; Commission on Science and Technology for Sustainable Development in the South (COMSATS), Pakistan; Pontificia Universidad Católica del Perú, Peru; Ministry of Education and Science, National Science Centre and WUT ID-UB, Poland; Korea Institute of Science and Technology Information and National Research Foundation of Korea (NRF), Republic of Korea; Ministry of Education and Scientific Research, Institute of Atomic Physics, Ministry of Research and Innovation and Institute of Atomic Physics and University Politehnica of Bucharest, Romania; Joint Institute for Nuclear Research (JINR), Ministry of Education and Science of the Russian Federation, National Research Centre Kurchatov Institute, Russian Science Foundation and Russian Foundation for Basic Research, Russia; Ministry of Education, Science, Research and Sport of the Slovak Republic, Slovakia; National Research Foundation of South Africa, South Africa; Swedish Research Council (VR) and Knut & Alice Wallenberg Foundation (KAW), Sweden; European Organization for Nuclear Research, Switzerland; Suranaree University of Technology (SUT), National Science and Technology Development Agency (NSTDA), Thailand Science Research and Innovation (TSRI) and National Science, Research and Innovation Fund (NSRF), Thailand; Turkish Energy, Nuclear and Mineral Research Agency (TENMAK), Turkey; National Academy of Sciences of Ukraine, Ukraine; Science and Technology Facilities Council (STFC), United Kingdom; National Science Foundation of the United States of America (NSF) and United States

Department of Energy, Office of Nuclear Physics (DOE NP), United States of America. In addition, individual groups or members have received support from: European Research Council, Strong 2020 - Horizon 2020 (grant nos. 950692, 824093), European Union; Academy of Finland (Center of Excellence in Quark Matter) (grant nos. 346327, 346328), Finland.

References

[1] **ALICE** Collaboration, "Letter of Intent: A Forward Calorimeter (FoCal) in the ALICE experiment," Tech. Rep. CERN-LHCC-2020-009. LHCC-I-036, CERN, Geneva, Jun, 2020. https://cds.cern.ch/record/2719928.

[2] A. Accardi *et al.*, "Electron Ion Collider: The next QCD Frontier: Understanding the glue that binds us all," *Eur. Phys. J. A* **52** no. 9, (2016) 268, arXiv:1212.1701 [nucl-ex].

[3] Y. V. Kovchegov and E. Levin, *Quantum Chromodynamics at high energy*, vol. 33 of *Cambridge Monographs on Particle Physics, Nuclear Physics and Cosmology (33)*. Cambridge University Press, 11, 2022.

[4] N. Armesto, "Nuclear shadowing," *J. Phys. G* **32** (2006) R367–R394, arXiv:hep-ph/0604108.

[5] F. Gelis, E. Iancu, J. Jalilian-Marian, and R. Venugopalan, "The Color Glass Condensate," *Ann. Rev. Nucl. Part. Sci.* **60** (2010) 463–489, arXiv:1002.0333 [hep-ph].

[6] P. J. Mulders and J. Rodrigues, "Transverse momentum dependence in gluon distribution and fragmentation functions," *Phys. Rev. D* **63** (2001) 094021, arXiv:hep-ph/0009343.

[7] **LHCb** Collaboration, J. Alves *et al.*, "The LHCb Detector at the LHC," *JINST* **3** (2008) S08005.

[8] **LHCb** Collaboration, R. Aaij *et al.*, "LHCb detector performance," *Int. J. Mod. Phys.* **A30** no. 07, (2015) 1530022, arXiv:1412.6352 [hep-ex].

[9] **LHCb** Collaboration, T. L. Collaboration, "LHCb projections for proton-lead collisions during LHC Runs 3 and 4," CERN. CERN, Geneva, 2018.

[10] D. R. Phillips *et al.*, "Get on the BAND Wagon: A Bayesian Framework for Quantifying Model Uncertainties in Nuclear Dynamics," *J. Phys. G* **48** no. 7, (2021) 072001, arXiv:2012.07704 [nucl-th].

[11] **JETSCAPE** Collaboration, D. Everett *et al.*, "Multisystem Bayesian constraints on the transport coefficients of QCD matter," *Phys. Rev. C* **103** no. 5, (2021) 054904, arXiv:2011.01430 [hep-ph].

[12] **JETSCAPE** Collaboration, S. Cao *et al.*, "Determining the jet transport coefficient $\hat{q}$ from inclusive hadron suppression measurements using Bayesian parameter estimation," *Phys. Rev. C* **104** no. 2, (2021) 024905, arXiv:2102.11337 [nucl-th].

[13] R. Venugopalan *et al.*, "EIC Theory Institute.". https://www.bnl.gov/eic-theory/.

[14] "SURGE collaboration.". https://www.bnl.gov/physics/surge/.

[15] C. Loizides, "Experimental overview on small collision systems at the LHC," *Nucl. Phys.* **A956** (2016) 200–207, arXiv:1602.09138 [nucl-ex].

[16] G.-Y. Qin and X.-N. Wang, "Jet quenching in high-energy heavy-ion collisions," *Int. J. Mod. Phys.* **E24** no. 11, (2015) 1530014, arXiv:1511.00790 [hep-ph]. [,309(2016)].

[17] **New Muon** Collaboration, M. Arneodo *et al.*, "The structure function ratios $F_2^{\mathrm{Li}}/F_2^{\mathrm{d}}$ and $F_2^{\mathrm{C}}/F_2^{\mathrm{D}}$ at small x," *Nucl. Phys.* **B441** (1995) 12–30, arXiv:hep-ex/9504002 [hep-ex].

[18] **New Muon** Collaboration, M. Arneodo *et al.*, "Measurement of the proton and the deuteron structure functions, F_2^{p} and F_2^{d}," *Phys. Lett.* **B364** (1995) 107–115, arXiv:hep-ph/9509406 [hep-ph].

[19] **New Muon** Collaboration, M. Arneodo *et al.*, "The Q^2 dependence of the structure function ratio $F_2^{\mathrm{Sn}}/F_2^{\mathrm{C}}$ and the difference $R^{\mathrm{Sn}} - R^{\mathrm{C}}$ in deep inelastic muon scattering," *Nucl. Phys.* **B481** (1996) 23–39.

[20] **European Muon** Collaboration, J. J. Aubert *et al.*, "The ratio of the nucleon structure functions $F2_n$ for iron and deuterium," *Phys. Lett.* **123B** (1983) 275–278.

[21] E.-C. Aschenauer *et al.*, "The RHIC Cold QCD Plan for 2017 to 2023: A Portal to the EIC," arXiv:1602.03922 [nucl-ex].

[22] J. Brandenburg, "STAR Forward Rapidity Upgrade," *PoS* **HardProbes2020** (2021) 179.

[23] **LHeC Study Group** Collaboration, J. L. Abelleira Fernandez *et al.*, "A Large Hadron Electron Collider at CERN: Report on the physics and design concepts for machine and detector," *J. Phys.* **G39** (2012) 075001, arXiv:1206.2913 [physics.acc-ph].

[24] **FCC** Collaboration, A. Abada *et al.*, "Future Circular Collider: Physics opportunities," *CERN-ACC-2018-0056* (2018) .

[25] **LHCb** Collaboration, T. Boettcher, "Direct photon production at LHCb," *Nucl. Phys.* **A982** (2019) 251–254.

[26] C. L. Da Silva, "Search for gluon saturation at Bjorken-x in $[10^{-6}, 10^{-4}]$ with the LHCb detector(ID:39)," May, 2018. https://cds.cern.ch/record/2319876.

[27] L. V. Gribov, E. M. Levin, and M. G. Ryskin, "Singlet structure function at small x: Unitarization of gluon ladders," *Nucl. Phys.* **B188** (1981) 555–576.

[28] A. H. Mueller and J.-w. Qiu, "Gluon Recombination and Shadowing at Small Values of x," *Nucl. Phys.* **B268** (1986) 427–452.

[29] A. M. Stasto, K. J. Golec-Biernat, and J. Kwiecinski, "Geometric scaling for the total γ^*p cross-section in the low x region," *Phys. Rev. Lett.* **86** (2001) 596–599, arXiv:hep-ph/0007192.

[30] T. Sjöstrand, S. Ask, J. R. Christiansen, R. Corke, N. Desai, P. Ilten, S. Mrenna, S. Prestel, C. O. Rasmussen, and P. Z. Skands, "An Introduction to PYTHIA 8.2," *Comput. Phys. Commun.* **191** (2015) 159–177, arXiv:1410.3012 [hep-ph].

[31] I. Helenius, K. J. Eskola, and H. Paukkunen, "Probing the small-x nuclear gluon distributions with isolated photons at forward rapidities in p–Pb collisions at the LHC," *JHEP* **09** (2014) 138, arXiv:1406.1689 [hep-ph].

[32] **LHCb** Collaboration, R. Aaij *et al.*, "Study of prompt D^0 meson production in p–Pb collisions at $\sqrt{s_{\mathrm{NN}}} = 5$ TeV," *JHEP* **10** (2017) 090, arXiv:1707.02750 [hep-ex].

[33] I. Helenius and H. Paukkunen, "Revisiting the D-meson hadroproduction in general-mass variable flavour number scheme," *JHEP* **05** (2018) 196, arXiv:1804.03557 [hep-ph].

[34] V. N. Gribov and L. N. Lipatov, "Deep inelastic e p scattering in perturbation theory," *Sov. J. Nucl. Phys.* **15** (1972) 438–450. [Yad. Fiz.15,781(1972)].

[35] G. Altarelli and G. Parisi, "Asymptotic freedom in parton language," *Nucl. Phys.* **B126** (1977) 298–318.

[36] Y. L. Dokshitzer, "Calculation of the structure functions for deep inelastic scattering and e^+e^- annihilation by perturbation theory in Quantum Chromodynamics.," *Sov. Phys. JETP* **46** (1977) 641–653. [Zh. Eksp. Teor. Fiz.73,1216(1977)].

[37] G. P. Salam, "An Introduction to leading and next-to-leading BFKL," *Acta Phys. Polon.* **B30** (1999) 3679–3705, arXiv:hep-ph/9910492 [hep-ph].

[38] A. H. Mueller, "A Simple derivation of the JIMWLK equation," *Phys. Lett.* **B523** (2001) 243–248, arXiv:hep-ph/0110169 [hep-ph].

[39] I. Balitsky, "Operator expansion for high-energy scattering," *Nucl. Phys. B* **463** (1996) 99–160, arXiv:hep-ph/9509348.

[40] Y. V. Kovchegov, "Small-x F(2) structure function of a nucleus including multiple pomeron exchanges," *Phys. Rev. D* **60** (1999) 034008, arXiv:hep-ph/9901281.

[41] R. Abdul Khalek *et al.*, "Science requirements and detector concepts for the Electron-Ion Collider: EIC Yellow Report," arXiv:2103.05419 [physics.ins-det].

[42] F. Dominguez, B.-W. Xiao, and F. Yuan, "k_t-factorization for Hard Processes in Nuclei," *Phys. Rev. Lett.* **106** (2011) 022301, arXiv:1009.2141 [hep-ph].

[43] F. Dominguez, C. Marquet, B.-W. Xiao, and F. Yuan, "Universality of Unintegrated Gluon Distributions at small x," *Phys. Rev. D* **83** (2011) 105005, arXiv:1101.0715 [hep-ph].

[44] H.-Y. Liu, X. Liu, J.-C. Pan, F. Yuan, and H. X. Zhu, "Nucleon Energy Correlators for the Color Glass Condensate," arXiv:2301.01788 [hep-ph].

[45] K. Devereaux, W. Fan, W. Ke, K. Lee, and I. Moult, "Imaging Cold Nuclear Matter with Energy Correlators," arXiv:2303.08143 [hep-ph].

[46] **H1, ZEUS** Collaboration, H. Abramowicz *et al.*, "Combination of measurements of inclusive deep inelastic $e^{\pm}p$ scattering cross sections and QCD analysis of HERA data," *Eur. Phys. J.* **C75** no. 12, (2015) 580, arXiv:1506.06042 [hep-ex].

[47] **NNPDF** Collaboration, R. Abdul Khalek, J. J. Ethier, and J. Rojo, "Nuclear parton distributions from lepton-nucleus scattering and the impact of an electron-ion collider," *Eur. Phys. J.* **C79** no. 6, (2019) 471, arXiv:1904.00018 [hep-ph].

[48] R. Abdul Khalek, J. J. Ethier, J. Rojo, and G. van Weelden, "nNNPDF2.0: quark flavor separation in nuclei from LHC data," *JHEP* **09** (2020) 183, arXiv:2006.14629 [hep-ph].

[49] S. Dulat, T.-J. Hou, J. Gao, M. Guzzi, J. Huston, P. Nadolsky, J. Pumplin, C. Schmidt, D. Stump, and C. P. Yuan, "New parton distribution functions from a global analysis of quantum chromodynamics," *Phys. Rev.* **D93** no. 3, (2016) 033006, arXiv:1506.07443 [hep-ph].

[50] J. L. Albacete, N. Armesto, J. G. Milhano, P. Quiroga-Arias, and C. A. Salgado, "AAMQS: A non-linear QCD analysis of new HERA data at small-x including heavy quarks," *Eur. Phys. J. C* **71** (2011) 1705, arXiv:1012.4408 [hep-ph].

[51] K. Kovarik *et al.*, "nCTEQ15 - Global analysis of nuclear parton distributions with uncertainties in the CTEQ framework," *Phys. Rev.* **D93** no. 8, (2016) 085037, arXiv:1509.00792 [hep-ph].

[52] K. J. Eskola, P. Paakkinen, H. Paukkunen, and C. A. Salgado, "EPPS16: Nuclear parton distributions with LHC data," *Eur. Phys. J.* **C77** no. 3, (2017) 163, arXiv:1612.05741 [hep-ph].

[53] K. J. Eskola, P. Paakkinen, H. Paukkunen, and C. A. Salgado, "EPPS21: a global QCD analysis of nuclear PDFs," *Eur. Phys. J. C* **82** no. 5, (2022) 413, arXiv:2112.12462 [hep-ph].

[54] N. Armesto, T. Lappi, H. Mäntysaari, H. Paukkunen, and M. Tevio, "Signatures of gluon saturation from structure-function measurements," *Phys. Rev. D* **105** no. 11, (2022) 114017, arXiv:2203.05846 [hep-ph].

[55] G. Nijs, W. van der Schee, U. Gürsoy, and R. Snellings, "Bayesian analysis of heavy ion collisions with the heavy ion computational framework Trajectum," *Phys. Rev. C* **103** no. 5, (2021) 054909, arXiv:2010.15134 [nucl-th].

[56] G. David, "Direct real photons in relativistic heavy ion collisions," *Rept. Prog. Phys.* **83** no. 4, (2020) 046301, arXiv:1907.08893 [nucl-ex].

[57] S. Catani, M. Fontannaz, J. P. Guillet, and E. Pilon, "Cross-section of isolated prompt photons in hadron hadron collisions," *JHEP* **05** (2002) 028, arXiv:hep-ph/0204023 [hep-ph].

[58] R. Ichou and D. d'Enterria, "Sensitivity of isolated photon production at TeV hadron colliders to the gluon distribution in the proton," *Phys. Rev.* **D82** (2010) 014015, arXiv:1005.4529 [hep-ph].

[59] G. A. Chirilli, B.-W. Xiao, and F. Yuan, "One-loop Factorization for Inclusive Hadron Production in *pA* Collisions in the Saturation Formalism," *Phys. Rev. Lett.* **108** (2012) 122301, arXiv:1112.1061 [hep-ph].

[60] H.-Y. Liu, Z.-B. Kang, and X. Liu, "Threshold resummation for hadron production in the small-x region," *Phys. Rev. D* **102** no. 5, (2020) 051502, arXiv:2004.11990 [hep-ph].

[61] Y. Shi, L. Wang, S.-Y. Wei, and B.-W. Xiao, "Pursuing the Precision Study for Color Glass Condensate in Forward Hadron Productions," *Phys. Rev. Lett.* **128** no. 20, (2022) 202302, arXiv:2112.06975 [hep-ph].

[62] J. Jalilian-Marian and A. H. Rezaeian, "Prompt photon production and photon-hadron correlations at RHIC and the LHC from the Color Glass Condensate," *Phys. Rev. D* **86** (2012) 034016, arXiv:1204.1319 [hep-ph].

[63] A. H. Rezaeian, "Semi-inclusive photon-hadron production in pp and pA collisions at RHIC and LHC," *Phys. Rev.* **D86** (2012) 094016, arXiv:1209.0478 [hep-ph].

[64] S. Benic, K. Fukushima, O. Garcia-Montero, and R. Venugopalan, "Probing gluon saturation with next-to-leading order photon production at central rapidities in proton-nucleus collisions," *JHEP* **01** (2017) 115, arXiv:1609.09424 [hep-ph].

[65] B. Ducloué, T. Lappi, and H. Mäntysaari, "Isolated photon production in proton-nucleus collisions at forward rapidity," *Phys. Rev.* **D97** no. 5, (2018) 054023, arXiv:1710.02206 [hep-ph].

[66] S. Benić, K. Fukushima, O. Garcia-Montero, and R. Venugopalan, "Photons as Probes of Gluon Saturation in Dilute + Dense Collisions," *MDPI Proc.* **10** no. 1, (2019) 33.

[67] G. Sampaio dos Santos, G. Gil da Silveira, and M. V. T. Machado, "Prompt photon production in high-energy *pA* collisions at forward rapidity," *Phys. Rev. C* **102** no. 5, (2020) 054901, arXiv:2006.15743 [hep-ph].

[68] S. Benić, O. Garcia-Montero, and A. Perkov, "Isolated photon-hadron production in high energy pp and pA collisions at RHIC and LHC," *Phys. Rev. D* **105** no. 11, (2022) 114052, arXiv:2203.01685 [hep-ph].

[69] A. H. Rezaeian, "CGC predictions for p+A collisions at the LHC and signature of QCD saturation," *Phys. Lett.* **B718** (2013) 1058–1069, arXiv:1210.2385 [hep-ph].

[70] G. Sampaio dos Santos, G. Gil da Silveira, and M. V. T. Machado, "Prompt photon production in high-energy *pA* collisions at forward rapidity," *Phys. Rev. C* **102** no. 5, (2020) 054901, arXiv:2006.15743 [hep-ph].

[71] J. Jalilian-Marian and A. H. Rezaeian, "Prompt photon production and photon-hadron correlations at RHIC and the LHC from the Color Glass Condensate," *Phys. Rev.* **D86** (2012) 034016, arXiv:1204.1319 [hep-ph].

[72] Z. Belghobsi, M. Fontannaz, J. P. Guillet, G. Heinrich, E. Pilon, and M. Werlen, "Photon–jet correlations and constraints on fragmentation functions," *Phys. Rev. D* **79** (2009) 114024, arXiv:0903.4834 [hep-ph].

[73] **ATLAS** Collaboration, M. Aaboud *et al.*, "Measurement of prompt photon production in $\sqrt{s_{\mathrm{NN}}} = 8.16$ TeV p–Pb collisions with ATLAS," *Phys. Lett. B* **796** (2019) 230–252, arXiv:1903.02209 [nucl-ex].

[74] **ALICE** Collaboration, S. Acharya *et al.*, "Measurement of the inclusive isolated photon production cross section in pp collisions at $\sqrt{s} = 7$ TeV," *Submitted to: Eur. Phys. J.* (2019) , arXiv:1906.01371 [nucl-ex].

[75] **NNPDF** Collaboration, R. D. Ball *et al.*, "Parton distributions from high-precision collider data," *Eur. Phys. J.* **C77** no. 10, (2017) 663, arXiv:1706.00428 [hep-ph].

[76] P. Aurenche, M. Fontannaz, J. P. Guillet, B. A. Kniehl, E. Pilon, and M. Werlen, "A Critical phenomenological study of inclusive photon production in hadronic collisions," *Eur. Phys. J.* **C9** (1999) 107–119, arXiv:hep-ph/9811382 [hep-ph].

[77] A. H. Rezaeian and A. Schafer, "Hadrons and direct photon in pp and pA collisions at LHC and saturation effects," *Phys. Rev.* **D81** (2010) 114032, arXiv:0908.3695 [hep-ph].

[78] S. Benic, K. Fukushima, O. Garcia-Montero, and R. Venugopalan, "Constraining unintegrated gluon distributions from inclusive photon production in proton–proton collisions at the LHC," *Phys. Lett.* **B791** (2019) 11–16, arXiv:1807.03806 [hep-ph].

[79] **LHCb** Collaboration, "Nuclear modification factor of neutral pions in the forward and backward regions in p–Pb collisions," arXiv:2204.10608 [nucl-ex].

[80] K. J. Eskola, I. Helenius, P. Paakkinen, and H. Paukkunen, "A QCD analysis of LHCb D-meson data in p–Pb collisions," arXiv:1906.02512 [hep-ph].

[81] T. Lappi and H. Mäntysaari, "Single inclusive particle production at high energy from HERA data to proton–nucleus collisions," *Phys. Rev. D* **88** (2013) 114020, arXiv:1309.6963 [hep-ph].

[82] **STAR** Collaboration, M. S. Abdallah *et al.*, "Evidence for Nonlinear Gluon Effects in QCD and Their Mass Number Dependence at STAR," *Phys. Rev. Lett.* **129** no. 9, (2022) 092501, arXiv:2111.10396 [nucl-ex].

[83] **ALICE** Collaboration, J. Adam *et al.*, "W and Z boson production in p-Pb collisions at $\sqrt{s_{\mathrm{NN}}} =$ 5.02 TeV," *JHEP* **02** (2017) 077, arXiv:1611.03002 [nucl-ex].

[84] **PHENIX** Collaboration, A. Adare *et al.*, "Suppression of back-to-back hadron pairs at forward rapidity in d+Au Collisions at $\sqrt{s_{NN}} = 200$ GeV," *Phys. Rev. Lett.* **107** (2011) 172301, arXiv:1105.5112 [nucl-ex].

[85] A. Stasto, S.-Y. Wei, B.-W. Xiao, and F. Yuan, "On the dihadron angular correlations in forward pA collisions," *Phys. Lett.* **B784** (2018) 301–306, arXiv:1805.05712 [hep-ph].

[86] H. Mäntysaari and H. Paukkunen, "Saturation and forward jets in proton-lead collisions at the LHC," *Phys. Rev. D* **100** no. 11, (2019) 114029, arXiv:1910.13116 [hep-ph].

[87] H.-y. Liu, K. Xie, Z. Kang, and X. Liu, "Single inclusive jet production in pA collisions at NLO in the small-x regime," *JHEP* **07** (2022) 041, arXiv:2204.03026 [hep-ph].

[88] L. Wang, L. Chen, Z. Gao, Y. Shi, S.-Y. Wei, and B.-W. Xiao, "Forward Inclusive Jet Productions in pA Collisions," arXiv:2211.08322 [hep-ph].

[89] A. van Hameren, P. Kotko, K. Kutak, C. Marquet, E. Petreska, and S. Sapeta, "Forward dijet production in p–Pb collisions in the small-x improved TMD factorization framework," *JHEP* **12** (2016) 034, arXiv:1607.03121 [hep-ph]. [Erratum: JHEP 02, 158 (2019)].

[90] M. A. Al-Mashad, A. van Hameren, H. Kakkad, P. Kotko, K. Kutak, P. van Mechelen, and S. Sapeta, "Dijet azimuthal correlations in pp and p–Pb collisions at forward LHC calorimeters," arXiv:2210.06613 [hep-ph].

[91] P. Kotko, K. Kutak, C. Marquet, E. Petreska, S. Sapeta, and A. van Hameren, "Improved TMD factorization for forward dijet production in dilute-dense hadronic collisions," *JHEP* **09** (2015) 106, arXiv:1503.03421 [hep-ph].

[92] A. van Hameren, "KaTie : For parton-level event generation with k_T-dependent initial states," *Comput. Phys. Commun.* **224** (2018) 371–380, arXiv:1611.00680 [hep-ph].

[93] **CMS** Collaboration, S. Chatrchyan *et al.*, "Studies of dijet transverse momentum balance and pseudorapidity distributions in pPb collisions at $\sqrt{s_{\mathrm{NN}}} = 5.02$ TeV," *Eur. Phys. J. C* **74** no. 7, (2014) 2951, arXiv:1401.4433 [nucl-ex].

[94] K. J. Eskola, H. Paukkunen, and C. A. Salgado, "EPS09: A new generation of NLO and LO nuclear parton distribution functions," *JHEP* **04** (2009) 065, arXiv:0902.4154 [hep-ph].

[95] B. Ducloué, T. Lappi, and H. Mäntysaari, "Forward J/ψ production in proton-nucleus collisions at high energy," *Phys. Rev. D* **91** no. 11, (2015) 114005, arXiv:1503.02789 [hep-ph].

[96] R. A. Khalek, R. Gauld, T. Giani, E. R. Nocera, T. R. Rabemananjara, and J. Rojo, "nNNPDF3.0: Evidence for a modified partonic structure in heavy nuclei," arXiv:2201.12363 [hep-ph].

[97] **ALICE** Collaboration, S. Acharya *et al.*, "Measurement of prompt D^0, D^+, D^{*+}, and D_s^+ production in p–Pb collisions at $\sqrt{s_{\mathrm{NN}}} = 5.02$ TeV," arXiv:1906.03425 [nucl-ex].

[98] **ALICE** Collaboration, B. B. Abelev *et al.*, "Long-range angular correlations of π, K and p in p–Pb collisions at $\sqrt{s_{\mathrm{NN}}}$ = 5.02 TeV," *Phys. Lett.* **B726** (2013) 164–177, arXiv:1307.3237 [nucl-ex].

[99] **ALICE** Collaboration, J. Adam *et al.*, "Forward-central two-particle correlations in p-Pb collisions at $\sqrt{s_{\mathrm{NN}}}$ = 5.02 TeV," *Phys. Lett.* **B753** (2016) 126–139, arXiv:1506.08032 [nucl-ex].

[100] **ALICE** Collaboration, S. Acharya *et al.*, "Search for collectivity with azimuthal J/ψ-hadron correlations in high multiplicity p–Pb collisions at $\sqrt{s_{\mathrm{NN}}}$ = 5.02 and 8.16 TeV," *Phys. Lett.* **B780** (2018) 7–20, arXiv:1709.06807 [nucl-ex].

[101] **ALICE** Collaboration, S. Acharya *et al.*, "Azimuthal anisotropy of heavy-flavour decay electrons in p–Pb collisions at $\sqrt{s_{\mathrm{NN}}}$=5.02 TeV," arXiv:1805.04367 [nucl-ex].

[102] **CMS** Collaboration, A. M. Sirunyan *et al.*, "Elliptic flow of charm and strange hadrons in high-multiplicity p–Pb collisions at $\sqrt{s_{\mathrm{NN}}} = 8.16$ TeV," *Phys. Rev. Lett.* **121** no. 8, (2018) 082301, arXiv:1804.09767 [hep-ex].

[103] S. Klein and P. Steinberg, "Photonuclear and two-photon interactions at high-energy nuclear colliders," *Ann. Rev. Nucl. Part. Sci.* **70** (2020) 323–354, arXiv:2005.01872 [nucl-ex].

[104] J. G. Contreras and J. D. Tapia Takaki, "Ultra-peripheral heavy-ion collisions at the LHC," *Int. J. Mod. Phys. A* **30** (2015) 1542012.

[105] Z. Citron *et al.*, "Future physics opportunities for high-density QCD at the LHC with heavy-ion and proton beams," in *HL/HE-LHC Workshop: Workshop on the Physics of HL-LHC, and Perspectives at HE-LHC Geneva, Switzerland, June 18-20, 2018*. 2018. arXiv:1812.06772 [hep-ph].

[106] A. Bylinkin, J. Nystrand, and D. Tapia Takaki, "Vector meson photoproduction in UPCs with FoCal," arXiv:2211.16107 [nucl-ex].

[107] S. Klein and J. Nystrand, "Exclusive vector meson production in relativistic heavy ion collisions," *Phys. Rev. C* **60** (1999) 014903, arXiv:hep-ph/9902259.

[108] S. P. Jones, A. D. Martin, M. G. Ryskin, and T. Teubner, "Probes of the small x gluon via exclusive J/ψ and Υ production at HERA and the LHC," *JHEP* **11** (2013) 085, arXiv:1307.7099 [hep-ph].

[109] K. J. Eskola, C. A. Flett, V. Guzey, T. Löytäinen, and H. Paukkunen, "Exclusive J/ψ photoproduction in ultraperipheral Pb+Pb collisions at the CERN Large Hadron Collider calculated at next-to-leading order perturbative QCD," *Phys. Rev. C* **106** no. 3, (2022) 035202, arXiv:2203.11613 [hep-ph].

[110] **ALICE** Collaboration, S. Acharya *et al.*, "Energy dependence of exclusive J/ψ photoproduction off protons in ultra-peripheral p–Pb collisions at $\sqrt{s_{\mathrm{NN}}} = 5.02$ TeV," *Eur. Phys. J. C* **79** no. 5, (2019) 402, arXiv:1809.03235 [nucl-ex].

[111] **ALICE** Collaboration, B. B. Abelev *et al.*, "Exclusive J/ψ photoproduction off protons in ultra-peripheral p–Pb collisions at $\sqrt{s_{\mathrm{NN}}} = 5.02$ TeV," *Phys. Rev. Lett.* **113** no. 23, (2014) 232504, arXiv:1406.7819 [nucl-ex].

[112] **H1** Collaboration, C. Alexa *et al.*, "Elastic and Proton-Dissociative Photoproduction of J/ψ Mesons at HERA," *Eur. Phys. J. C* **73** no. 6, (2013) 2466, arXiv:1304.5162 [hep-ex].

[113] **LHCb** Collaboration, R. Aaij *et al.*, "Exclusive J/ψ and ψ(2S) production in pp collisions at $\sqrt{s} = 7$ TeV," *J. Phys. G* **40** (2013) 045001, arXiv:1301.7084 [hep-ex].

[114] **LHCb** Collaboration, R. Aaij *et al.*, "Updated measurements of exclusive J/ψ and ψ(2S) production cross-sections in pp collisions at $\sqrt{s} = 7$ TeV," *J. Phys. G* **41** (2014) 055002, arXiv:1401.3288 [hep-ex].

[115] **LHCb** Collaboration, R. Aaij *et al.*, "Central exclusive production of J/ψ and $\psi(2S)$ mesons in pp collisions at $\sqrt{s} = 13$ TeV," *JHEP* **10** (2018) 167, arXiv:1806.04079 [hep-ex].

[116] S. R. Klein and J. Nystrand, "Interference in exclusive vector meson production in heavy ion collisions," *Phys. Rev. Lett.* **84** (2000) 2330–2333, arXiv:hep-ph/9909237.

[117] **ALICE** Collaboration, S. Acharya *et al.*, "Energy dependence of exclusive J/ψ photoproduction off protons in ultra-peripheral p–Pb collisions at $\sqrt{s_{\mathrm{NN}}} = 5.02$ TeV," *Eur. Phys. J.* **C79** no. 5, (2019) 402, arXiv:1809.03235 [nucl-ex].

[118] **ZEUS** Collaboration, S. Chekanov *et al.*, "Exclusive photoproduction of J/ψ mesons at HERA," *Eur. Phys. J. C* **24** (2002) 345–360, arXiv:hep-ex/0201043.

[119] J. Cepila, J. G. Contreras, and J. D. Tapia Takaki, "Energy dependence of dissociative J/ψ photoproduction as a signature of gluon saturation at the LHC," *Phys. Lett.* **B766** (2017) 186–191, arXiv:1608.07559 [hep-ph].

[120] I. Bautista, A. Fernandez Tellez, and M. Hentschinski, "BFKL evolution and the growth with energy of exclusive J/ψ and Υ photoproduction cross sections," *Phys. Rev. D* **94** no. 5, (2016) 054002, arXiv:1607.05203 [hep-ph].

[121] N. Armesto and A. H. Rezaeian, "Exclusive vector meson production at high energies and gluon saturation," *Phys. Rev. D* **90** no. 5, (2014) 054003, arXiv:1402.4831 [hep-ph].

[122] S. R. Klein, J. Nystrand, J. Seger, Y. Gorbunov, and J. Butterworth, "STARlight: A Monte Carlo simulation program for ultra-peripheral collisions of relativistic ions," *Comput. Phys. Commun.* **212** (2017) 258–268, arXiv:1607.03838 [hep-ph].

[123] M. Hentschinski *et al.*, "White Paper on Forward Physics, BFKL, Saturation Physics and Diffraction," arXiv:2203.08129 [hep-ph].

[124] **H1** Collaboration, C. Adloff *et al.*, "Diffractive photoproduction of ψ(2S) mesons at HERA," *Phys. Lett. B* **541** (2002) 251–264, arXiv:hep-ex/0205107.

[125] **ZEUS** Collaboration, I. Abt *et al.*, "Measurement of the cross-section ratio $\sigma_{\psi(2S)}/\sigma_{J/\psi}$ in exclusive photoproduction at HERA," *JHEP* **12** (2022) 164, arXiv:2206.13343 [hep-ex].

[126] H. Mäntysaari and B. Schenke, "Evidence of strong proton shape fluctuations from incoherent diffraction," *Phys. Rev. Lett.* **117** no. 5, (2016) 052301, arXiv:1603.04349 [hep-ph].

[127] H. Mäntysaari and B. Schenke, "Revealing proton shape fluctuations with incoherent diffraction at high energy," *Phys. Rev. D* **94** no. 3, (2016) 034042, arXiv:1607.01711 [hep-ph].

[128] S. R. Klein and H. Mäntysaari, "Imaging the nucleus with high-energy photons," *Nature Rev. Phys.* **1** no. 11, (2019) 662–674, arXiv:1910.10858 [hep-ex].

[129] S. R. Klein, "Challenges to the Good-Walker paradigm in coherent and incoherent photoproduction," arXiv:2301.01408 [hep-ph].

[130] J. Cepila, J. G. Contreras, M. Krelina, and J. D. Tapia Takaki, "Mass dependence of vector meson photoproduction off protons and nuclei within the energy-dependent hot-spot model," *Nucl. Phys. B* **934** (2018) 330–340, arXiv:1804.05508 [hep-ph].

[131] **ALICE** Collaboration, B. Abelev *et al.*, "Coherent J/ψ photoproduction in ultra-peripheral Pb-Pb collisions at $\sqrt{s_{NN}} = 2.76$ TeV," *Phys. Lett. B* **718** (2013) 1273–1283, arXiv:1209.3715 [nucl-ex].

[132] **ALICE** Collaboration, S. Acharya *et al.*, "Coherent J/ψ and ψ' photoproduction at midrapidity in ultra-peripheral Pb–Pb collisions at $\sqrt{s_{\rm NN}} = 5.02$ TeV," arXiv:2101.04577 [nucl-ex].

[133] **ALICE** Collaboration, S. Acharya *et al.*, "Coherent J/ψ photoproduction at forward rapidity in ultra-peripheral Pb–Pb collisions at $\sqrt{s_{\rm NN}} = 5.02$ TeV," arXiv:1904.06272 [nucl-ex].

[134] **ALICE** Collaboration, E. Abbas *et al.*, "Charmonium and e^+e^- pair photoproduction at mid-rapidity in ultra-peripheral Pb-Pb collisions at $\sqrt{s_{\rm NN}}$=2.76 TeV," *Eur. Phys. J.* **C73** no. 11, (2013) 2617, arXiv:1305.1467 [nucl-ex].

[135] **ALICE** Collaboration, J. Adam *et al.*, "Coherent ρ^0 photoproduction in ultra-peripheral Pb-Pb collisions at $\sqrt{s_{\rm NN}} = 2.76$ TeV," *JHEP* **09** (2015) 095, arXiv:1503.09177 [nucl-ex].

[136] **ALICE** Collaboration, "Coherent ψ(2S) photo-production in ultra-peripheral Pb Pb collisions at $\sqrt{s_{NN}}$ = 2.76 TeV," *Phys. Lett.* **B751** (2015) 358–370, arXiv:1508.05076 [nucl-ex].

[137] V. Guzey, M. Strikman, and M. Zhalov, "Disentangling coherent and incoherent quasielastic J/ψ photoproduction on nuclei by neutron tagging in ultraperipheral ion collisions at the LHC," *Eur. Phys. J.* **C74** no. 7, (2014) 2942, arXiv:1312.6486 [hep-ph].

[138] **STAR** Collaboration, L. Adamczyk *et al.*, "Coherent diffractive photoproduction of ρ^0mesons on gold nuclei at 200 GeV/nucleon-pair at the Relativistic Heavy Ion Collider," *Phys. Rev. C* **96** no. 5, (2017) 054904, arXiv:1702.07705 [nucl-ex].

[139] **STAR** Collaboration, S. R. Klein, "Dipion photoproduction and the Q^2 evolution of the shape of the gold nucleus," *PoS* **DIS2018** (2018) 047, arXiv:1807.00455 [nucl-ex].

[140] **ATLAS** Collaboration, A. Angerami, "Measurements of photo-nuclear jet production in Pb–Pb collisions with ATLAS," *Nucl. Phys.* **A967** (2017) 277–280.

[141] **CMS** Collaboration, "Azimuthal correlations within exclusive dijets with large momentum transfer in photon-lead collisions," arXiv:2205.00045 [nucl-ex].

[142] J. L. Nagle and W. A. Zajc, "Small system collectivity in relativistic hadronic and nuclear collisions," *Ann. Rev. Nucl. Part. Sci.* **68** (2018) 211–235, arXiv:1801.03477 [nucl-ex].

[143] **ALICE** Collaboration, B. Abelev *et al.*, "Long-range angular correlations on the near and away side in p–Pb collisions at $\sqrt{s_{\rm NN}} = 5.02$ TeV," *Phys. Lett.* **B719** (2013) 29–41, arXiv:1212.2001 [nucl-ex].

[144] **ATLAS** Collaboration, "Measurement of the long–range pseudorapidity correlations between muons and charged-particles in $\sqrt{s_{\rm NN}}$=8.16 TeV proton-lead collisions with the ATLAS detector," Tech. Rep. ATLAS-CONF-2017-006, CERN, Geneva, Feb, 2017. http://cds.cern.ch/record/2244808.

[145] J.-Y. Ollitrault, "Anisotropy as a signature of transverse collective flow," *Phys. Rev.* **D46** (1992) 229–245.

[146] **ALICE** Collaboration, "Measurements of azimuthal anisotropies at forward and backward rapidity with muons in high-multiplicity p–Pb collisions at $\sqrt{s_{\rm NN}} = 8.16$ TeV," arXiv:2210.08980 [nucl-ex].

[147] J. L. Albacete, P. Guerrero-Rodríguez, and C. Marquet, "Initial correlations of the Glasma energy-momentum tensor," arXiv:1808.00795 [hep-ph].

[148] T. Altinoluk, N. Armesto, and D. E. Wertepny, "Correlations and the ridge in the Color Glass Condensate beyond the glasma graph approximation," *JHEP* **05** (2018) 207, arXiv:1804.02910 [hep-ph].

[149] A. Kurkela, U. A. Wiedemann, and B. Wu, "Nearly isentropic flow at sizeable η/s," arXiv:1803.02072 [hep-ph].

[150] A. Kurkela, U. A. Wiedemann, and B. Wu, "Kinetic transport is needed to reliably extract shear viscosity from pA and AA data," arXiv:1805.04081 [hep-ph].

[151] C. Zhang, C. Marquet, G.-Y. Qin, Y. Shi, L. Wang, S.-Y. Wei, and B.-W. Xiao, "Collectivity of heavy mesons in proton-nucleus collisions," *Phys. Rev. D* **102** no. 3, (2020) 034010, arXiv:2002.09878 [hep-ph].

[152] X. Du and R. Rapp, "In-medium charmonium production in proton–nucleus collisions," *JHEP* **03** (2019) 015, arXiv:1808.10014 [nucl-th].

[153] B. Schenke, S. Schlichting, and P. Singh, "Rapidity dependence of initial state geometry and momentum correlations in p+Pb collisions," *Phys. Rev. D* **105** no. 9, (2022) 094023, arXiv:2201.08864 [nucl-th].

[154] B. Schenke, C. Shen, and P. Tribedy, "Hybrid Color Glass Condensate and hydrodynamic description of the Relativistic Heavy Ion Collider small system scan," *Phys. Lett. B* **803** (2020) 135322, arXiv:1908.06212 [nucl-th].

[155] **PHENIX** Collaboration, C. Aidala *et al.*, "Measurements of azimuthal anisotropy and charged-particle multiplicity in d+Au collisions at $\sqrt{s_{NN}}$ =200, 62.4, 39, and 19.6 GeV," *Phys. Rev. C* **96** no. 6, (2017) 064905, arXiv:1708.06983 [nucl-ex].

[156] L.-G. Pang, H. Petersen, and X.-N. Wang, "Pseudorapidity distribution and decorrelation of anisotropic flow within the open-computing-language implementation CLVisc hydrodynamics," *Phys. Rev. C* **97** no. 6, (2018) 064918, arXiv:1802.04449 [nucl-th].

[157] D. E. Kharzeev and E. M. Levin, "Deep inelastic scattering as a probe of entanglement," *Phys. Rev. D* **95** no. 11, (2017) 114008, arXiv:1702.03489 [hep-ph].

[158] Z. Tu, D. E. Kharzeev, and T. Ullrich, "Einstein-Podolsky-Rosen paradox and quantum entanglement at subnucleonic scales," *Phys. Rev. Lett.* **124** no. 6, (2020) 062001, arXiv:1904.11974 [hep-ph].

[159] **PHENIX** Collaboration, A. Adare *et al.*, "Suppression pattern of neutral pions at high transverse momentum in Au–Au collisions at $\sqrt{s_{\rm NN}}$ = 200 GeV and constraints on medium transport coefficients," *Phys. Rev. Lett.* **101** (2008) 232301, arXiv:0801.4020 [nucl-ex].

[160] **BRAHMS** Collaboration, I. Arsene *et al.*, "Nuclear modification factor for charged pions and protons at forward rapidity in central Au–Au collisions at 200-GeV," *Phys. Lett.* **B650** (2007) 219–223, arXiv:nucl-ex/0610021 [nucl-ex].

[161] T. Renk, "The rapidity dependence of jet quenching," arXiv:1406.6784 [hep-ph].

[162] **ATLAS** Collaboration, G. Aad *et al.*, "Measurement of charged-particle spectra in Pb–Pb collisions at $\sqrt{s_{\rm NN}} = 2.76$ TeV with the ATLAS detector at the LHC," *JHEP* **09** (2015) 050, arXiv:1504.04337 [hep-ex].

[163] **ALICE** Collaboration, B. Abelev *et al.*, "J/ψ suppression at forward rapidity in Pb–Pb collisions at $\sqrt{s_{\rm NN}} = 2.76$ TeV," *Phys. Rev. Lett.* **109** (2012) 072301, arXiv:1202.1383 [hep-ex].

[164] **ALICE** Collaboration, B. B. Abelev *et al.*, "Centrality, rapidity and transverse momentum dependence of J/ψ suppression in Pb–Pb collisions at $\sqrt{s_{\rm NN}}$=2.76 TeV," *Phys. Lett.* **B734** (2014) 314–327, arXiv:1311.0214 [nucl-ex].

A The ALICE Collaboration

S. Acharya [126], D. Adamová [87], A. Adler[70], G. Aglieri Rinella [33], M. Agnello [30], N. Agrawal [51], Z. Ahammed [133], S. Ahmad [16], S.U. Ahn [71], I. Ahuja [38], A. Akindinov [141], M. Al-Turany [98], D. Aleksandrov [141], B. Alessandro [56], H.M. Alfanda [6], R. Alfaro Molina [67], B. Ali [16], A. Alici [26], N. Alizadehvandchali [115], A. Alkin [33], J. Alme [21], G. Alocco [52], T. Alt [64], A.R. Altamura [50], I. Altsybeev [96], M.N. Anaam [6], C. Andrei [46], A. Andronic [136], V. Anguelov [95], F. Antinori [54], P. Antonioli [51], N. Apadula [75], L. Aphecetche [104], H. Appelshäuser [64], C. Arata [74], S. Arcelli [26], M. Aresti [52], R. Arnaldi [56], J.G.M.C.A. Arneiro [111], I.C. Arsene [20], M. Arslandok [138], A. Augustinus [33], R. Averbeck [98], M.D. Azmi [16], H. Baba[123], A. Badalà [53], J. Bae [105], Y.W. Baek [41], X. Bai [119], R. Bailhache [64], Y. Bailung [48], A. Balbino [30], A. Baldisseri [129], B. Balis [2], D. Banerjee [4], Z. Banoo [92], R. Barbera [27], F. Barile [32], L. Barioglio [96], M. Barlou[79], G.G. Barnaföldi [137], L.S. Barnby [86], V. Barret [126], L. Barreto [111], C. Bartels [118], K. Barth [33], E. Bartsch [64], N. Bastid [126], S. Basu [76], G. Batigne [104], D. Battistini [96], B. Batyunya [142], D. Bauri[47], J.L. Bazo Alba [102], I.G. Bearden [84], C. Beattie [138], P. Becht [98], D. Behera [48], I. Belikov [128], A.D.C. Bell Hechavarria [136], F. Bellini [26], R. Bellwied [115], S. Belokurova [141], G. Bencedi [137], S. Beole [25], A. Bercuci [46], Y. Berdnikov [141], A. Berdnikova [95], L. Bergmann [95], M.G. Besoiu [63], L. Betev [33], P.P. Bhaduri [133], A. Bhasin [92], M.A. Bhat [4], B. Bhattacharjee [42], L. Bianchi [25], N. Bianchi [49], J. Bielčík [36], J. Bielčíková [87], J. Biernat [108], A.P. Bigot [128], A. Bilandzic [96], G. Biro [137], S. Biswas [4], N. Bize [104], J.T. Blair [109], D. Blau [141], M.B. Blidaru [98], N. Bluhme[39], C. Blume [64], G. Boca [22,55], F. Bock [88], T. Bodova [21], A. Bogdanov[141], S. Boi [23], J. Bok [58], L. Boldizsár [137], M. Bombara [38], P.M. Bond [33], G. Bonomi [132,55], H. Borel [129], A. Borissov [141], A.G. Borquez Carcamo [95], H. Bossi [138], E. Botta [25], Y.E.M. Bouziani [64], L. Bratrud [64], P. Braun-Munzinger [98], M. Bregant [111], M. Broz [36], G.E. Bruno [97,32], M.D. Buckland [24], D. Budnikov [141], H. Buesching [64], S. Bufalino [30], P. Buhler [103], N. Burmasov [141], Z. Buthelezi [68,122], A. Bylinkin [21], S.A. Bysiak[108], M. Cai [6], H. Caines [138], A. Caliva [29], E. Calvo Villar [102], J.M.M. Camacho [110], P. Camerini [24], F.D.M. Canedo [111], M. Carabas [125], A.A. Carballo [33], F. Carnesecchi [33], R. Caron [127], L.A.D. Carvalho [111], J. Castillo Castellanos [129], F. Catalano [33,25], C. Ceballos Sanchez [142], I. Chakaberia [75], P. Chakraborty [47], S. Chandra [133], S. Chapeland [33], M. Chartier [118], S. Chattopadhyay [133], S. Chattopadhyay [100], T.G. Chavez [45], T. Cheng [98,6], C. Cheshkov [127], B. Cheynis [127], V. Chibante Barroso [33], D.D. Chinellato [112], E.S. Chizzali [I,96], J. Cho [58], S. Cho [58], P. Chochula [33], P. Christakoglou [85], C.H. Christensen [84], P. Christiansen [76], T. Chujo [124], M. Ciacco [30], C. Cicalo [52], F. Cindolo [51], M.R. Ciupek[98], G. Clai[II,51], F. Colamaria [50], J.S. Colburn[101], D. Colella [97,32], M. Colocci [26], G. Conesa Balbastre [74], Z. Conesa del Valle [73], G. Contin [24], J.G. Contreras [36], M.L. Coquet [129], P. Cortese [131,56], M.R. Cosentino [113], F. Costa [33], S. Costanza [22,55], C. Cot [73], J. Crkovská [95], P. Crochet [126], R. Cruz-Torres [75], P. Cui [6], A. Dainese [54], M.C. Danisch [95], A. Danu [63], P. Das [81], P. Das [4], S. Das [4], A.R. Dash [136], S. Dash [47], A. De Caro [29], G. de Cataldo [50], J. de Cuveland[39], A. De Falco [23], D. De Gruttola [29], N. De Marco [56], C. De Martin [24], S. De Pasquale [29], R. Deb[132], S. Deb [48], R. Del Grande [96], L. Dello Stritto [29], W. Deng [6], P. Dhankher [19], D. Di Bari [32], A. Di Mauro [33], B. Diab [129], R.A. Diaz [142,7], T. Dietel [114], Y. Ding [6], R. Divià [33], D.U. Dixit [19], Ø. Djuvsland[21], U. Dmitrieva [141], A. Dobrin [63], B. Dönigus [64], J.M. Dubinski[134], A. Dubla [98], S. Dudi [91], P. Dupieux [126], M. Durkac[107], N. Dzalaiova[13], T.M. Eder [136], R.J. Ehlers [75], F. Eisenhut [64], R. Ejima[93], D. Elia [50], B. Erazmus [104], F. Ercolessi [26], F. Erhardt [90], M.R. Ersdal[21], B. Espagnon [73], G. Eulisse [33], D. Evans [101], S. Evdokimov [141], L. Fabbietti [96], M. Faggin [28], J. Faivre [74], F. Fan [6], W. Fan [75], A. Fantoni [49], M. Fasel [88], P. Fecchio[30], A. Feliciello [56], G. Feofilov [141], A. Fernández Téllez [45], L. Ferrandi [111], M.B. Ferrer [33], A. Ferrero [129], C. Ferrero [56], A. Ferretti [25], V.J.G. Feuillard [95], V. Filova [36], D. Finogeev [141], F.M. Fionda [52], F. Flor [115], A.N. Flores [109], S. Foertsch [68], I. Fokin [95], S. Fokin [141], E. Fragiacomo [57], E. Frajna [137], U. Fuchs [33], N. Funicello [29], C. Furget [74], A. Furs [141], T. Fusayasu [99], J.J. Gaardhøje [84], M. Gagliardi [25], A.M. Gago [102], T. Gahlaut[47], C.D. Galvan [110], D.R. Gangadharan [115], P. Ganoti [79], C. Garabatos [98], A.T. Garcia [73], J.R.A. Garcia [45], E. Garcia-Solis [9], C. Gargiulo [33], K. Garner[136], P. Gasik [98], A. Gautam [117], M.B. Gay Ducati [66], M. Germain [104], A. Ghimouz[124], C. Ghosh[133], M. Giacalone [51], G. Gioachin [30], P. Giubellino [98,56], P. Giubilato [28], A.M.C. Glaenzer [129], P. Glässel [95], E. Glimos [121], D.J.Q. Goh[77], V. Gonzalez [135], M. Gorgon [2], K. Goswami [48], S. Gotovac[34], V. Grabski [67], L.K. Graczykowski [134], E. Grecka [87], A. Grelli [59], C. Grigoras [33], V. Grigoriev [141], S. Grigoryan [142,1], F. Grosa [33], J.F. Grosse-Oetringhaus [33], R. Grosso [98], D. Grund [36], G.G. Guardiano [112], R. Guernane [74], M. Guilbaud [104], K. Gulbrandsen [84], T. Gundem [64], T. Gunji [123], W. Guo [6], A. Gupta [92],

R. Gupta [92], R. Gupta [48], S.P. Guzman [45], K. Gwizdziel [134], L. Gyulai [137], C. Hadjidakis [73], F.U. Haider [92], H. Hamagaki [77], A. Hamdi [75], M. Hamid[6], Y. Han [139], B.G. Hanley [135], R. Hannigan [109], J. Hansen [76], M.R. Haque [134], J.W. Harris [138], A. Harton [9], H. Hassan [88], D. Hatzifotiadou [51], P. Hauer [43], L.B. Havener [138], S.T. Heckel [96], E. Hellbär [98], H. Helstrup [35], M. Hemmer [64], T. Herman [36], G. Herrera Corral [8], F. Herrmann[136], S. Herrmann [127], K.F. Hetland [35], B. Heybeck [64], H. Hillemanns [33], B. Hippolyte [128], F.W. Hoffmann [70], B. Hofman [59], G.H. Hong [139], M. Horst [96], A. Horzyk [2], Y. Hou [6], P. Hristov [33], C. Hughes [121], P. Huhn[64], L.M. Huhta [116], T.J. Humanic [89], A. Hutson [115], D. Hutter [39], R. Ilkaev[141], H. Ilyas [14], M. Inaba [124], G.M. Innocenti [33], M. Ippolitov [141], A. Isakov [85,87], T. Isidori [117], M.S. Islam [100], M. Ivanov[13], M. Ivanov [98], V. Ivanov [141], K.E. Iversen [76], M. Jablonski [2], B. Jacak [75], N. Jacazio [26], P.M. Jacobs [75], S. Jadlovska[107], J. Jadlovsky[107], S. Jaelani [83], C. Jahnke [112], M.J. Jakubowska [134], M.A. Janik [134], T. Janson[70], S. Ji [17], S. Jia [10], A.A.P. Jimenez [65], F. Jonas [88], D.M. Jones [118], J.M. Jowett [33,98], J. Jung [64], M. Jung [64], A. Junique [33], A. Jusko [101], M.J. Kabus [33,134], J. Kaewjai[106], P. Kalinak [60], A.S. Kalteyer [98], A. Kalweit [33], V. Kaplin [141], A. Karasu Uysal [72], D. Karatovic [90], O. Karavichev [141], T. Karavicheva [141], P. Karczmarczyk [134], E. Karpechev [141], U. Kebschull [70], R. Keidel [140], D.L.D. Keijdener[59], M. Keil [33], B. Ketzer [43], S.S. Khade [48], A.M. Khan [119,6], S. Khan [16], A. Khanzadeev [141], Y. Kharlov [141], A. Khatun [117], A. Khuntia [36], M.B. Kidson[114], B. Kileng [35], B. Kim [105], C. Kim [17], D.J. Kim [116], E.J. Kim [69], J. Kim [139], J.S. Kim [41], J. Kim [58], J. Kim [69], M. Kim [19], S. Kim [18], T. Kim [139], K. Kimura [93], S. Kirsch [64], I. Kisel [39], S. Kiselev [141], A. Kisiel [134], J.P. Kitowski [2], J.L. Klay [5], J. Klein [33], S. Klein [75], C. Klein-Bösing [136], M. Kleiner [64], T. Klemenz [96], A. Kluge [33], A.G. Knospe [115], C. Kobdaj [106], T. Kollegger[98], A. Kondratyev [142], N. Kondratyeva [141], E. Kondratyuk [141], J. Konig [64], S.A. Konigstorfer [96], P.J. Konopka [33], G. Kornakov [134], S.D. Koryciak [2], A. Kotliarov [87], V. Kovalenko [141], M. Kowalski [108], V. Kozhuharov [37], I. Králik [60], A. Kravčáková [38], L. Krcal [33,39], M. Krivda [101,60], F. Krizek [87], K. Krizkova Gajdosova [33], M. Kroesen [95], M. Krüger [64], D.M. Krupova [36], E. Kryshen [141], V. Kučera [58], C. Kuhn [128], P.G. Kuijer [85], T. Kumaoka[124], D. Kumar[133], L. Kumar [91], N. Kumar[91], S. Kumar [32], S. Kundu [33], P. Kurashvili [80], A. Kurepin [141], A.B. Kurepin [141], A. Kuryakin [141], S. Kushpil [87], M.J. Kweon [58], Y. Kwon [139], S.L. La Pointe [39], P. La Rocca [27], A. Lakrathok[106], M. Lamanna [33], R. Langoy [120], P. Larionov [33], E. Laudi [33], L. Lautner [33,96], R. Lavicka [103], R. Lea [132,55], H. Lee [105], I. Legrand [46], G. Legras [136], J. Lehrbach [39], T.M. Lelek[2], R.C. Lemmon [86], I. León Monzón [110], M.M. Lesch [96], E.D. Lesser [19], P. Lévai [137], X. Li[10], X.L. Li[6], J. Lien [120], R. Lietava [101], I. Likmeta [115], B. Lim [25], S.H. Lim [17], V. Lindenstruth [39], C. Lippmann [98], A. Liu [19], D.H. Liu [6], J. Liu [118], G.S.S. Liveraro [112], I.M. Lofnes [21], C. Loizides [88], S. Lokos [108], J. Lomker [59], P. Loncar [34], X. Lopez [126], E. López Torres [7], P. Lu [98,119], J.R. Luhder [136], M. Lunardon [28], G. Luparello [57], Y.G. Ma [40], M. Mager [33], A. Maire [128], M.V. Makariev [37], M. Malaev [141], G. Malfattore [26], N.M. Malik [92], Q.W. Malik[20], S.K. Malik [92], L. Malinina [V,142], D. Mallick [81], N. Mallick [48], G. Mandaglio [31,53], S.K. Mandal [80], V. Manko [141], F. Manso [126], V. Manzari [50], Y. Mao [6], R.W. Marcjan [2], G.V. Margagliotti [24], A. Margotti [51], A. Marín [98], C. Markert [109], P. Martinengo [33], M.I. Martínez [45], G. Martínez García [104], M.P.P. Martins [111], S. Masciocchi [98], M. Masera [25], A. Masoni [52], L. Massacrier [73], O. Massen [59], A. Mastroserio [130,50], O. Matonoha [76], S. Mattiazzo [28], P.F.T. Matuoka[111], A. Matyja [108], C. Mayer [108], A.L. Mazuecos [33], F. Mazzaschi [25], M. Mazzilli [33], J.E. Mdhluli [122], A.F. Mechler[64], Y. Melikyan [44], A. Menchaca-Rocha [67], E. Meninno [103,29], A.S. Menon [115], M. Meres [13], S. Mhlanga[114,68], Y. Miake[124], L. Micheletti [33], L.C. Migliorin[127], D.L. Mihaylov [96], K. Mikhaylov [142,141], A.N. Mishra [137], D. Miśkowiec [98], A. Modak [4], A.P. Mohanty [59], B. Mohanty[81], M. Mohisin Khan [III,16], M.A. Molander [44], S. Monira [134], Z. Moravcova [84], C. Mordasini [116], D.A. Moreira De Godoy [136], I. Morozov [141], A. Morsch [33], T. Mrnjavac [33], V. Muccifora [49], S. Muhuri [133], J.D. Mulligan [75], A. Mulliri[23], M.G. Munhoz [111], R.H. Munzer [64], H. Murakami [123], S. Murray [114], L. Musa [33], J. Musinsky [60], J.W. Myrcha [134], B. Naik [122], A.I. Nambrath [19], B.K. Nandi [47], R. Nania [51], E. Nappi [50], A.F. Nassirpour [18,76], A. Nath [95], C. Nattrass [121], M.N. Naydenov [37], A. Neagu[20], A. Negru[125], L. Nellen [65], R. Nepeivoda [76], S. Nese [20], G. Neskovic [39], B.S. Nielsen [84], E.G. Nielsen [84], S. Nikolaev [141], S. Nikulin [141], V. Nikulin [141], F. Noferini [51], S. Noh [12], P. Nomokonov [142], J. Norman [118], N. Novitzky [124], P. Nowakowski [134], A. Nyanin [141], J. Nystrand [21], M. Ogino [77], S. Oh [18], A. Ohlson [76], V.A. Okorokov [141], J. Oleniacz [134], A.C. Oliveira Da Silva [121], M.H. Oliver [138], A. Onnerstad [116], C. Oppedisano [56], A. Ortiz Velasquez [65], J. Otwinowski [108], M. Oya[93], K. Oyama [77], Y. Pachmayer [95], S. Padhan [47], D. Pagano [132,55], G. Paić [65], A. Palasciano [50],

S. Panebianco [129], H. Park [124], H. Park [105], J. Park [58], J.E. Parkkila [33], Y. Patley [47], R.N. Patra[92], B. Paul [23], H. Pei [6], T. Peitzmann [59], X. Peng [11], M. Pennisi [25], S. Perciballi [25], D. Peresunko [141], G.M. Perez [7], Y. Pestov[141], V. Petrov [141], M. Petrovici [46], R.P. Pezzi [104,66], S. Piano [57], M. Pikna [13], P. Pillot [104], O. Pinazza [51,33], L. Pinsky[115], C. Pinto [96], S. Pisano [49], M. Płoskoń [75], M. Planinic[90], F. Pliquett[64], M.G. Poghosyan [88], B. Polichtchouk [141], S. Politano [30], N. Poljak [90], A. Pop [46], S. Porteboeuf-Houssais [126], V. Pozdniakov [142], I.Y. Pozos [45], K.K. Pradhan [48], S.K. Prasad [4], S. Prasad [48], R. Preghenella [51], F. Prino [56], C.A. Pruneau [135], I. Pshenichnov [141], M. Puccio [33], S. Pucillo [25], Z. Pugelova[107], S. Qiu [85], L. Quaglia [25], R.E. Quishpe[115], S. Ragoni [15], A. Rakotozafindrabe [129], L. Ramello [131,56], F. Rami [128], S.A.R. Ramirez [45], T.A. Rancien[74], M. Rasa [27], S.S. Räsänen [44], R. Rath [51], M.P. Rauch [21], I. Ravasenga [85], K.F. Read [88,121], C. Reckziegel [113], A.R. Redelbach [39], K. Redlich [IV,80], C.A. Reetz [98], A. Rehman[21], F. Reidt [33], H.A. Reme-Ness [35], Z. Rescakova[38], K. Reygers [95], A. Riabov [141], V. Riabov [141], R. Ricci [29], M. Richter [20], A.A. Riedel [96], W. Riegler [33], A.G. Riffero [25], C. Ristea [63], M.V. Rodriguez [33], M. Rodríguez Cahuantzi [45], K. Røed [20], R. Rogalev [141], E. Rogochaya [142], T.S. Rogoschinski [64], D. Rohr [33], D. Röhrich [21], P.F. Rojas[45], S. Rojas Torres [36], P.S. Rokita [134], G. Romanenko [26], F. Ronchetti [49], A. Rosano [31,53], E.D. Rosas[65], K. Roslon [134], A. Rossi [54], A. Roy [48], S. Roy [47], N. Rubini [26], O.V. Rueda [115], D. Ruggiano [134], R. Rui [24], P.G. Russek [2], R. Russo [85], A. Rustamov [82], E. Ryabinkin [141], Y. Ryabov [141], A. Rybicki [108], H. Rytkonen [116], J. Ryu [17], W. Rzesa [134], O.A.M. Saarimaki [44], S. Sadhu [32], S. Sadovsky [141], J. Saetre [21], K. Šafařík [36], P. Saha[42], S.K. Saha [4], S. Saha [81], B. Sahoo [47], B. Sahoo [48], R. Sahoo [48], S. Sahoo[61], D. Sahu [48], P.K. Sahu [61], J. Saini [133], K. Sajdakova[38], S. Sakai [124], M.P. Salvan [98], S. Sambyal [92], D. Samitz [103], I. Sanna [33,96], T.B. Saramela[111], D. Sarkar [135], N. Sarkar[133], P. Sarma [42], V. Sarritzu [23], V.M. Sarti [96], M.H.P. Sas [138], J. Schambach [88], H.S. Scheid [64], C. Schiaua [46], R. Schicker [95], A. Schmah[98], C. Schmidt [98], H.R. Schmidt[94], M.O. Schmidt [33], M. Schmidt[94], N.V. Schmidt [88], A.R. Schmier [121], R. Schotter [128], A. Schröter [39], J. Schukraft [33], K. Schweda [98], G. Scioli [26], E. Scomparin [56], J.E. Seger [15], Y. Sekiguchi[123], D. Sekihata [123], M. Selina [85], I. Selyuzhenkov [98], S. Senyukov [128], J.J. Seo [95,58], D. Serebryakov [141], L. Šerkšnytė [96], A. Sevcenco [63], T.J. Shaba [68], A. Shabetai [104], R. Shahoyan[33], A. Shangaraev [141], A. Sharma[91], B. Sharma [92], D. Sharma [47], H. Sharma [54,108], M. Sharma [92], S. Sharma [77], S. Sharma [92], U. Sharma [92], A. Shatat [73], O. Sheibani[115], K. Shigaki [93], M. Shimomura[78], J. Shin[12], S. Shirinkin [141], Q. Shou [40], Y. Sibiriak [141], S. Siddhanta [52], T. Siemiarczuk [80], T.F. Silva [111], D. Silvermyr [76], T. Simantathammakul[106], R. Simeonov [37], B. Singh[92], B. Singh [96], K. Singh [48], R. Singh [81], R. Singh [92], R. Singh [48], S. Singh [16], V.K. Singh [133], V. Singhal [133], T. Sinha [100], B. Sitar [13], M. Sitta [131,56], T.B. Skaali[20], G. Skorodumovs [95], M. Slupecki [44], N. Smirnov [138], R.J.M. Snellings [59], E.H. Solheim [20], J. Song [115], A. Songmoolnak[106], C. Sonnabend [33,98], F. Soramel [28], A.B. Soto-hernandez [89], R. Spijkers [85], I. Sputowska [108], J. Staa [76], J. Stachel [95], I. Stan [63], P.J. Steffanic [121], S.F. Stiefelmaier [95], D. Stocco [104], I. Storehaug [20], P. Stratmann [136], S. Strazzi [26], C.P. Stylianidis[85], A.A.P. Suaide [111], C. Suire [73], M. Sukhanov [141], M. Suljic [33], R. Sultanov [141], V. Sumberia [92], S. Sumowidagdo [83], S. Swain[61], I. Szarka [13], M. Szymkowski [134], S.F. Taghavi [96], G. Taillepied [98], J. Takahashi [112], G.J. Tambave [81], S. Tang [6], Z. Tang [119], J.D. Tapia Takaki [117], N. Tapus[125], L.A. Tarasovicova [136], M.G. Tarzila [46], G.F. Tassielli [32], A. Tauro [33], G. Tejeda Muñoz [45], A. Telesca [33], L. Terlizzi [25], C. Terrevoli [115], S. Thakur [4], D. Thomas [109], A. Tikhonov [141], A.R. Timmins [115], M. Tkacik[107], T. Tkacik [107], A. Toia [64], R. Tokumoto[93], K. Tomohiro[93], N. Topilskaya [141], M. Toppi [49], T. Tork [73], V.V. Torres [104], A.G. Torres Ramos [32], A. Trifiró [31,53], A.S. Triolo [33,31,53], S. Tripathy [51], T. Tripathy [47], S. Trogolo [33], V. Trubnikov [3], W.H. Trzaska [116], T.P. Trzcinski [134], A. Tumkin [141], R. Turrisi [54], T.S. Tveter [20], K. Ullaland [21], B. Ulukutlu [96], A. Uras [127], G.L. Usai [23], M. Vala[38], N. Valle [22], L.V.R. van Doremalen[59], M. van Leeuwen [85], C.A. van Veen [95], R.J.G. van Weelden [85], P. Vande Vyvre [33], D. Varga [137], Z. Varga [137], M. Vasileiou [79], A. Vasiliev [141], O. Vázquez Doce [49], V. Vechernin [141], E. Vercellin [25], S. Vergara Limón[45], R. Verma[47], L. Vermunt [98], R. Vértesi [137], M. Verweij [59], L. Vickovic[34], Z. Vilakazi[122], O. Villalobos Baillie [101], A. Villani [24], G. Vino [50], A. Vinogradov [141], T. Virgili [29], M.M.O. Virta [116], V. Vislavicius[76], A. Vodopyanov [142], B. Volkel [33], M.A. Völkl [95], K. Voloshin[141], S.A. Voloshin [135], G. Volpe [32], B. von Haller [33], I. Vorobyev [96], N. Vozniuk [141], J. Vrláková [38], J. Wan[40], C. Wang [40], D. Wang[40], Y. Wang [40], Y. Wang [6], A. Wegrzynek [33], F.T. Weiglhofer[39], S.C. Wenzel [33], J.P. Wessels [136], S.L. Weyhmiller [138], J. Wiechula [64], J. Wikne [20], G. Wilk [80], J. Wilkinson [98], G.A. Willems [136], B. Windelband [95], M. Winn [129], J.R. Wright [109], W. Wu[40], Y. Wu [119], R. Xu [6], A. Yadav [43], A.K. Yadav [133], S. Yalcin [72], Y. Yamaguchi [93], S. Yang[21],

S. Yano [93], Z. Yin [6], I.-K. Yoo [17], J.H. Yoon [58], H. Yu[12], S. Yuan[21], A. Yuncu [95], V. Zaccolo [24], C. Zampolli [33], F. Zanone [95], N. Zardoshti [33], A. Zarochentsev [141], P. Závada [62], N. Zaviyalov[141], M. Zhalov [141], B. Zhang [6], C. Zhang [129], L. Zhang [40], S. Zhang [40], X. Zhang [6], Y. Zhang[119], Z. Zhang [6], M. Zhao [10], V. Zherebchevskii [141], Y. Zhi[10], D. Zhou [6], Y. Zhou [84], J. Zhu [98,6], Y. Zhu[6], S.C. Zugravel [56], N. Zurlo [132,55]

Affiliation Notes

[I] Also at: Max-Planck-Institut für Physik, Munich, Germany
[II] Also at: Italian National Agency for New Technologies, Energy and Sustainable Economic Development (ENEA), Bologna, Italy
[III] Also at: Department of Applied Physics, Aligarh Muslim University, Aligarh, India
[IV] Also at: Institute of Theoretical Physics, University of Wroclaw, Poland
[V] Also at: An institution covered by a cooperation agreement with CERN

Collaboration Institutes

[1] A.I. Alikhanyan National Science Laboratory (Yerevan Physics Institute) Foundation, Yerevan, Armenia
[2] AGH University of Science and Technology, Cracow, Poland
[3] Bogolyubov Institute for Theoretical Physics, National Academy of Sciences of Ukraine, Kiev, Ukraine
[4] Bose Institute, Department of Physics and Centre for Astroparticle Physics and Space Science (CAPSS), Kolkata, India
[5] California Polytechnic State University, San Luis Obispo, California, United States
[6] Central China Normal University, Wuhan, China
[7] Centro de Aplicaciones Tecnológicas y Desarrollo Nuclear (CEADEN), Havana, Cuba
[8] Centro de Investigación y de Estudios Avanzados (CINVESTAV), Mexico City and Mérida, Mexico
[9] Chicago State University, Chicago, Illinois, United States
[10] China Institute of Atomic Energy, Beijing, China
[11] China University of Geosciences, Wuhan, China
[12] Chungbuk National University, Cheongju, Republic of Korea
[13] Comenius University Bratislava, Faculty of Mathematics, Physics and Informatics, Bratislava, Slovak Republic
[14] COMSATS University Islamabad, Islamabad, Pakistan
[15] Creighton University, Omaha, Nebraska, United States
[16] Department of Physics, Aligarh Muslim University, Aligarh, India
[17] Department of Physics, Pusan National University, Pusan, Republic of Korea
[18] Department of Physics, Sejong University, Seoul, Republic of Korea
[19] Department of Physics, University of California, Berkeley, California, United States
[20] Department of Physics, University of Oslo, Oslo, Norway
[21] Department of Physics and Technology, University of Bergen, Bergen, Norway
[22] Dipartimento di Fisica, Università di Pavia, Pavia, Italy
[23] Dipartimento di Fisica dell'Università and Sezione INFN, Cagliari, Italy
[24] Dipartimento di Fisica dell'Università and Sezione INFN, Trieste, Italy
[25] Dipartimento di Fisica dell'Università and Sezione INFN, Turin, Italy
[26] Dipartimento di Fisica e Astronomia dell'Università and Sezione INFN, Bologna, Italy
[27] Dipartimento di Fisica e Astronomia dell'Università and Sezione INFN, Catania, Italy
[28] Dipartimento di Fisica e Astronomia dell'Università and Sezione INFN, Padova, Italy
[29] Dipartimento di Fisica 'E.R. Caianiello' dell'Università and Gruppo Collegato INFN, Salerno, Italy
[30] Dipartimento DISAT del Politecnico and Sezione INFN, Turin, Italy
[31] Dipartimento di Scienze MIFT, Università di Messina, Messina, Italy
[32] Dipartimento Interateneo di Fisica 'M. Merlin' and Sezione INFN, Bari, Italy
[33] European Organization for Nuclear Research (CERN), Geneva, Switzerland
[34] Faculty of Electrical Engineering, Mechanical Engineering and Naval Architecture, University of Split, Split, Croatia
[35] Faculty of Engineering and Science, Western Norway University of Applied Sciences, Bergen, Norway
[36] Faculty of Nuclear Sciences and Physical Engineering, Czech Technical University in Prague, Prague, Czech Republic
[37] Faculty of Physics, Sofia University, Sofia, Bulgaria
[38] Faculty of Science, P.J. Šafárik University, Košice, Slovak Republic

[39] Frankfurt Institute for Advanced Studies, Johann Wolfgang Goethe-Universität Frankfurt, Frankfurt, Germany
[40] Fudan University, Shanghai, China
[41] Gangneung-Wonju National University, Gangneung, Republic of Korea
[42] Gauhati University, Department of Physics, Guwahati, India
[43] Helmholtz-Institut für Strahlen- und Kernphysik, Rheinische Friedrich-Wilhelms-Universität Bonn, Bonn, Germany
[44] Helsinki Institute of Physics (HIP), Helsinki, Finland
[45] High Energy Physics Group, Universidad Autónoma de Puebla, Puebla, Mexico
[46] Horia Hulubei National Institute of Physics and Nuclear Engineering, Bucharest, Romania
[47] Indian Institute of Technology Bombay (IIT), Mumbai, India
[48] Indian Institute of Technology Indore, Indore, India
[49] INFN, Laboratori Nazionali di Frascati, Frascati, Italy
[50] INFN, Sezione di Bari, Bari, Italy
[51] INFN, Sezione di Bologna, Bologna, Italy
[52] INFN, Sezione di Cagliari, Cagliari, Italy
[53] INFN, Sezione di Catania, Catania, Italy
[54] INFN, Sezione di Padova, Padova, Italy
[55] INFN, Sezione di Pavia, Pavia, Italy
[56] INFN, Sezione di Torino, Turin, Italy
[57] INFN, Sezione di Trieste, Trieste, Italy
[58] Inha University, Incheon, Republic of Korea
[59] Institute for Gravitational and Subatomic Physics (GRASP), Utrecht University/Nikhef, Utrecht, Netherlands
[60] Institute of Experimental Physics, Slovak Academy of Sciences, Košice, Slovak Republic
[61] Institute of Physics, Homi Bhabha National Institute, Bhubaneswar, India
[62] Institute of Physics of the Czech Academy of Sciences, Prague, Czech Republic
[63] Institute of Space Science (ISS), Bucharest, Romania
[64] Institut für Kernphysik, Johann Wolfgang Goethe-Universität Frankfurt, Frankfurt, Germany
[65] Instituto de Ciencias Nucleares, Universidad Nacional Autónoma de México, Mexico City, Mexico
[66] Instituto de Física, Universidade Federal do Rio Grande do Sul (UFRGS), Porto Alegre, Brazil
[67] Instituto de Física, Universidad Nacional Autónoma de México, Mexico City, Mexico
[68] iThemba LABS, National Research Foundation, Somerset West, South Africa
[69] Jeonbuk National University, Jeonju, Republic of Korea
[70] Johann-Wolfgang-Goethe Universität Frankfurt Institut für Informatik, Fachbereich Informatik und Mathematik, Frankfurt, Germany
[71] Korea Institute of Science and Technology Information, Daejeon, Republic of Korea
[72] KTO Karatay University, Konya, Turkey
[73] Laboratoire de Physique des 2 Infinis, Irène Joliot-Curie, Orsay, France
[74] Laboratoire de Physique Subatomique et de Cosmologie, Université Grenoble-Alpes, CNRS-IN2P3, Grenoble, France
[75] Lawrence Berkeley National Laboratory, Berkeley, California, United States
[76] Lund University Department of Physics, Division of Particle Physics, Lund, Sweden
[77] Nagasaki Institute of Applied Science, Nagasaki, Japan
[78] Nara Women's University (NWU), Nara, Japan
[79] National and Kapodistrian University of Athens, School of Science, Department of Physics , Athens, Greece
[80] National Centre for Nuclear Research, Warsaw, Poland
[81] National Institute of Science Education and Research, Homi Bhabha National Institute, Jatni, India
[82] National Nuclear Research Center, Baku, Azerbaijan
[83] National Research and Innovation Agency - BRIN, Jakarta, Indonesia
[84] Niels Bohr Institute, University of Copenhagen, Copenhagen, Denmark
[85] Nikhef, National institute for subatomic physics, Amsterdam, Netherlands
[86] Nuclear Physics Group, STFC Daresbury Laboratory, Daresbury, United Kingdom
[87] Nuclear Physics Institute of the Czech Academy of Sciences, Husinec-Řež, Czech Republic
[88] Oak Ridge National Laboratory, Oak Ridge, Tennessee, United States
[89] Ohio State University, Columbus, Ohio, United States
[90] Physics department, Faculty of science, University of Zagreb, Zagreb, Croatia
[91] Physics Department, Panjab University, Chandigarh, India

[92] Physics Department, University of Jammu, Jammu, India
[93] Physics Program and International Institute for Sustainability with Knotted Chiral Meta Matter (SKCM2), Hiroshima University, Hiroshima, Japan
[94] Physikalisches Institut, Eberhard-Karls-Universität Tübingen, Tübingen, Germany
[95] Physikalisches Institut, Ruprecht-Karls-Universität Heidelberg, Heidelberg, Germany
[96] Physik Department, Technische Universität München, Munich, Germany
[97] Politecnico di Bari and Sezione INFN, Bari, Italy
[98] Research Division and ExtreMe Matter Institute EMMI, GSI Helmholtzzentrum für Schwerionenforschung GmbH, Darmstadt, Germany
[99] Saga University, Saga, Japan
[100] Saha Institute of Nuclear Physics, Homi Bhabha National Institute, Kolkata, India
[101] School of Physics and Astronomy, University of Birmingham, Birmingham, United Kingdom
[102] Sección Física, Departamento de Ciencias, Pontificia Universidad Católica del Perú, Lima, Peru
[103] Stefan Meyer Institut für Subatomare Physik (SMI), Vienna, Austria
[104] SUBATECH, IMT Atlantique, Nantes Université, CNRS-IN2P3, Nantes, France
[105] Sungkyunkwan University, Suwon City, Republic of Korea
[106] Suranaree University of Technology, Nakhon Ratchasima, Thailand
[107] Technical University of Košice, Košice, Slovak Republic
[108] The Henryk Niewodniczanski Institute of Nuclear Physics, Polish Academy of Sciences, Cracow, Poland
[109] The University of Texas at Austin, Austin, Texas, United States
[110] Universidad Autónoma de Sinaloa, Culiacán, Mexico
[111] Universidade de São Paulo (USP), São Paulo, Brazil
[112] Universidade Estadual de Campinas (UNICAMP), Campinas, Brazil
[113] Universidade Federal do ABC, Santo Andre, Brazil
[114] University of Cape Town, Cape Town, South Africa
[115] University of Houston, Houston, Texas, United States
[116] University of Jyväskylä, Jyväskylä, Finland
[117] University of Kansas, Lawrence, Kansas, United States
[118] University of Liverpool, Liverpool, United Kingdom
[119] University of Science and Technology of China, Hefei, China
[120] University of South-Eastern Norway, Kongsberg, Norway
[121] University of Tennessee, Knoxville, Tennessee, United States
[122] University of the Witwatersrand, Johannesburg, South Africa
[123] University of Tokyo, Tokyo, Japan
[124] University of Tsukuba, Tsukuba, Japan
[125] University Politehnica of Bucharest, Bucharest, Romania
[126] Université Clermont Auvergne, CNRS/IN2P3, LPC, Clermont-Ferrand, France
[127] Université de Lyon, CNRS/IN2P3, Institut de Physique des 2 Infinis de Lyon, Lyon, France
[128] Université de Strasbourg, CNRS, IPHC UMR 7178, F-67000 Strasbourg, France, Strasbourg, France
[129] Université Paris-Saclay Centre d'Etudes de Saclay (CEA), IRFU, Départment de Physique Nucléaire (DPhN), Saclay, France
[130] Università degli Studi di Foggia, Foggia, Italy
[131] Università del Piemonte Orientale, Vercelli, Italy
[132] Università di Brescia, Brescia, Italy
[133] Variable Energy Cyclotron Centre, Homi Bhabha National Institute, Kolkata, India
[134] Warsaw University of Technology, Warsaw, Poland
[135] Wayne State University, Detroit, Michigan, United States
[136] Westfälische Wilhelms-Universität Münster, Institut für Kernphysik, Münster, Germany
[137] Wigner Research Centre for Physics, Budapest, Hungary
[138] Yale University, New Haven, Connecticut, United States
[139] Yonsei University, Seoul, Republic of Korea
[140] Zentrum für Technologie und Transfer (ZTT), Worms, Germany
[141] Affiliated with an institute covered by a cooperation agreement with CERN
[142] Affiliated with an international laboratory covered by a cooperation agreement with CERN.